Four Branch Diversity Combining And Adaptive Beamforming Measurements using Mobile Arrays at 2.05 GHz

Gaurav Joshi

Thesis submitted to the Faculty of the Virginia Polytechnic Institute and State University in partial fulfillment of the requirements for the degree of

Masters of Science
in
Electrical Engineering

Dr. Warren L. Stutzman, Chair
Dr. Jeffrey Reed
Dr. Dennis Sweeney

July 15, 2002
Blacksburg, Virginia
Keywords: Mobile Arrays, Antenna Diversity, Rayleigh Channel, Maximal Ratio, Switched Diversity, Diversity Gain, Interference Rejection, Vehicular Measurements

Four Branch Diversity Combining And Adaptive Beamforming Measurements using Mobile Arrays at 2.05 GHz

Gaurav Joshi

Abstract

Mobile arrays employing diversity combining and adaptive beamforming techniques overcome multipath fading, improve coverage, and increase capacity in wireless communications systems. In this thesis, diversity combining and adaptive beamforming performance of different four element arrays for mobile (vehicular speed) and portable (pedestrian speed) terminals is investigated. The performance of four element arrays with different configurations and with different element patterns is compared using the square array of four half-wave dipole elements as the baseline. Results from diversity and beamforming measurements, performed in urban and suburban environments for both line-of-sight (LOS) and obstructed multipath channels are used to analyze and compare the performances of different four element arrays. At cumulative probabilities of 10%, 1% and 0.1%, diversity gain and improvement in signal-to-interference-plus-noise-ratio (SINR) are calculated from the diversity combining measurements and interference rejection measurements respectively.

Experimental results illustrating the dependence of diversity gain on power imbalance, envelope correlation and diversity-combining scheme are presented. Measurements were performed at 2.05 GHz using the handheld antenna array testbed (HAAT). Low profile linear arrays are shown to provide diversity gain values of 5 to 8 dB and 11 to 16 dB, respectively for switched and maximal ratio combining at the 99% reliability level in non-line-of-sight urban channel. Interference cancellation of 24 to 28 dB was recorded in urban and suburban line-of-sight (LOS) channels for the sectorized square array. Results of vehicular measurements with the arrays mounted on a ground plane supported above the vehicle roof are also reported.

Acknowledgement

I would like to thank my advisor, Dr. Warren L. Stutzman, for his invaluable support, encouragement and guidance over the past year. My sincere appreciation goes to my committee members Dr. Jeffrey Reed and Dr. Dennis Sweeney for their help and support in reviewing my thesis. I would like to express my gratitude to Dr. Carl Dietrich for his persistent help and inspiration. Without his encouragement, it would not have been possible to complete this thesis.

I would like to thank all my fellow students in the Virginia Tech Antenna Group, for creating a friendly and competitive atmosphere, especially Derek, Kai, Stani, Ko, Minh Chau, Seong-Youp, Nathan, Christian and Laure. I would like to thank the assistance of the VTAG staff, especially Randal Nealy for his support. I am also thankful to the students and faculty of MPRG for giving me the opportunity and pleasure to work with on numerous occasions.

I would like to express my deepest gratitude to Darrell Cook, Trey McCoy and their families for their emotional support. Most of all, I am grateful to my parents, my friends at B.S.U., Vidhi and my sister Khushi for everything in my life.

Chapter 1
Introduction

1.1 Introduction and Motivation

Wireless communication reliability is severely limited by multipath fading and capacity is limited by co-channel interference. Multipath fading caused by the time varying nature of the channel introduces fades as deep as 25 dB – 35 dB, whereas co-channel interference limits the number of users that can be offered service in the system. Adaptive antenna arrays are normally deployed at a base station to mitigate multipath fading and interference. However, significant improvement in system capacity and reliability can be achieved if adaptive arrays are also deployed at the mobile terminals [Vau88].

The transmitted signal reaches the receiver along different paths with different phase offsets because of the dynamic environment with stationary and moving scatterers. Sometimes, these signals arrive with different phase offsets to combine destructively, thus, causing severe fluctuations in the amplitude of the received signal called as **fading**. Multipath fading affects the reliability (quality) of the signal. On the other hand, interference limits the efficiency with which channels can be reused, thus, limiting the capacity of the system.

Smart antenna applications offer considerable performance gain by exploiting the diversity and beam forming capability of the array to reduce interference and increase capacity. Spatial separation of receiving antennas offers space diversity that provides virtual channels in the space domain [Win94]. Diversity combining techniques combine signals from different

antenna elements sufficiently uncorrelated to give greater reliability. All antenna elements in the array are most unlikely to be in a fade simultaneously and combining the signal outputs from these array elements reduces the likelihood of experiencing a fade because a simultaneous deep fade on both antennas is unlikely. Adaptive beamforming techniques cancel interfering signals with spatial characteristics different from the desired signal. Smart antennas with beamforming capabilities adaptively put a null in the direction of the interfering signal. The potential performance gain achievable through diversity combining and adaptive beam forming motivates investigation of different array configurations at the mobile unit to overcome multipath fading and interference, respectively.

1.2 Objective

In 1988, Vaughn [Vau88] first proposed performance gain due to diversity combining at handsets. Braun performed diversity and optimum beamforming measurements [Bra99] with two-element arrays at mobile handsets in 1999. In 2000, Dietrich [Die00] demonstrated performance improvement of handheld array configurations using co-polarized and dual-polarized arrays. In this thesis, diversity combining and adaptive beamforming performances of different four-element arrays for mobile (vehicular speed) and portable (pedestrian speed) terminals are investigated. Experimental results from diversity combining and interference rejection measurements performed with different scenarios are analyzed. These measured results are used to compare performances of different four element arrays in overcoming multipath fading and co-channel interference.

Growth in mobile and personal communication systems has offered opportunities to explore the role of antennas at the handset. The handset antennas are required to be small, lightweight and low profile. This thesis investigates the performance of various low profile mobile arrays that are robust, inexpensive and that can be mounted on vehicles. Diversity combining and interference rejection performances of linear and square arrays are compared. The array elements for the linear and square arrays are low-profile broadband omni directional monopoles. Arrays with elements mounted on a high impedance ground plane having a short

separation from the ground plane are also investigated along with a square sectorized array of four monopole elements that are backed by corner reflectors to generate directional patterns.

1.3 Thesis Outline

This thesis begins with an overview of multipath fading and diversity combining (Chapter 2). In Chapter 2, radio-wave propagation in mobile wireless communications channels (Section 2.1) is briefly introduced. Slow and fast fading channels with flat fading are also discussed in Section 2.1. Various diversity combining techniques and parameters affecting the diversity performance are addressed respectively, in Section 2.2 and Section 2.3. Section 2.2 discusses selection diversity, switch diversity, maximal ratio combining and equal gain combining techniques. The effect of power imbalance in branches and envelope correlation on diversity combining is briefly discussed in Section 2.3.

Chapter 3 describes interference cancellation using antenna arrays with adaptive beamforming techniques. A brief introduction to adaptive beamforming in mobile communication channels is given in Section 3.1. Section 3.2 offers a brief introduction to antenna arrays for adaptive beamforming. Sections 3.3 and 3.4 discuss different fixed and adaptive beam forming techniques used to effectively reduce co-channel interference and subsequently increase system capacity. Least mean square algorithm, recursive least square algorithm and constant modulus blind adaptive algorithms are briefly discussed in Section 3.4.

Measurements were performed at 2.05 GHz using the four-channel Handheld Antenna Array Testbed (HAAT) [Die01]. Chapter 4 gives an overview of this measurement testbed. Section 4.1 discusses the HAAT system and its supporting data processing software. Different linear and square antenna arrays used in the measurements are described in Section 4.2. Section 4.2.2 discusses impedance measurement results and Section 4.2.3 presents results from co-polarized H-plane radiation pattern measurement.

In Chapter 5, diversity measurement results are discussed using the HAAT measurement testbed described in Chapter 4. The performance of four element arrays described in Section 4.2 in overcoming multipath fading was investigated for pedestrian and vehicular

speeds. Chapter 5 begins with a short discussion on experiment objectives and measurement scenarios in Section 5.1. Measurement results from diversity combining measurements for arrays mounted on the linear positioner are described in Section 5.2.1. Section 5.2.2 describes results from the measurements performed in urban and suburban environments for both line-of-sight (LOS) and obstructed multipath channels with arrays mounted on a vehicle rooftop. Section 5.3 briefly analyzes and compares the diversity combining performances of different arrays.

Chapter 6 reports results from interference rejection measurements performed in urban, suburban and rural environments. Section 6.1 describes experiment objectives and scenarios followed by Section 6.2 discussing adaptive beamforming measured results with arrays mounted on the linear positioner and on vehicle rooftops. Section 6.3 compares interference rejection performance of arrays described in Section 4.2 in different scenarios. Finally, Chapter 7 summarizes the content and results presented in this thesis. A short discussion on future work is also presented in this chapter.

References

[Win94] Winters J.H., Salz J. and Gitlin R. D., *'The impact of antenna diversity on the Capacity of the Wireless Comm. Systems'*, IEEE Transaction on Communications, vol. 42, pp 1740-1751, 1994.

[Fuj01] Fujimoto K., James J. R., *Mobile Antenna Systems Handbook*, 2nd edition, Artech House, 2001.

[Vau88] Vaughn R. G., *'On Optimum Combining at the Mobile'*, IEEE Transactions on Vehicular Technology, vol. 37, No. 4, pp. 181-188, November 1988.

[Bra99] Braun C., Nilsson M. and Murch R. D., *' Measurement of the Interference Rejection Capacity of Smart Antennas on Mobile Telephones'*, IEEE Vehicular Technology Conference, 1999.

[Die00] Dietrich C. B. Jr., *'Adaptive Arrays and Diversity Antenna configurations for Handheld Wireless Communication Terminals'*, Ph.D. Dissertation, Virginia Tech, 2000.

[Die01] Dietrich C. B. Jr., Dietze K., Nealy J. R, Stutzman W. L., '*Spatial, polarization, and pattern diversity for wireless handheld terminals*', IEEE Transactions on Antennas and Propagation, vol. 49, September 2001.

Chapter 2

Multipath Fading and Diversity Combining

Multipath fading, co-channel interference, noise, and signal de-polarization mismatch all affect mobile radio communications. These characteristics reduce reliability and bandwidth efficiency. Diversity combining using smart antennas helps to ensure reliable communications with sufficient service quality and system capacity. A **smart antenna** is an antenna array used with signal-processing algorithms for adapting its radiation pattern to time varying channel conditions in order to improve link performance [War95]. Such an intelligent multibeam antenna array can dynamically change the system configurations to achieve performance gain in a cost effective manner [Bac97].

The use of smart antennas at base stations has shown significant performance gain in system reliability [Lee82]. One of the most elementary smart antennas use **antenna diversity**, where the signals received by multiple antennas are weighted and then combined [Win98]. Antenna diversity at base station employs two or more array elements to overcome multipath fading. For spatial antenna diversity, an antenna separation of ten or more wavelengths is required because of narrow angle spread of signal arrival as observed by the base station [Jak93]. However, the mobile handsets are often surrounded by scatterers, leading to wide angle spread. This allows small spacing between antenna elements at the handsets [Jak93]. At a given level of reliability, diversity-combining increases the overall received signal strength and, thus permits the use of lower transmit power. Employing antenna diversity using smart

antennas at the handsets decreases the required base station transmit power, thus reducing interference [Bra98].

Diversity combining techniques combine signals from different antennas that are sufficiently uncorrelated to give greater reliability. Individual antenna elements experience different multipath fading conditions. All antenna elements are unlikely to be in a fade simultaneously and this gives sufficient redundancy to extract information from the elements that are not in a fade, thus overcoming fading. Diversity schemes can be classified as:

1. Frequency Diversity
2. Time Diversity
3. Antenna Diversity
    (a) Space Diversity
    (b) Polarization Diversity
    (c) Angle Diversity

In a mobile communication channel characterized by multipath fading, diversity combining improves the overall received signal strength and hence improves reliability. At a given reliability (or outage probability) diversity reduces the average fade level [Jak93]. Diversity performance is commonly quantified using the parameter of diversity gain. Diversity gain is usually defined as the improvement of signal-to-noise ratio of the combined signal over the strongest branch in the diversity system. It is a function of envelope correlation, power imbalance between array elements, combining techniques and bandwidth of the signal relative to the coherence bandwidth of the channel. Diversity Gain is directly dependent upon the fades present in the signal. The direct relationship shows that deeper the fades, the larger the possible diversity gain. This can be seen from the fact that fading is less severe in Ricean fading channels, and so the available diversity gain is less than that in Rayleigh fading channels. This is the case in the measurements reported in Section 5.2.

This chapter examines diversity combining techniques at mobile handsets. The chapter begins with a brief introduction of the mobile multipath radio channel in Section 2.1. The performance of the combining techniques is determined by the envelope correlation,

polarization and individual element pattern. This is addressed in Section 2.2 with a discussion on diversity combining techniques. Section 2.3 addresses the diversity performance as a function of power imbalance, envelope correlation, and channel characteristics. As the power imbalance increases, the contribution from each branch becomes unequal and this results in reduced diversity gain. Diversity gain varies inversely with the envelope correlation between the signals from individual antenna array elements; that is, the less correlated the signals are, the more diversity gain is experienced.

2.1 The Wireless Mobile Communication Channel

Clear line-of-sight (LOS) communication has all the signal energy passing directly from the transmitter to the receiver. When scatterers, reflectors, or LOS blockage is present, there are multiple propagation paths with different total path lengths connecting the transmitter and the receiver. This results in multiple copies of the same signal arriving at the receiver from different directions at different time instants, causing an 'echo effect'. Due to the different path lengths of the multipath signals, the signal components have different phase shifts [$e^{j2p\ (R/?)}$], superimposed at the receiver causing constructive and destructive interference. The resulting fading is dynamic because either the receiving terminal or scatterers are moving,. The received signal envelope undergoes random fluctuations called **multipath fading**. In a multipath channel the received signal can be represented as sum of delayed, attenuated and phase-shifted versions of the transmitted signal [Rap99].

$$r(t) = \sum_{i=1}^{N} a_i(t)\, e^{j[2\pi f_c t_i(t) + f_i(t)]}\, s\left(t - t_i(t)\right) + n(t) \qquad (2.1)$$

where N is the total number of multipaths $a_i(t)$ is the time varying attenuation factor of the i^{th} path, $t_i(t)$ is the time varying delay associated with the i^{th} path, $f_i(t)$ is the phase shift due to the path length and reflection or scattering associated with the i^{th} path and $n(t)$ is the receiver noise.

Smart antennas are known to improve reliability, talk time, coverage and the capacity in wireless communication systems characterized by multipath fading channel [Lib99]. Transmit signal power can be increased to prevent a received signal from undergoing deep fades but this is not advisable because it increases interference to other users. An alternative to increased power is to employ multi-receiver diversity combining techniques. Diversity essentially offers redundancy at the receiver by using different independently fading branches. However, it should be noted that diversity cannot overcome large-scale path loss due to spreading of the wave front with distance from the transmitter, but diversity combining is a suitable tool to combat small-scale fading due to multipath.

Three major factors determine fading in a mobile channel. The first is the time delay characteristics of the channel and the second is the relative motion of the receiver compared to the scatterers in the channel and the third is the angle of arrival at the receiver. The time delay characteristic of the channel is given by [Rap99]:

Mean excess time delay: $$\bar{t} = E[t] \tag{2.2}$$

Rms delay spread: $$t_{rms} = \sqrt{E[(t - \bar{t})^2]} \tag{2.3}$$

where $t = t_i - t_1$ is the excess time delay of arrival of the i^{th} signal as compared to the arrival time t_1 of the first multipath or direct line of sight signal. Finally, the superposition of the multipath components depends on the antenna pattern.

Narrowband signals undergo flat fading, i.e. all frequency components of the narrowband signal are similarly affected by the channel and the frequency content of the signal is not distorted. In a typical flat fading channel, the inverse of the signal bandwidth $t_s = 1/\Delta f_s$ is greater than the delay spread t_{rms} or the signal bandwidth Δf_s is smaller than the *coherence bandwidth* Δf_c of the channel. Coherence bandwidth [Pro95] is defined as the bandwidth over which two transmitted signals are strongly correlated. In flat fading, every frequency component of the transmitted signal undergoes the same attenuation and phase shift

as introduced by the channel, because the bandwidth of the signal is smaller than the coherence bandwidth of the channel. Flat fading can be represented as multiplicative noise.

The relative motion of the receiver compared to its surroundings results in Doppler frequency shift. In a multipath channel the motion of scatterers or the receivers results in different multipath components arriving with different Doppler shifts, called *Doppler spread*. The Doppler spread introduced by the channel is normally given as the inverse of the coherence time T_c of the channel. *Coherence time* [Pro95] is defined as the time duration over which two transmitted signals are strongly correlated. Doppler spread or the coherence time of the channel describes the time variant nature of the channel.

At pedestrian and slow vehicular speeds the transmitted signal undergoes slow fading, i.e. the time rate of change of the channel is much slower than that of the signal. In a typical slow fading channel, the Doppler spread Δf_D is much smaller than the signal bandwidth Δf_s or the inverse of the signal bandwidth $t_s = 1/\Delta f_s$ is much smaller than the coherence time T_c of the channel [Rap99]. Flat fading is illustrated with narrowband data collected at Virginia Tech using the Handheld Antenna Array Testbed (HAAT) over a slow fading channel at pedestrian speeds. The normalized signal envelope observed at 2.05 GHz is shown in Fig. 2.1.

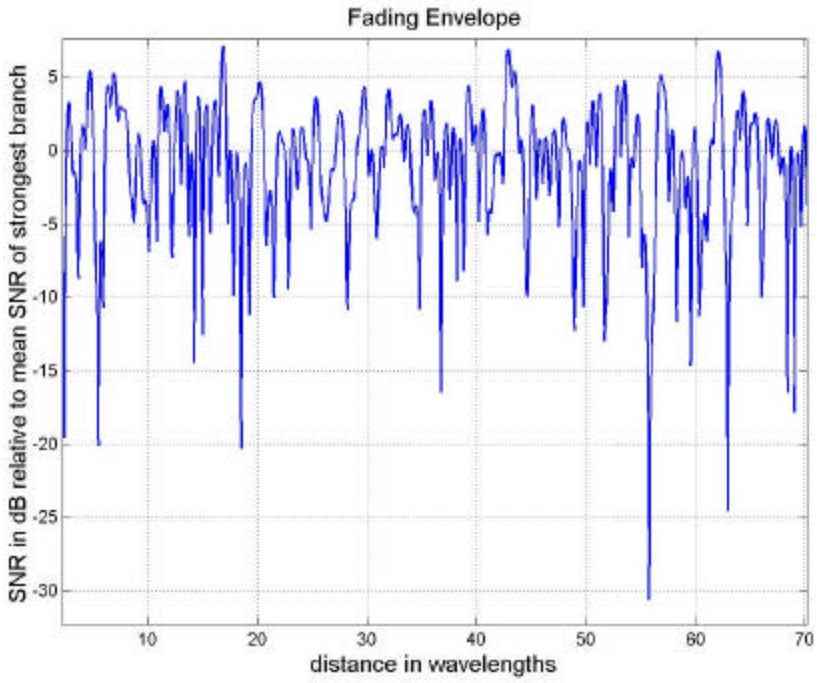

Figure 2.1 Signal envelope over a slow flat fading channel at 2.05 GHz [Jos01]

2.2 Diversity Combining Techniques

Diversity combining is very effective in reducing the average outage rate defined for a given threshold, or outage level. Linear summation of weighted received signals from different antenna elements is called diversity combining. Linear diversity combining techniques are classified as:

- Selection Diversity
- Switched Diversity
- Maximal Ratio Combining
- Equal Gain Combining

The simplest diversity combining technique, called selection diversity, selects the strongest signal. It selects the branch having the highest instantaneous power level. However, it requires as many receiver front-ends as the number of branches. A simpler way to implement the same idea with a single receiver would be to select a receiver output until its power drops

below an acceptable level, after which the next branch is selected. This technique is called switched diversity.

Another diversity combining technique is maximal ratio combining, which involves weighting the branch signal outputs proportional to their signal-to-noise ratio and cophasing them before combining. This is the optimum combining method as it maximizes the SNR of the combined signal. Weighting the branch signals proportional to their SNR is a difficult task as it requires pre-detection processing. Equal gain combining avoids this task by equally weighting the branch signals and cophasing them before combining. Equal gain combining performs almost as well as optimal maximal ratio combining [Jak93].

2.2.1 Selection Diversity

Selection diversity is the simplest diversity combining technique. Consider an array with N elements as shown in Fig. 2.2.1. Selection diversity selects among all branches the output from the branch with maximum signal-to-noise ratio (SNR) and connects it to the receiver. If the number of array elements and subsequent branches N is large then the probability of having large SNR at the receiver output is high.

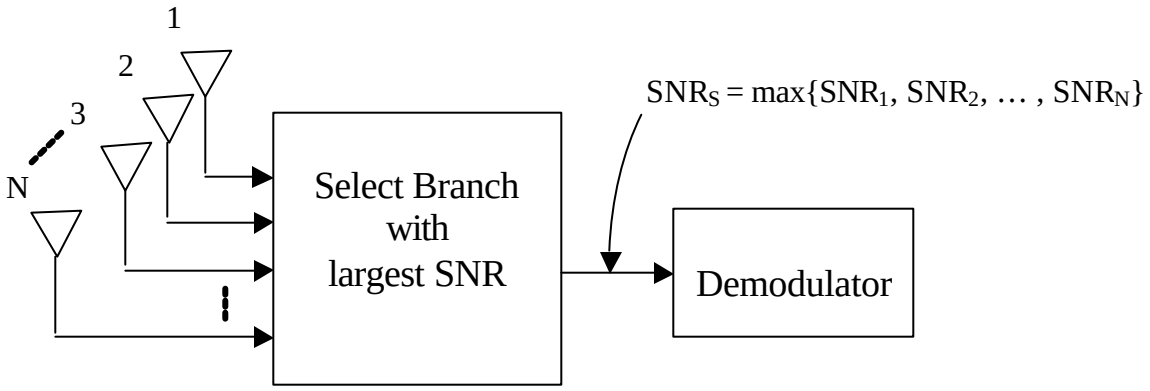

Figure 2.2.1 Block diagram for selection diversity combining

A major disadvantage of using selection diversity combining is that the receiver has to monitor the SNR of each of the branches and compare them in real time and must connect the

branch with the highest instantaneous signal-to-noise ratio (SNR) to the receiver demodulator. Also, the receiver must have multiple RF front ends, which are expensive. Another drawback of this technique is that it requires the signals in all branches to be co-phased so that when the receiver switches between branches to select the best signal, phase discontinuities are avoided. When the noise in all the branches is equal the branch with the strongest received signal power may be selected. Selection diversity offers maximum performance gain when the signal strength of each of the branch outputs is equal and the fading is uncorrelated [Jak93].

The performance gain achieved from selection diversity is quantified using the cumulative distribution of the signal envelope after diversity combining. Consider independent flat Rayleigh fading on each of the N diversity branches. If $\{\gamma_k\}$ are the instantaneous signal-to-noise ratios in each of the N branches and Γ be the time average of the signal envelope over a short duration, then the cumulative probability that the signal envelope drops below a predefined level of fading as γ_o is given as [Sch96]

$$P_r(\gamma \le \gamma_o) = \prod_{k=1}^{N} P_r(\gamma_k \le \gamma_o) = \left[1 - e^{-\left(\frac{\gamma_o}{\Gamma}\right)}\right]^N \tag{2.4}$$

Four-branch diversity combining measurements using a four-monopole linear array, shown in Fig. 4.2.3 (a), were performed at Virginia Tech Drillfield, to observe the advantage of selection diversity in suburban line-of-sight scenario. The measured data from two of the four branches was processed offline using the HAAT diversity combining software described in Section 4.1.2. The fading envelope of each of the four branches and the signal after selection diversity combining is shown in Fig. 2.2.2 (a). Note that the envelope of the signal combined using selection diversity undergoes little fading. Even though the individual branches undergo a fade as deep as –40 dB, the signal envelope after selection diversity combining never goes below –12 dB, reducing the fade level crossing rate. Cumulative probabilities of the signal-to-noise ratio (SNR) in each branch are shown in Fig. 2.2.2 (b).

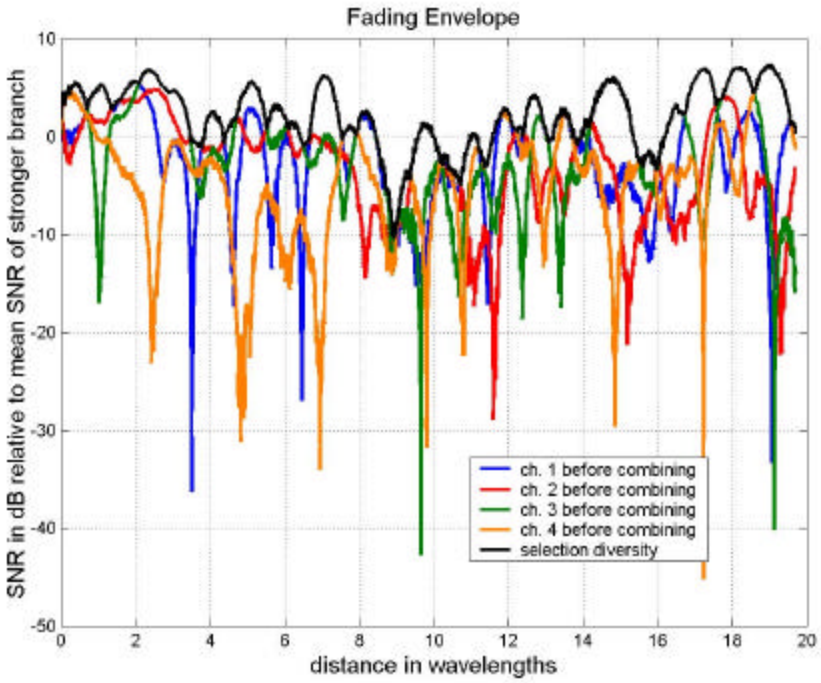

(a) Fading Envelope

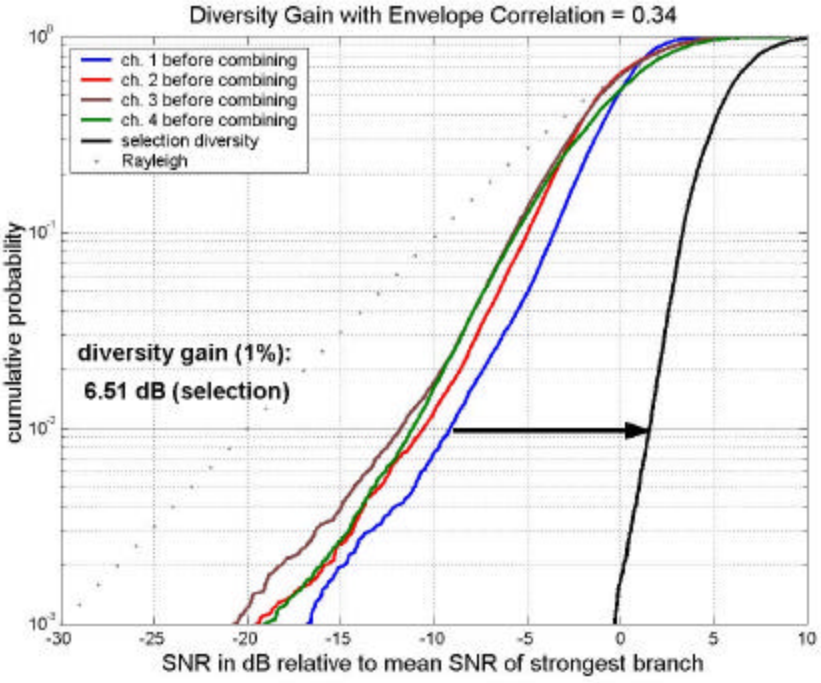

(b) Diversity Gain and Cumulative Distribution of the signal envelopes

Figure 2.2.2 Fading envelope and cumulative distribution of each of the four branches and the signal combined with selection diversity using four-monopole linear array shown in Fig. 4.2.3 (a) in a suburban line-of-sight scenario at the Virginia Tech Drillfield.

2.2.2 Switched Diversity

Switched diversity can be considered to be a form of selection diversity. Instead of selecting the strongest signal from all possible branches, switched diversity preselects a branch and connects it to the receiver till its signal-to-noise (SNR) ratio drops below a given threshold. The advantage that switched diversity offers over selection diversity is that the receiver need not monitor all the branches simultaneously and so a single receiver suffices. Initially the receiver connects the first branch to the demodulator input and monitors the SNR or simply the signal strength. If the SNR or the signal strength drops below a certain threshold limit, then the receiver 'switches' to the next branch and connects it to the demodulator while also monitoring its SNR.

The switched diversity technique is sensitive to the threshold level selected for switching to the next strongest branch. This can be seen in the measurement results performed for four-branch diversity combining at Drillfield, Virginia Tech campus using four-element linear array, shown in Fig 4.2.3 (a). For threshold of –10 dB at 99% reliability (1% cumulative probability), switched diversity offers 6.4 dB gain over the strongest signal as shown in Fig. 2.2.3 (a). However, for the threshold of –5 dB switched diversity offers a gain of 7.27 dB over the strongest signal at 1% cumulative distribution as shown in Fig 2.2.3 (b). It shows that diversity gain increases as the switching threshold lowers. The switching threshold puts a lower limit on the fades of the combined signal and increases the achievable gain over the strongest branch.

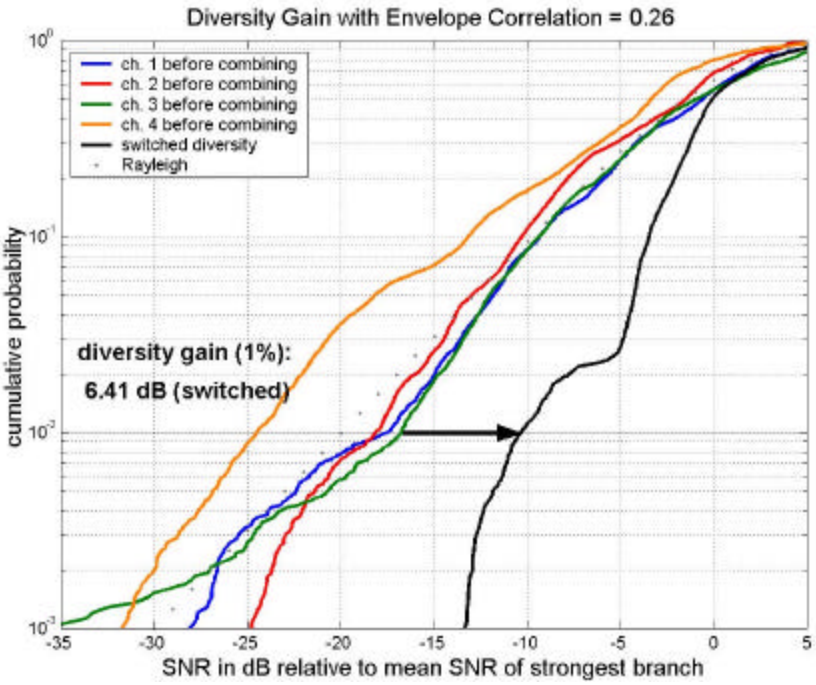

(a) Threshold = -10 dB

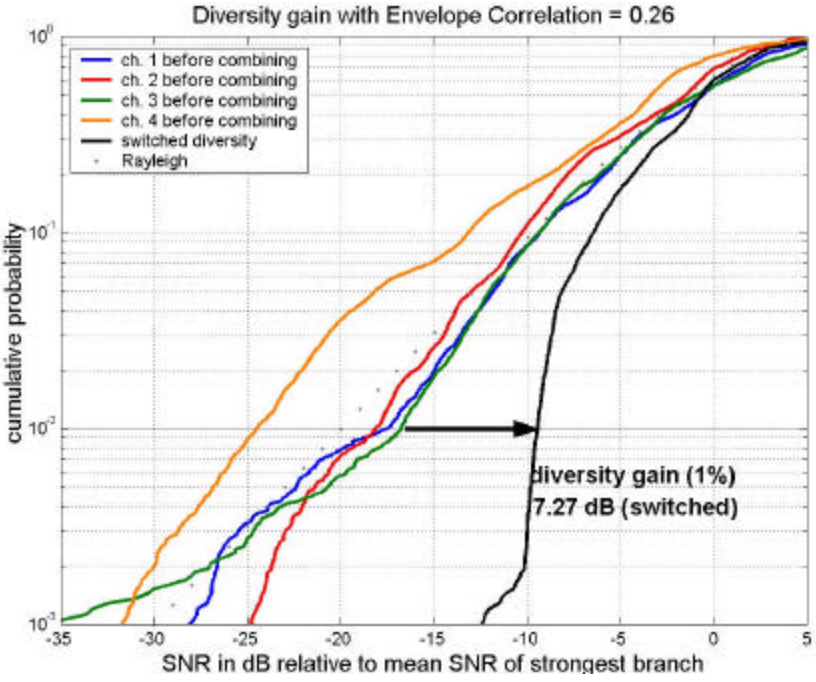

(b) threshold = -5 dB

Figure 2.2.3 CDF plot of SNR for each branch of four-element linear array of monopoles shown in Fig 4.2.3 (a) and the signal after switched diversity combining showing the effect of switching threshold on switched diversity combining technique. Measurements were taken at Virginia Tech Drillfield using the HAAT system described in Section 4.1

Switched diversity technique is not optimal because switching to the next branch occurs only when the signal-to-noise ratio (SNR) of the selected branch drops below the threshold [Sch96]. Since the switched diversity technique does not use information available from all branches but rather uses only one branch output, it does not offer optimum performance. It is quite possible that the selected branch may not be the strongest branch and may still remain selected as long as its signal strength is above the threshold. This can be seen in Fig 2.2.4, which shows that the branch selected is not the optimal since there is a stronger signal available.

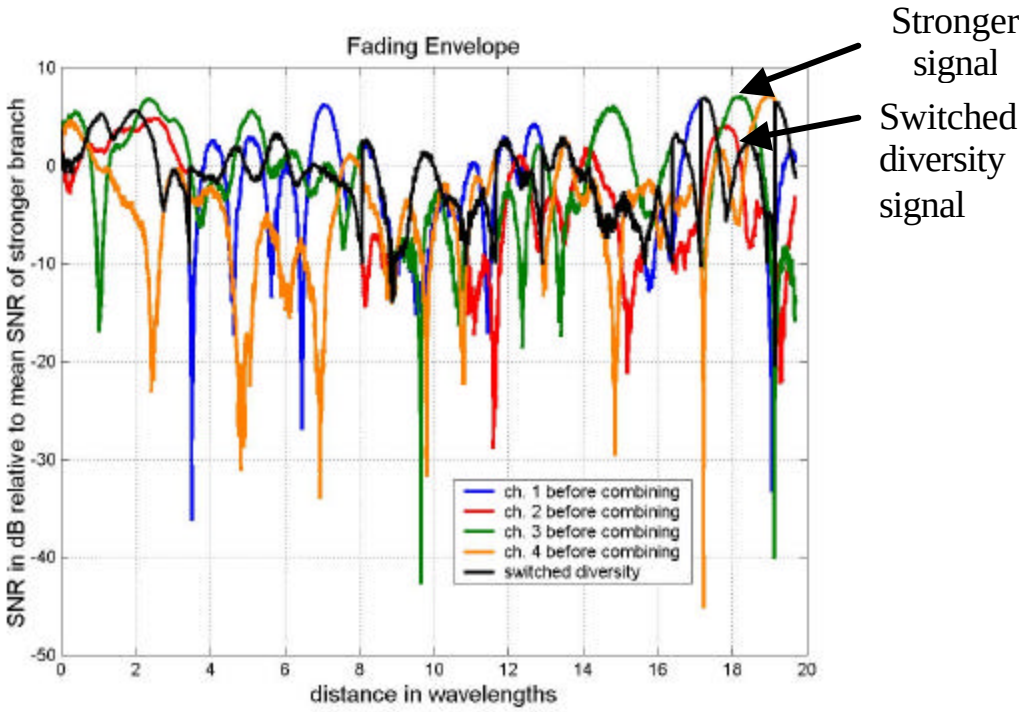

Figure 2.2.4 Signal Envelope from four branches with Switched Diversity using the four-element linear array shown in Fig. 4.2.3 (a) in suburban environment at Virginia Tech. The threshold used is – 10 dB.

2.2.3 Maximal Ratio Combining (MRC)

Maximal Ratio Combining is the optimal diversity combining technique [Vau88], since it makes use of information from all branches. The principle behind MRC is to maximize the

SNR at the input to the demodulator. Weighting each branch output with its instantaneous SNR and co-phasing them prior to addition results in maximum SNR at the output of the receiver. Fig 2.2.5 shows block diagram of Maximal Ratio Combining where the gain coefficients a_i for $i = 1,2,\ldots,N$ are proportional to SNR_i of the i^{th} branch. It gives optimal output but not without a price. MRC is more complicated than any of the other diversity combining techniques, primarily because MRC requires correct co-phasing for coherent addition. MRC requires regular estimates of the instantaneous signal-to-noise ratio for each branch. MRC also requires the gain coefficients a_i for $i = 1,2,\ldots,N$ to be constantly updated.

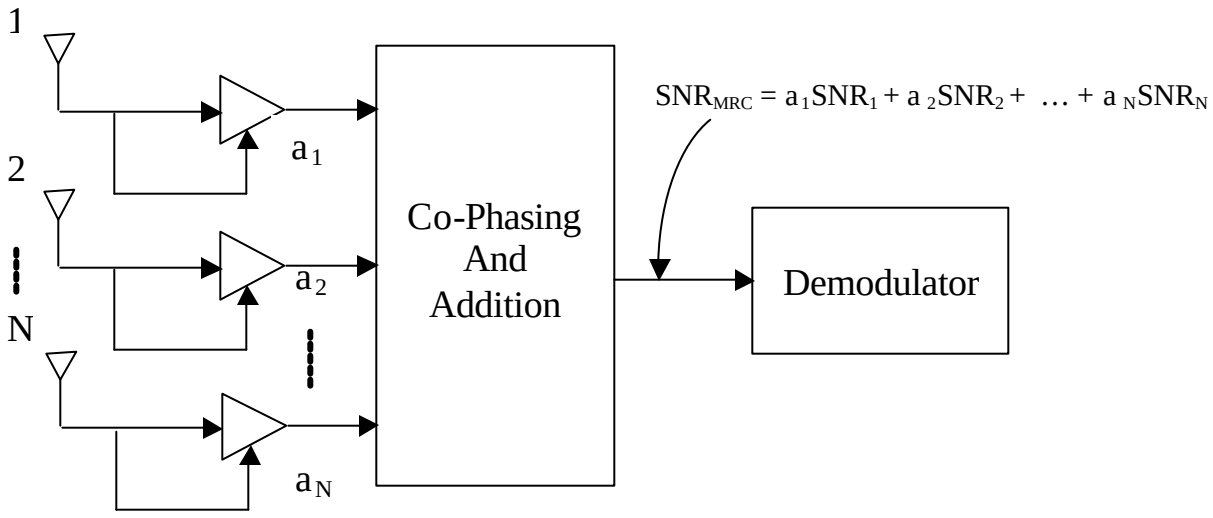

Figure 2.2.5 Block diagram of Maximal Ratio Combining (MRC) diversity technique

The measured data for four-element linear array with broadband monopoles at Virginia Tech Drillfield, as used in selection diversity and switched diversity, was also processed using MRC and is shown in Fig 2.2.6. Note that MRC significantly increases the signal strength of the combined signal at the input to the demodulator and is shown in Fig. 2.2.6 (a). Moreover, MRC being an optimum combining technique, offers maximum diversity gain. Note that compared to 6.5 dB for selection diversity and 6.4 dB for switched diversity with a threshold at –10 dB, MRC offers a diversity gain of 13.3 dB at 1% outage probability as shown in Fig. 2.2.6 (b).

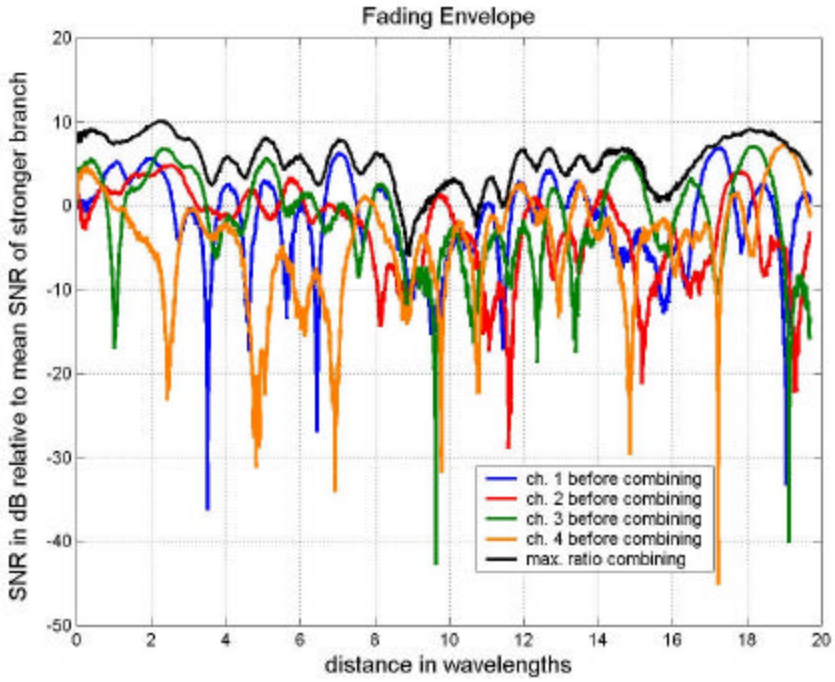

(a) Fading envelope from four-branch MRC diversity combining measurement

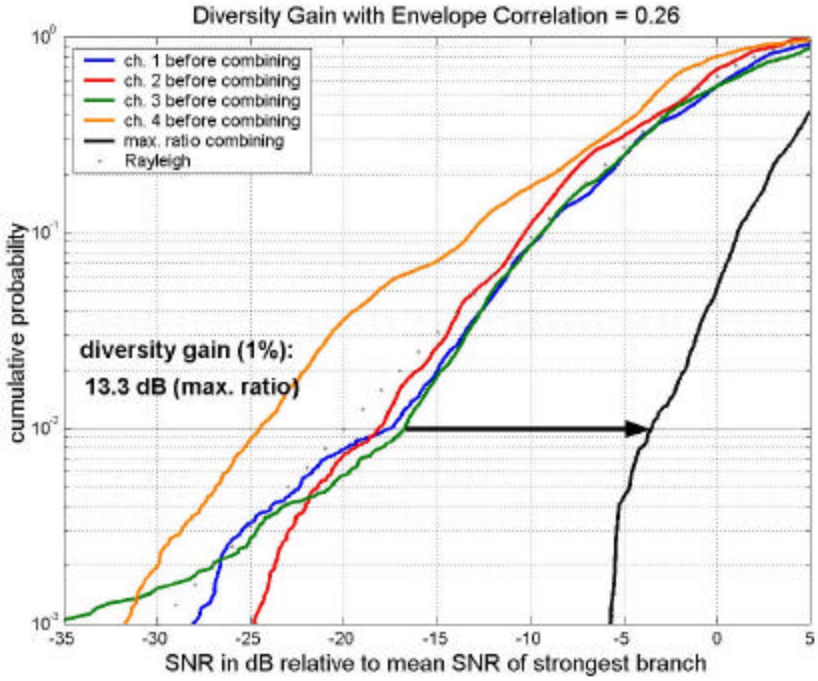

(b) Cumulative Probability of the SNR of each branch relative to the mean SNR of the strongest branch from four-branch MRC diversity combining measurement

Figure 2.2.6 Fading envelope and CDF plots for four-branch diversity combining using four-element linear array (Fig. 4.2.3 (a)) of monopoles in suburban scenario (Virginia Tech Drillfield)

Cumulative distribution of the signals from each branch and of the signal obtained by diversity combining is used to determine the diversity gain. The performance gain achieved from maximal ratio combining is viewed using the cumulative distribution of the signal envelope after diversity combining. Consider a flat fading Rayleigh channel with independent fading on each of the N diversity branches as mentioned in Section 2.2.1. If γ_k be the instantaneous signal-to-noise ratio in each of the N branches and Γ be the time average over a short duration, then the cumulative probability that the signal envelope drops below a predefined level of fading as γ_o for maximal ratio combining is given as [Sch96]

$$P_r(\gamma \leq \gamma_o) = \frac{1}{N!}\frac{\gamma_o^{\,N}}{\Gamma^N} \tag{2.5}$$

2.2.4 Equal Gain Combining

Equal gain combining is a variation of maximal-ratio combining, where the gain coefficients are all set equal to some constant (usually 1), i.e. $a_1 = a_2 = \ldots = a_N = a$. However, the branch signals are co-phased before summation to give an approximately optimal, combined signal output. It has been observed that equal gain combining offers marginal degradation in performance as compared to MRC for large SNRs at the branch inputs [Jak93].

The cumulative probability for the outage that the signal envelope drops below a predefined level of fading, γ_o, for equal gain combining is given as [Sch96]

$$P_r(\gamma \leq \gamma_o) = \frac{(2N)^N}{(2N)!}\frac{\gamma_o^{\,N}}{\prod_{k=1}^{N}\Gamma_k} \tag{2.6}$$

where Γ_k is the average signal-to-noise ratio over a short duration of time.

2.3 Diversity Performance and Diversity Gain

The performance achieved in diversity combining is quantified by the 'diversity gain', which quantifies the improvement in the signal strength at a certain level of reliability (say 99% corresponding to 1% cumulative probability) compared to the case when no diversity is employed. The diversity gain at cumulative probability *p* is expressed as [Die01]

$$G_d(p) = g_d - g_s \tag{2.7}$$

where $?_d$ is the SNR after diversity combining and $?_S$ is the SNR of the strongest branch before diversity combining [Jak93] at '*p*' cumulative probability. As shown in Fig 2.3.1 the cumulative distribution functions (CDFs) are plotted for the envelopes of all the branches as well as the calculated envelope of the signal formed after maximal ratio combining. The diversity gain for a given cumulative probability is the length of a horizontal line segment drawn between the strongest signal and the signal formed after combining. Measured data for four-element sectored square array (shown in Fig. 4.2.3 (c)) in urban obstructed scenario as described in Table 6.1 was processed using maximal ratio combining. The diversity gain of 11 dB at 1% cumulative probability for this measurement is shown in Fig. 2.3.1, which means that the diversity gain equals or exceeds 11 dB during the most severe 1% of signal fading. Note that the CDFs are normalized to the time average of the strongest branch.

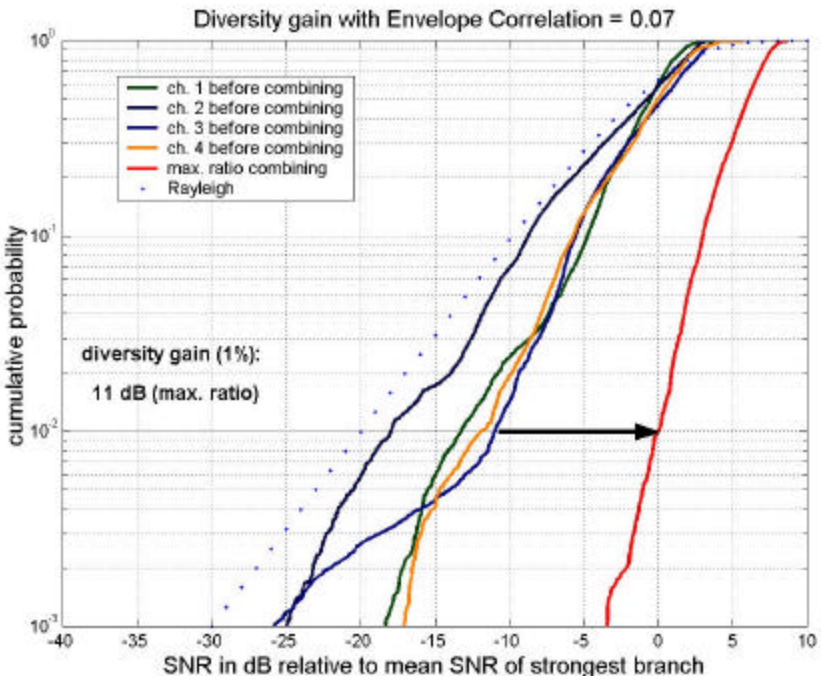

Figure 2.3.1 Cumulative probability of SNR from each branch as well as of the signal after MRC for diversity measurement performed using four-element sectored square array (shown in Fig. 4.2.3 (c)) in urban obstructed scenario as described in Table 6.1

Diversity gain performance depends on the following factors:

- Envelope correlation
- Branch power imbalance
- Diversity combining technique
- Antenna Array configuration

The first two of these are discussed in the following section. Diversity combining techniques were discussed in Section 2.3 and finally antenna arrays are discussed in Section 3.2.

2.3.1 Power Imbalance

Power imbalance is defined as the difference in average power of the branches in a diversity system. The effect of power imbalance in spatial antenna diversity is typically not significant, however, it can be a factor in polarization and angle diversity systems [Jak93].

Severe power imbalance results in the strong branch determining the output signal-to-noise ratio (SNR) with little contribution from the weaker branch.

Experiments performed at Whittemore Hall, Virginia Tech using the four-wire antenna shown in Fig. 4.2.3 (d) have shown that line-of-sight (LOS) measurements with significant direct to multipath component power imbalance offer less diversity gain [Jos01]. This is because fading is less severe in the line-of-sight channel. The LOS channel offers one direct signal which is dominant with little fade that in turn reduces the diversity gain, as there is little room for improvement. The Fig 2.3.2 (a) and Fig 2.3.2 (b) compare the diversity gain for line-of-sight (LOS) and N-LOS experimental setup in the urban channel with nearly equal envelope correlation coefficient. Note that in the LOS condition with substantial power imbalance, as shown in Fig 2.3.2 (a), diversity gain is less by 5.0 dB as compared to the obstructed non-line-of-sight condition at 99% reliability level.

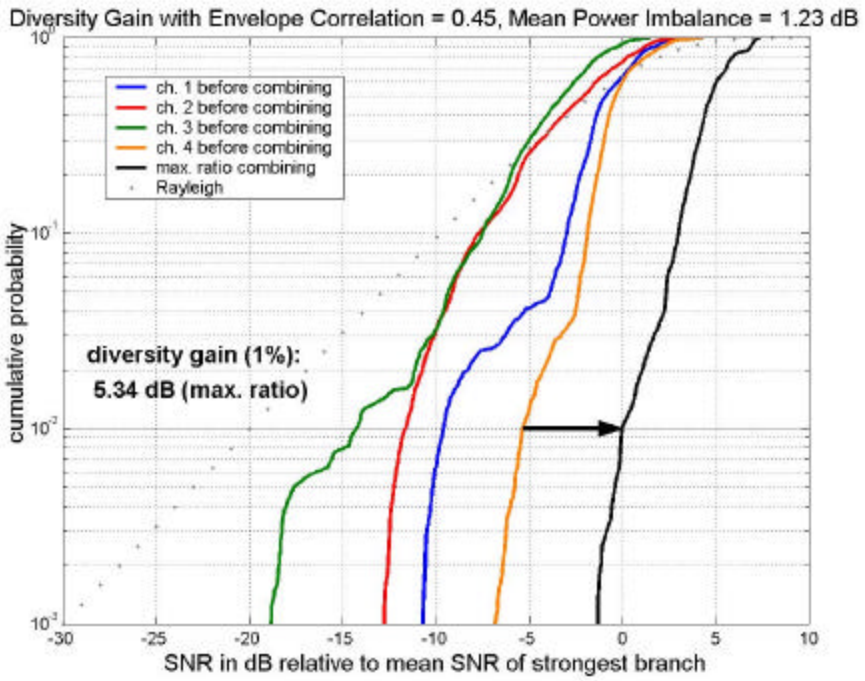

(a) Line-of-sight (LOS) scenario with power imbalance of 1.23 dB

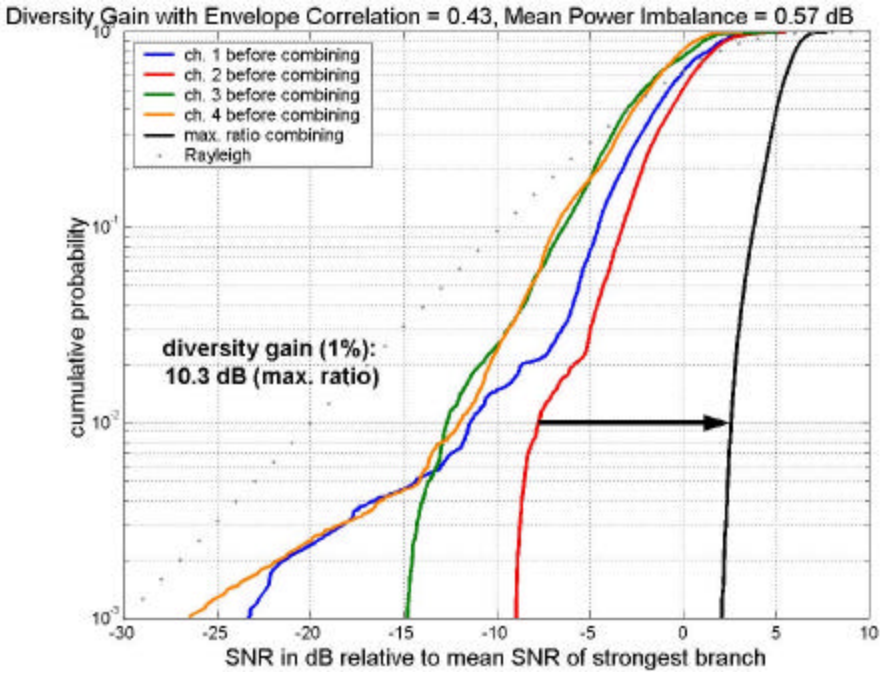

(b) Non-Line-of-sight (N-LOS) scenario with power imbalance of 0.57 dB

Figure 2.3.2 Diversity gain comparison for the effect of power imbalance in LOS and N-LOS scenarios using four-wire antenna (shown in Fig. 4.2.3 (d)) in an urban environment near Whittemore Hall, Virginia Tech with envelope correlation = 0.44º±0.01

2.3.2 Envelope Correlation

Diversity performance significantly depends on the envelope correlation $?_e$, which in turn depends on the spacing d between the antenna elements. Low envelope cross-correlation ensures high diversity gain. Analytically, envelope correlation $?_e$ is given by

$$r_e = \frac{E\left[\left(x_i - \overline{x_i}\right)\left(x_j - \overline{x_j}\right)\right]}{\sqrt{s_{xi}\, s_{xj}}} \tag{2.8}$$

where $\overline{x}$ and s_x respectively indicate the mean and the variance of the signal envelope x. Envelope correlation is a measure of how closely the signals fom two branches are related. If the signals are completely correlated then $?_e$ = 1, and the signals in the branches may fade simultaneously.

As the element spacing in an array goes to zero, the signals received by the antenna array elements fade at the same time offering no gain. The objective is to space the antenna array elements such that they fade independently. Correlation between the different antenna elements decreases as the spacing between them increases. Also the diversity techniques offer maximum gain when the signals on all branches have nearly equal strength. Analytically, the dependence of envelope correlation $?_e$ on element spacing in the array for angle of arrival having uniform distribution in azimuth and all elements having omni-directional pattern is shown to be [Jak93]

$$r_e = J_o^{\,2}\left(\frac{2pd}{l}\right) \tag{2.9}$$

where J_o is Bessel function of the first kind, order zero, and d is the element spacing. The above expression is valid if there is no polarization mismatch and all the scatterers lie in the azimuth plane. Individual element patterns of the antenna array elements are affected by mutual coupling due to close spacing. Mutual coupling distorts the individual element radiation pattern and this decreases envelope correlation.

The experimental results from measurements performed at Virginia Tech show that as the envelope correlation coefficient decreases diversity gain increases [Jos01]. This is because the reduced envelope correlation indicates that the array elements are uncorrelated and the signals received fade independently. Note that the measurements to determine the effect of envelope correlation on diversity performance were performed under identical conditions at west end of Virginia Tech Drillfield. Power imbalance in the two experiments differs by 0.3 dB and can be considered to be identical. Diversity gain of 8.2 dB is achieved for envelope correlation of $?_e$ = 0.76 as compared to 11 dB for envelope correlation of $?_e$ = 0.06 as shown in Fig 2.3.3 (a) and Fig 2.3.3 (b) respectively for the linear array.

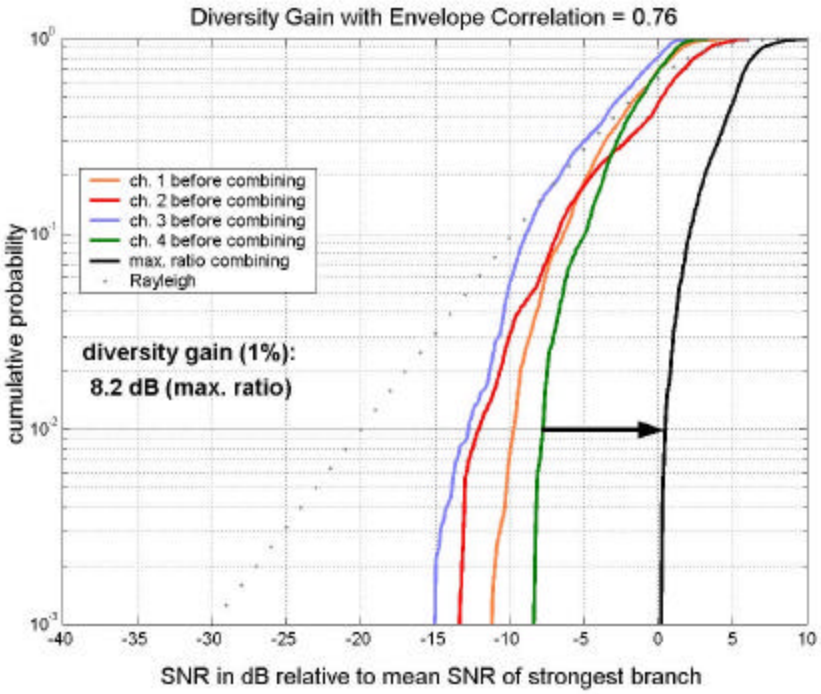

(a) Envelope correlation: $?_e$ = 0.76

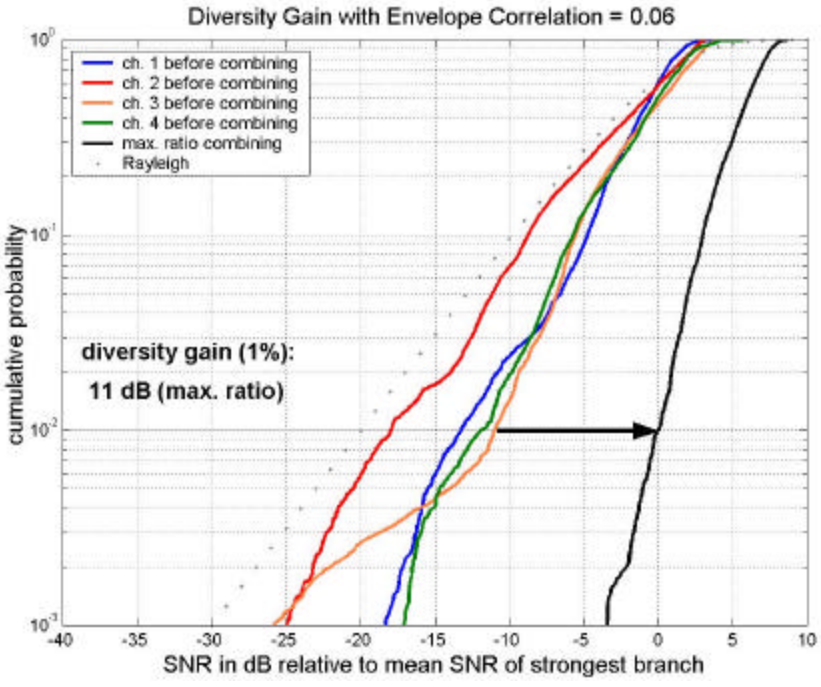

(b) Envelope correlation: $?_e$ = 0.06

Figure 2.3.3 Diversity gain comparison for the effect of envelope correlation under identical power imbalance condition in LOS and N-LOS scenarios using four-monopole square array (shown in Fig. 4.2.3 (b)) in a suburban environment at Virginia Tech Drillfield

The envelope cross-correlation of signals received by array elements having different radiation pattern is low. Pattern diversity, which exploits the different radiation pattern of individual elements to increase reliability, takes advantage of the resulting low envelope correlation.

It is difficult to experimentally determine the effect of power imbalance on diversity combining and vice versa. In most multipath environments, it was difficult to distinguish the effect of envelope correlation and power imbalance. After several trials at several different measurement locations, constant envelope correlation was observed at the space between the Whittemore Hall and Hancock Hall on Virginia Tech campus (shown in Fig.2.3.2).

References

[War95] Ward, C. R., Hudson, J. E., Searle J. G., "*Smart Antenna solutions for mobile radio systems*", 9th International Conference on Antennas and Propagation, 1995, Volume 1, pp: 130-136.

[Bac97] Bachman, H. L., "*Smart Antennas – the practical realities*", IEEE Proceedings Aerospace Conference, 1997, Volume 1, pp: 63-70.

[Lee82] Lee W. C. Y., "*Mobile Communications Engineering*," McGraw-Hill, New York 1982.

[Win98] Winters, J. H., "*Smart Antennas for Wireless Systems*", IEEE Personal Communications, February 1998, Volume 5, pp: 23-27.

[Jak93] Jakes W. C., "*Microwave Mobile Communications*", New York, IEEE Press 1993.

[Bra98] Braun, C., Engblorn, G., Beekman, C., "*Antenna diversity for mobile telephones*", IEEE Antennas and Propagation Society International Symposium, 1998. Volume 4, pp: 2220-2223.

[Lib99] Liberti, J.C., Rappaport T.S., "*Smart Antennas for Wireless Communications: CDMA Applications*", Prentice Hall, 1999

[Rap99] T. S. Rappaport, "*Wireless Communications; Principles & Practice*", Prentice Hall, NJ 1999.

[Pro95] J. G. Proakis, "*Digital Communications*", McGraw-Hill, New York, NY 1995.

[Jos01] Joshi G. G., Dietrich C. B., Reed J. H., Davis W. A., "*Investigation of Diversity and Adaptive beamforming using the four-wire antenna*", report to HRL Labs, 2001.

[Sch96] Schwartz M., Bennett W. R., Stein S., "*Communication Systems and Techniques*", IEEE Press, 1996.

[Vau88] Vaughan R. G., "*On Optimum combining at the mobile*", IEEE Transactions on Vehicular Technology, November 1988, Volume 37, pp: 181-188.

[Die01] C. B. Dietrich Jr., K. Dietze, J. R. Nealy, W. L. Stutzman, "*Spatial, polarization, and pattern diversity for wireless handheld terminals*", IEEE Transactions on Antennas and Propagation, Volume 49, Sept.2001.

[DieK01] Kai Dietze, "*Analysis of a Two-Branch Maximal Ratio and Selection Diversity System with Unequal Branch Powers and Correlated Inputs for a Rayleigh Fading Channe*l", Master's Thesis, Virginia Tech, 2001.

Chapter 3

Adaptive Beamforming

Capacity in mobile radio communications is severely limited by the co-channel interference, which limits reuse of the channels. An array of antenna elements, used with an adaptive beamforming algorithm can mitigate multipath fading and overcome interference. Adaptive beamforming techniques employed at the base station have shown improvement in system capacity [Lee98]. Further increase in system performance can be achieved by utilizing beamforming at the mobile handsets [Vau88]. Measurement results in Chapter 6 demonstrate the interference rejection achieved by using smart antenna arrays with beamforming techniques.

Adaptive beamforming differentiates the interfering signal from the desired signal on the basis of different spatial characteristics. Adaptive beamforming can be seen as spatial filtering. A beamforming algorithm dynamically steers the array pattern to place maximum possible gain in the direction of the incoming desired signal while simultaneously placing a null or nulls in the direction of arrival of interfering signals. This increases the signal-to-interference ratio. However, if the angles of arrival of the desired and the interfering signals are the same, then a spatial beamforming could theoretically fail. In this case, polarization sensitive adaptive arrays can reject interference provided the polarization of the desired signal is not the same as the interfering signal [Com81]. The received signals from the array elements are weighted before combining thus optimizing some parameter (normally the SINR) of the combined signal.

For a cellular radio system in an urban populated environment, capacity is the most important issue. Allowing frequency re-use in the same cell (Spatial Division Multiple Access or SDMA) increases capacity and this requires reduction in frequency reuse factor through proper interference cancellation. Interference rejection allows increase in the capacity of the system and corresponding increase in the revenue for the service provider.

Section 3.1 introduces the advantages of employing adaptive beamforming in mobile communications. Antenna array configurations are briefly discussed in Section 3.2. Effects of the geometry of the array and the element pattern on beamforming are briefly addressed. Different fixed and adaptive beamforming techniques are discussed respectively in Sections 3.3 and 3.4.

3.1 Adaptive Beamforming in Mobile Radio Communications

Kohno et al. [Koh90] proposed the use of antenna arrays to overcome co-channel interference in mobile radio communications systems. Using simulation results, they demonstrated co-channel interference rejection by steering nulls in the direction of the interferers with arrival angles different from that of the desired users. The main objective of using beamforming in mobile radio communications is to combat co-channel interference when the direction of arrival of the interfering signal is different from that of the desired signal.

Adaptive beamforming with antenna arrays allows modification of the array pattern to reject interference and enhance signal-to-interference-plus-noise ratio (SINR). The performance in interference rejection using beamforming techniques is quantified by the signal-to-interference-plus-noise ratio (SINR) improvement achieved after implementing the beamforming. High SINR improvement can be achieved for large spatial separation in the angle of arrival of interfering and the desired signal. Measurements were performed at Virginia Tech Drillfield, using the four-element linear array of monopoles shown in Fig. 4.2.3 (a) and two transmitters to demonstrate interference rejection. SINR plotted with respect to time from the experimental results is shown in Fig 3.1.1. Observe large variations in the SINR before beamforming due to fading of both desired and interfering signals on all four channels. The

SINR of the combined signal after beamforming showed rapid fluctuations but no severe fading due to interference. In this particular measurement the SINR fluctuates about ±10 dB about 40 dB.

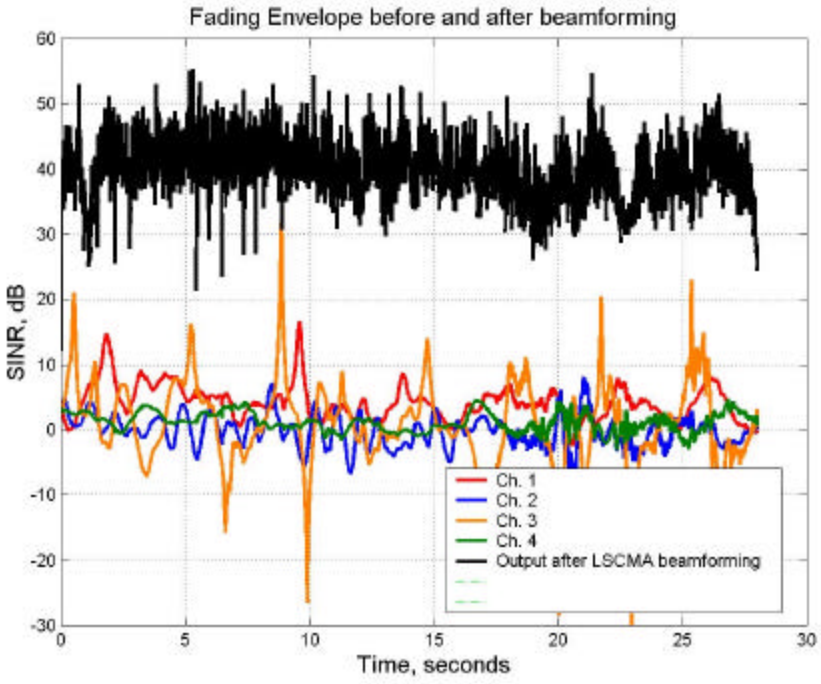

Figure 3.1.1 Measured signal-to-interference-plus-noise ratio (SINR) for four-element linear array of monopoles as receiving antenna, taken at Virginia Tech Drillfield [Jos01]

A sample plot of cumulative probability of SINR from each of the four branches is shown in Fig 3.1.2. This plot shows the improvement in SINR at 1% cumulative probability for measured signal-to-interference-plus-noise ratio (SINR) for four-element linear array of monopoles at Virginia Tech Drillfield. For a cumulative probability of 10^{-2} or 1%, the signal from the strongest channel shows SINR of about -1 dB, while the weighted signal after beamforming using a constant modulus algorithm (CMA) gives SINR of 28 dB. This shows that the SINR remains above this level 99% of the time. The CMA algorithm in this particular case achieves an improvement of about 29 dB over the SINR measured on the strongest branch.

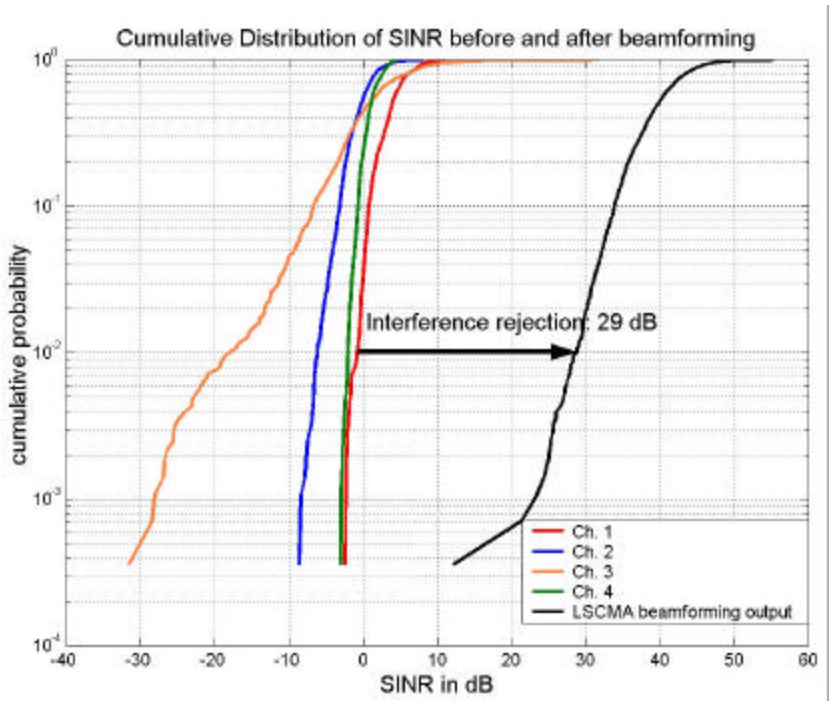

Figure 3.1.2 Cumulative Probability Distribution of SINR of each of the four branches and the branches combined to maximize SINR [Jos01]

Theoretically, any four-element antenna array can null three interferers [Hud81], which means that if four users in a mobile environment are sufficiently separated spatially, then interference rejection using adaptive beamforming forms near optimum radiation pattern that directs nulls in the direction of the interferers. The geometry, pattern and orientation of elements in the array influence the beamforming capability of the array.

3.2 Antenna Array

A single antenna element offers a wide radiation pattern with low directivity because antenna directivity and beam width are inversely related. A high gain directional beam can be achieved using an array with a number of elements spatially separated and fed from a feed structure. The array pattern is determined by the vector addition of fields radiated or received by individual array elements. For transmit beamforming, the objective is to space and feed the array elements such that fields from these elements undergo constructive superposition in the desired direction and destructively add in the direction of interference. For beamforming at the

receiver, algorithms that exploit the spatial characteristics of the desired signal to cancel the interfering signal are employed. The factors that affect the array performance are:

- Geometry of the array
- Radiation pattern of individual elements
- Relative excitation of the array elements

The radiation pattern of an antenna array consists of isotropically radiating elements is called *array factor* and it depends on the geometry and relative excitation of array elements. However, if the radiation pattern of the array elements is not isotropic and the orientations of the elements are identical, then the radiation pattern of the array is the product of the array factor and the individual array element pattern.

Linear Arrays

A linear array has all elements positioned along a single line. An equally spaced array as shown in Fig 3.1.3 has equal distance *d* between its elements. The angle *?* is called the direction of arrival.

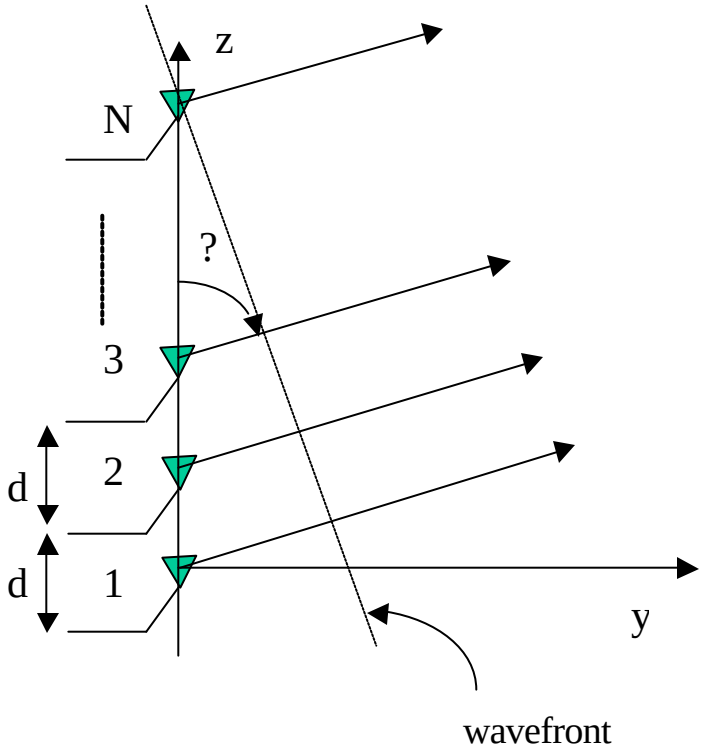

Figure 3.2.1 Geometry for a linear array antenna

The signal received at the first element may be shown as

$$x_{1n} = a_n e^{jj_n} \tag{3.1}$$

where the subscript n denotes the time instant, a_n and j_n respectively describes the amplitude and phase of the received signal. Note that $\{a_n\} = \{1\}$ for uniformly illuminated array. The signal received at the ith array element relative to that received at the first element is given as

$$x_{in} = x_{1n}\, e^{-j\{b(i-1)d\sin q\}} \tag{3.2}$$

The array $a(q) = \begin{bmatrix} 1 & e^{-jbd\sin q} & \cdots & e^{-j(N-1)bd\sin q} \end{bmatrix}$ is the called the *steering vector*, which is a function of the individual array element response and the array geometry. The response of individual array element to the received signal is digitized and used as input to the digital beamforming techniques.

3.3 Fixed Beamforming Techniques

Beamforming can be implemented using two basic techniques: switched beamforming and adaptive beamforming. Switched beamforming chooses from a set of fixed beams such that SINR is minimized. However, this is not the optimal approach. Adaptive antenna arrays typically use digital signal processing to dynamically alter the beam pattern to achieve optimal performance.

The simplest beamforming technique is selection of one of multiple fixed beams. An antenna array with a switched-beam technique yields numerous fixed beams, with high gain and low sidelobes as required. Switched beam technique can be implemented easily using a beamforming network with controlled switching as shown in Fig 3.3.1. A switched beam array uses highly directive beams and so offers some multipath rejection. Fixed beams with high gain allow increased coverage. However, this technique cannot reject interference with angle of arrival very close to that of the desired signal. Switched beamforming is very popular

technique on the downlink from the base station to the mobile terminals as it increases range and capacity.

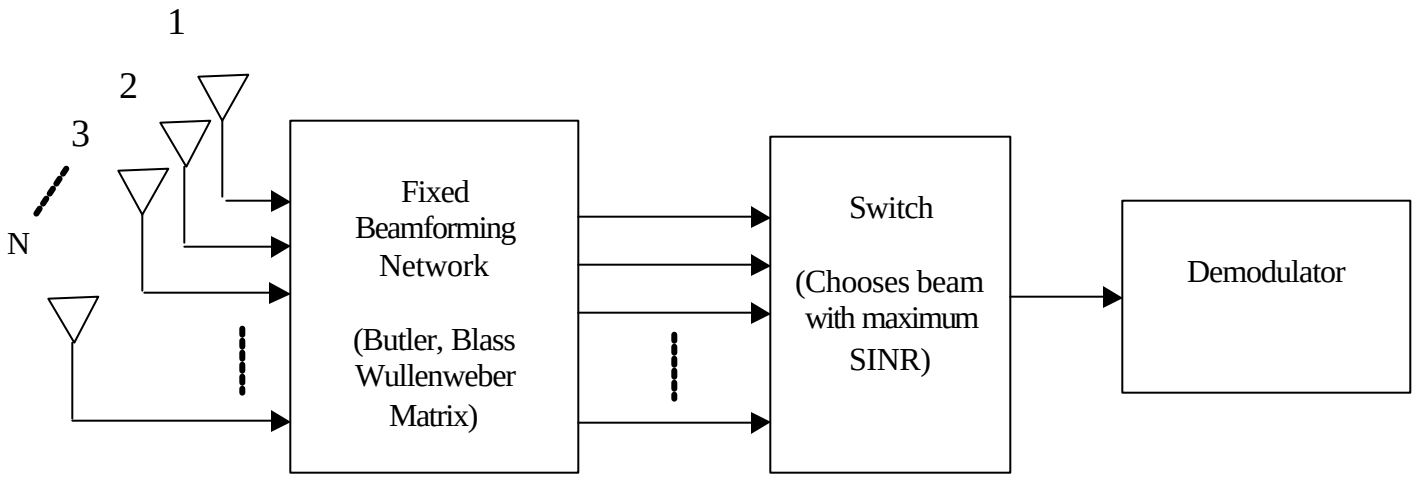

Figure 3.3.1 Switched Beamforming

The most common method used to achieve multiple-fixed beams using beamforming network consisting of hybrids and phase shifters is the use of Butler Matrix. The Butler matrix [Lit96] beamformer is equivalent to a spatial fast Fourier transform process. It uses hybrids and phase shifters to achieve mutually orthogonal fixed beams. Linearly independent combinations of the individual array element patterns produce these orthogonal beams. A Butler matrix, when applied to circular arrays, helps achieve fixed beams that cover the entire range of azimuth angles.

Fixed beams can also be formed using a Blass Matrix or a Wullenweber array [Lit96].

3.4 Adaptive Beamforming Techniques

Adaptive Beamforming algorithms approximate optimum beamforming using iterative approaches. The array pattern is dynamically adjusted to optimize some parameter of the received signal, which usually is the mean signal-to-interference-plus-noise ratio (SINR).

The amplitude and phase of the signal captured by different elements of the antenna array form what is known as the spatial signature of the signal. A beamformer weights and sums the signal's in-phase and quadrature-phase components captured by each antenna element such that the desired beam is formed. The spacing between the elements, the pattern of individual elements, the relative amplitude and phase of the current fed to the individual elements, the polarization of the elements and many other factors affect beamforming. The improvement in SINR largely depends upon the experimental scenario and the type of adaptive beamforming algorithm used.

Fig 3.4.1 [Lit96] is a block diagram of adaptive beamforming network and it shows that the output of the array $r(t)$ at any time instant is the complex weighted sum of the branch received signals $r_i(t)$ for $i = 1,2,\ldots,N$. Assume that the received branch signals include the array element pattern, gain and locally generated thermal noise. The received signal in each branch is a superposition of the desired signal $d(t)$, interfering signals and their multipaths. The array output $r(t)$ is compared to a reference signal, a replica of the desired signal $d(t)$ to update the complex weights w_i for each branch $i = 1,2,\ldots,N$. Optimum weights are determined iteratively to minimize the mean square error (MSE) between the array output $r(t)$ and the desired signal $d(t)$.

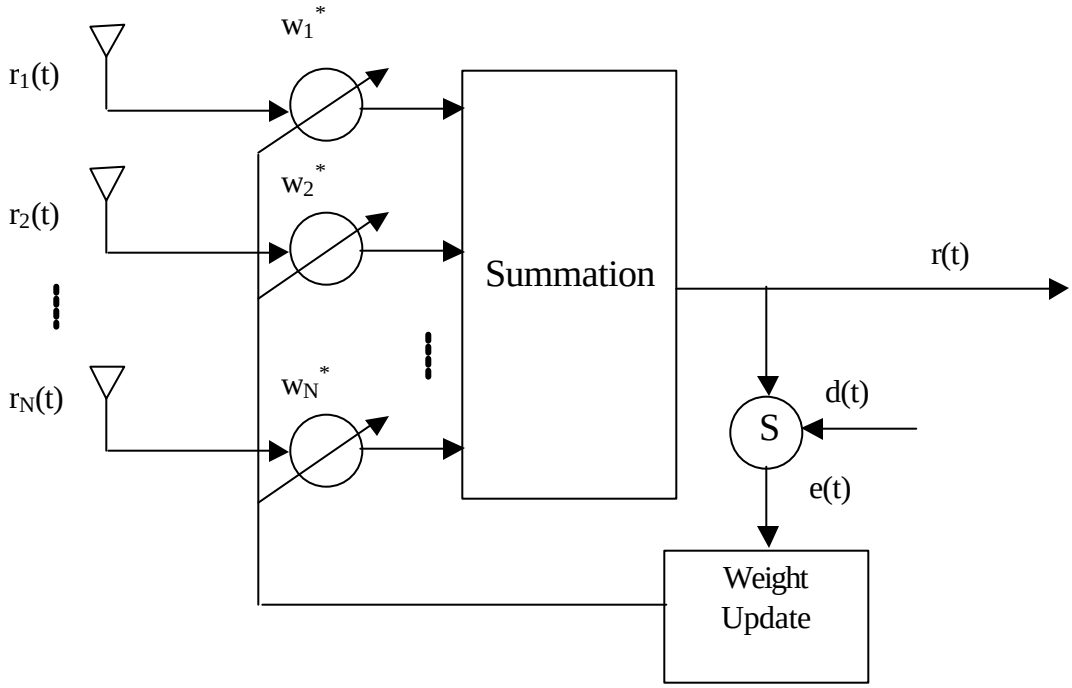

Figure 3.4.1 Block Diagram of adaptive beamforming network

The objective is to minimize the error *e(t)* and this gives optimum complex weights that alter the amplitude and phase of the received branch signals such that the output of the array is given as:

$$r(t) = \left[w_1^* \; w_2^* \; \cdots \; w_N^*\right] \left[r_1(t) \; r_2(t) \cdots r_N(t)\right]^T \tag{3.3}$$

Adaptive beamforming algorithms can be classified as blind or non-blind algorithms based on their need for a training sequence. Blind algorithms are robust and do not require training sequences. Beamforming techniques that require training sequences determine optimum weights by minimizing the mean square error (MSE) between the output of the beam former and a reference signal. Blind algorithms optimize beamforming weights based on the criterion of optimizing some property of the received signal that is shown to be related to SINR.

Optimal performance of any algorithm requires knowledge of channel characteristics. Channel characteristics can be estimated using a training sequence in case of non-blind

algorithm or can be determined from known signal characteristic in the case of blind algorithm. Three major adaptive beamforming algorithms are:

1. The **Least Mean Square** (LMS) algorithm is the simplest to implement and follows the steepest descent method. But it converges slowly and requires the knowledge of the desired signal.
2. The **Recursive Least Square** (RLS) algorithm recursively estimates the matrix inversion and converges must faster than LMS algorithm. But it too requires a reference signal.
3. The **Constant Modulus Algorithm** (CMA) is a blind adaptive algorithm, as it does not require any training sequence. It exploits the constant amplitude property of the envelope of the signal. Also being a blind adaptive algorithm it is not guaranteed to converge. A version of CMA called LS-CMA uses a direct matrix inversion.

3.4.1 Least Mean Square (LMS) Algorithm

The LMS algorithm follows the method of steepest descent. The criterion is to recursively estimate the weights proportional to the negative gradient of the mean square error (MSE). The proportionality is determined by a constant *?*, which in turn determines the convergence of the algorithm. LMS algorithm iteratively determines the weights such that the MSE given by $E\left(e^2\right)$ is minimized.

$$w_{n+1} = w_n - r\,\nabla E\left(e^2\right) \tag{3.4}$$

The LMS algorithm is very easy to implement due to its low complexity. However, it has a few drawbacks. The LMS algorithm requires knowledge of the desired signal to determine the MSE $E\left(e^2\right)$. The steepest descent method that the LMS algorithm employs does not allow quick convergence. An optimal value of ? needs to be determined to tradeoff between the rate of convergence and the stability of the algorithm [Ree02].

3.4.2 Recursive Least Square (RLS) Algorithm

The RLS algorithm follows the method of least squares, which determines the beamforming weights w such that the sum of error-squared $|e|^2$ is minimized. The sum of error-squared is given as

$$|e|^2 = \sum_{n=1}^{N} |e_n|^2 = \sum_{n=1}^{N} |d_n - w_n^H x_n|^2 \tag{3.5}$$

where the total number of array elements is N, the received signal is x and the desired signal is d. The optimal weight vector $\boldsymbol{w}$ that satisfies the criterion of achieving minimum least square error is given as

$$w = \left(XX^H\right)^{-1} x \left(Xd^H\right) = R_{xx}^{-1} x R_{xd} \tag{3.6}$$

Note that in order to determine the least square solution matrix inversion operation needs to be undertaken. The Direct Matrix Inversion (DMI) approach becomes impractical due to complexity as the matrix dimension increases. RLS algorithm recursively estimates the matrix inversion and converges must faster than LMS algorithm.

The time-varying correlated channel requires weighting of the previous information symbols. The RLS algorithm introduces exponential weighting. The RLS algorithm recursively alters the received signal covariance matrix R_{xx}^{-1}. Introducing 'forget factor' ? [Lit96] to estimate the received signal covariance matrix:

$$R_n = \sum_{j=1}^{N} z^{n-j} x_j x_j^H \tag{3.7}$$

The received signal covariance matrix R_{xx}^{-1} is updated recursively as:

$$R_n = z\ R_{n-1} + x_n x_n^{\ H} \tag{3.8}$$

The weights are updated as:

$$w_n = w_{n-1} + y_n \left\{ d_n - w_{n-1}^{\ H} x_n \right\} \tag{3.9}$$

where $y_n = \dfrac{z^{-1} R_{n-1}^{-1} x_n}{1 + z^{-1} x_n^{\ H} R_{n-1}^{-1} x_n}$

The RLS algorithm is faster than the LMS algorithm and its rate of convergence is about an order of magnitude faster than that of the LMS algorithm given the signal-to-noise ratio is high [Hay91].

3.4.3 Constant Modulus Algorithm (CMA)

CMA is a blind algorithm and it exploits the constant amplitude property of the envelope of the signal. CMA is particularly suitable for the narrowband measurements undertaken because it does not require any carrier synchronization. Moreover, an unmodulated tone at 2.05 GHz has a near constant envelope. Multipath fading and interference affect the constant envelope property of the desired signal. CMA when applied to beamforming aims to restore the constant envelope property of the desired signal. CMA optimizes a cost function based on the constant amplitude property of the envelope of the signal to obtain a near accurate estimate of the desired signal.

CMA updates the beam former weights $\boldsymbol{w}$ such that it minimizes the cost function e that measures average deviation of the envelope from the constant modulus condition, given as [Lit96]:

$$e = E\left[\left\{\frac{E\left(\left|x_n\right|^4\right)}{E\left(\left|x_n\right|^2\right)} - \left|x_n\right|^2\right\}^2\right] \tag{3.10}$$

The weights are updated as:

$$w_{i(n+1)} = w_{in} + z\left[1 - \left|r_n\right|^2\right] r_n\, x_{in} \qquad \text{for } i = 1,2,\ldots,N \tag{3.11}$$

where z is the step size used to update the weights, r_n is the beam former output.

There are many ways to determine the beam former weight vector ***w.*** The simplest method is to minimize e using steepest descent method. CMA is optimal if it converges, i.e. minimizing CMA cost function e is equivalent to determining the minimum MSE. CMA requires proper scaling of the weights, which makes convergence of the algorithm uncertain. CMA algorithm is not guaranteed to converge. Moreover, CMA can converge to an interfering signal.

Least Square CMA (LS – CMA)

Different methods can be used to update the beamformer weights such that the CMA cost function e is minimized. Usually steepest descent method is used to determine the weights but is very slow to converge as seen in Section 3.4.1. An alternative would be use least square CMA which minimizes the cost function given as:

$$\left|e\right|^2 = \sum_{n=1}^{N} \left|e_n\right|^2 = \sum_{n=1}^{N} \left|1 - \left| w_n^H x_n \right|\right|^2 \tag{3.12}$$

Least Square CMA can either determine the weights by matrix inversion as given by

$$w = R_{xx}^{-1} R_{xd} \tag{3.13}$$

where the estimate of the desired signal having unity envelope is given by $dn = \frac{r_n}{|r_n|}$, (r_n is the beamformer output).

Multi-Target Constant Modulus Algorithm (MT-CMA)

There is a possibility that the CMA and LS - CMA algorithm may capture a strong undesired signal and reject the desired signal as interference. Multi-target variations of CMA and LS – CMA successively extract up to N signals that have the constant modulus property. For an N – element array a set of N orthogonal weight vector is used which can extract up to N signals independently.

3.5 Summary

Chapter 3 gives an overview of the basic principles in adaptive beamforming. Section 3.1 discusses the advantage and application of adaptive beamforming techniques in mobile wireless communications. Section 3.2 discusses the array theory using the example of an equally spaced linear array. Section 3.3 offers an overview on fixed beamforming techniques followed by adaptive beamforming techniques in Section 3.4. Adaptive beamforming dynamically steers a null in the direction of the interfering signal and increases the signal-to-interference-plus-noise ratio. Various beamforming algorithms are presented with their cost functions, advantages and drawbacks.

References

[Lee98] Lee W. C. Y., *Mobile Communications Engineering*, Second Edition, New York, McGraw-Hill, 1998.

[Vau88] Vaughan R. G., *"On Optimum Combining at the Mobile,"* IEEE Transactions on Vehicular Technology, November 1988, pp.181-188.

[Com81] Compton R. T., Jr., *"On the Performance of a Polarization Sensitive Adaptive Array*," IEEE Transactions on Antennas and Propagation, September 1981, pp. 718-725.

[Koh90] Kohno R., Imai H., Hatori M., Pasupathy S., "*Combinations of an adaptive array antenna and a canceller of interference for direct-sequence spread-spectrum multiple-access system***",** IEEE Journal on Selected Areas in Communications, May 1990, Volume 8, pp: 675-682.

[Jos01] Joshi G. G., Dietrich C. B., Reed J. H., Davis W. A., *"Investigation of Diversity and Adaptive beamforming using the four-wire antenna*", report to HRL Labs, 2001.

[Hud81] Hudson J. E., *Adaptive Array Principles*, Institution of Electrical Engineers, Peter Peregrinus Ltd. 1981.

[Lit96] Litva J. and Lo T. K., *Digital Beamforming in Wireless Communication*, Artech House Publishers, 1996,

[Ree02] Reed J. H., *Software Radios: A Modern Approach to Radio Design*, Prentice Hall, May 2002.

[Hay91] Haykin S., *Adaptive Filter Theory*, Prentice Hall, Englewood Cliffs, NJ, 1991.

[But61] Butler J. and Lowe R., "*Beam-Forming Matrix Simplifies Design of Electronically Scanned Antennas*," Electronic Design, April 1961, pp. 170-173

Chapter 4

Diversity and Adaptive Beamforming Measurement System

The diversity combining and adaptive beamforming performance of the four element arrays was evaluated using the Handheld Antenna Array Testbed (HAAT). The HAAT system is a custom designed and constructed measurement apparatus that is portable and is used to test hand-held and vehicle mounted antenna configurations. Randall Nealy and Carl Dietrich [Car00] of the Virginia Tech Antenna Group (VTAG) developed the HAAT system for four channel narrowband space diversity and adaptive beamforming experiments. The four-channel HAAT measurement system operates at 2.05 GHz and consists of a four-channel narrowband receiver, two transmitters, and data processing and evaluating software.

This chapter gives a brief overview of the HAAT measurement testbed. Section 4.1 discusses the HAAT system and its supporting data processing software. Interested readers are referred to [Car00] for more information. The antenna arrays used in the measurements are described in Section 4.2. This section also discusses impedance and pattern measurement results.

4.1 HAAT Overview

The Handheld Antenna Array Testbed operates at 2.05 GHz. A system-level diagram of the HAAT is shown in Fig 4.1.1. The HAAT components include two transmitters, a four-

channel receiver with digital data recorders, and data processing software to evaluate diversity combining and adaptive beamforming performance. Arrays can be mounted on a linear positioning system for measurements at pedestrian speeds or can be mounted on a vehicle rooftop for measurements at vehicular speeds. Continuous wave (CW) tone signals are transmitted from portable, battery powered transmitters. The signals received at the four branches of an array are down converted to an audio IF using a four-channel receiver, which is also portable. The digitized IF signals are recorded using digital audio tapes (DAT) in stereo mode. The data are processed and analyzed in non-real time to allow comparison of different combining techniques and different beamforming algorithms.

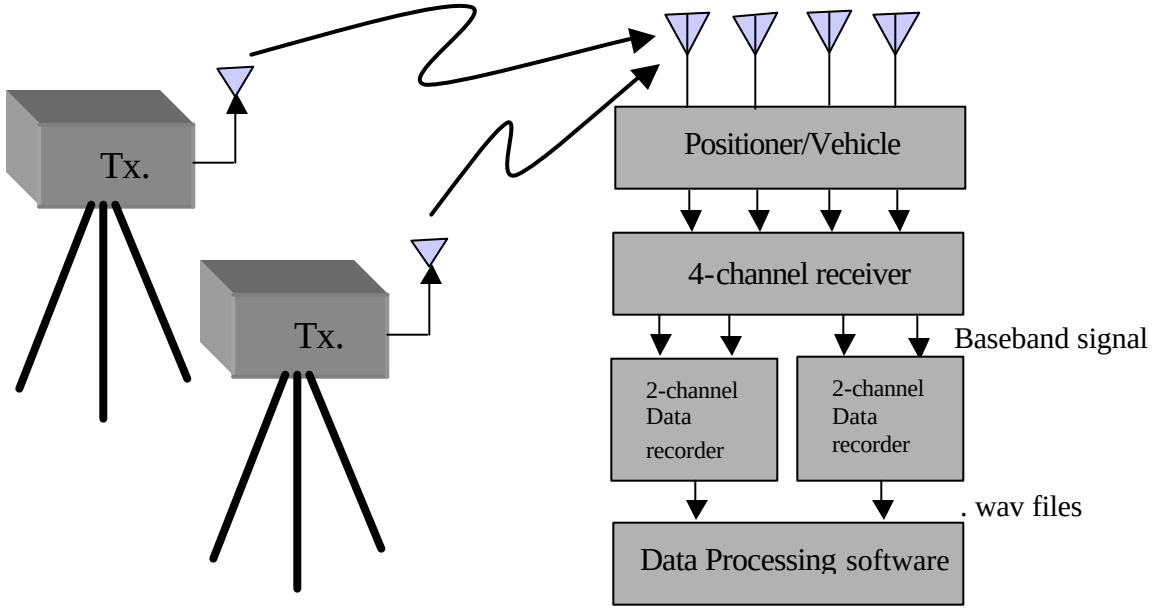

Figure 4.1.1 System level block diagram of HAAT system

Diversity measurements can be undertaken using a single transmitter, and interference rejection measurements can be performed by activating the second transmitter that is offset in frequency by 1 kHz. Investigations at pedestrian speeds are taken using a linear positioner run by a stepper motor. However, to investigate the performance at vehicular speeds, measurements can be taken by mounting the arrays on a ground plane suspended above the vehicle rooftop.

The HAAT data processing system is used to analyze the collected data offline [Car00]. The data processing system consists of a data recorder interfaced to a computer and Matlab files that process the measured data to extract statistical information. This in turn is used to determine the performance of different combining techniques and beamforming algorithms for each antenna array configuration.

4.1.1. HAAT Hardware

Each of the two HAAT transmitters transmit a 2.05 GHz continuous wave (CW) signal with a transmit power of approximately 500 mW (27 dBm). The two transmit frequencies are offset by 1 kHz to differentiate them at the receiver. For diversity measurements a single transmitter was used while for interference rejection measurements two interfering transmitters were used. For spatial diversity measurements the transmitters employed vertically oriented half-wave dipole antennas. The battery-powered transmitter is mounted on a tripod giving it an approximate height of 1.5 meters and it is portable. Using a bandwidth of 100 Hz in the data processing software, a noise floor of approximately –122 dBm is achieved [Car00]. For the worst case fading, the HAAT system offers a range of about 50 meters in obstructed non-line-of-sight channel.

To investigate the performance at pedestrian speeds, controlled measurements were taken using a linear positioner, run by a stepper motor. The linear positioner, shown in picture Fig 4.1.2, has a fiberglass structure and is approximately 3m long. The linear positioner is portable and is mounted on a tripod. The drive motor moves the four-element antenna and the four-channel receiver assembly along the stationary track at a speed of 0.115 m/sec and is controlled by a control circuit that provides pulses for synchronization of the digital audiotape recorders.

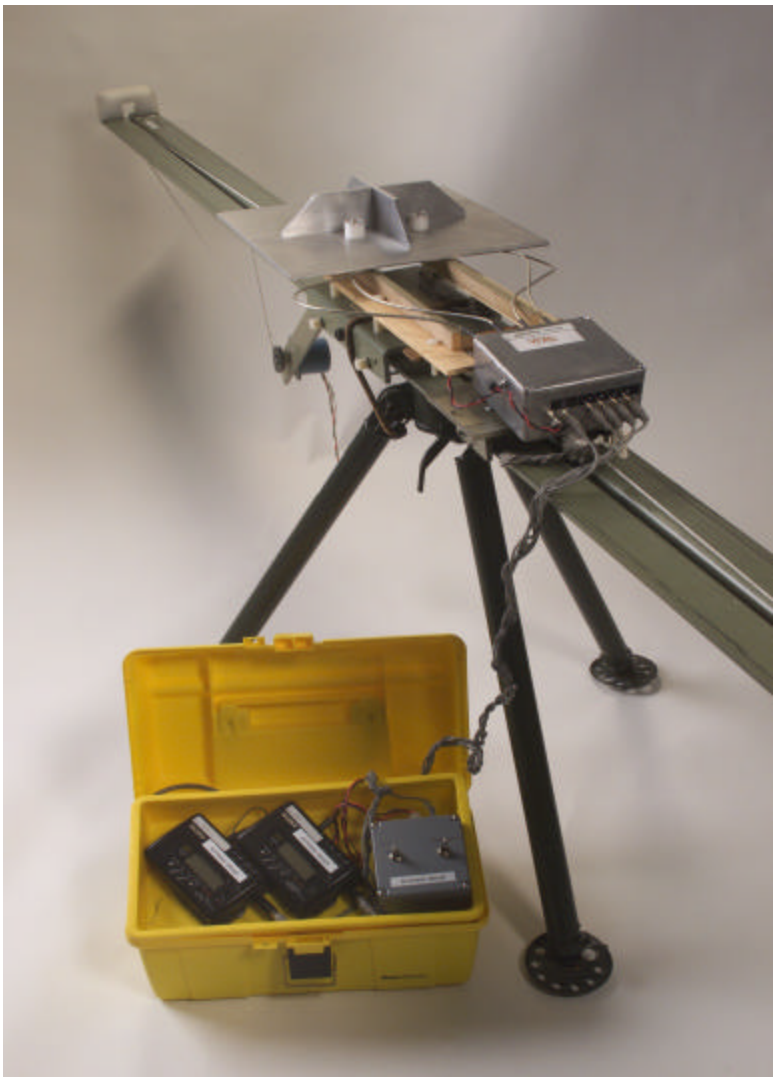

Figure 4.1.2 HAAT linear positioner with four-channel receiver and DAT recorders.

Diversity combining and adaptive beamforming measurements were conducted at vehicular speeds with the arrays mounted on a ground plane suspended above a vehicle rooftop as shown in Fig. 4.1.3. Two sheets of metal formed a false rooftop that was used to mount arrays in the slot between them. Four coaxial cables connect each of the four array elements to the four-channel receiver.

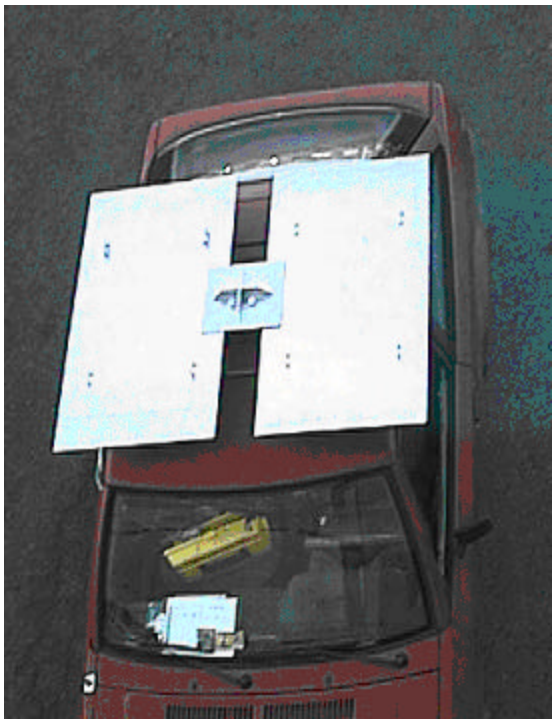

Figure 4.1.3 Vehicle mount for measurements at vehicular speeds

The HAAT four-channel receiving unit down converts the received signal from 2.05 GHz to audio frequencies using an internal local oscillator. The down converted signal with envelope variation information is recorded on Digital Audio Tape (DAT) cassettes. For each channel, a different antenna element is connected directly to a mixer and the received RF signal at 2.05 GHz is mixed down directly to baseband as shown in Fig 4.1.4. Data recording is performed in stereo mode to record two channels on a single DAT cassette. The data is sampled at 32 kHz and is recorded with a resolution of 16 bits/sample.

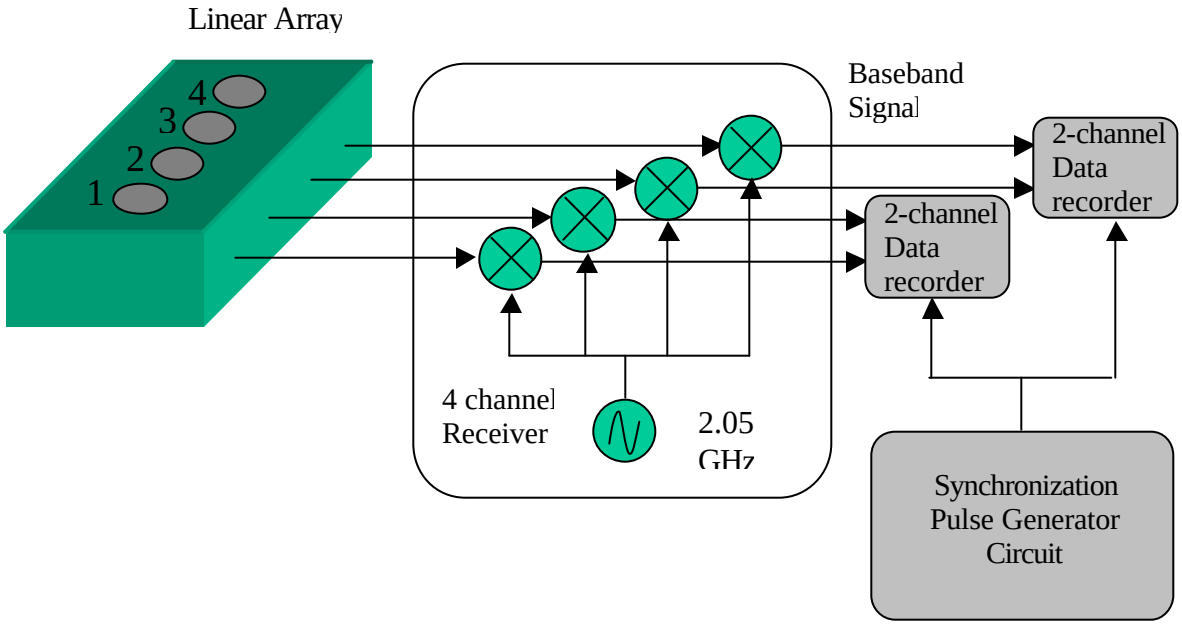

Figure 4.1.4 Four-channel receiver with DAT recorder and synchronization circuit of the HAAT system.

Synchronization pulses are inserted in the receiver baseband output at the beginning and end of each measurement. The pulses have two purposes. First, they mark the beginning and end of a measurement. Second, the pulses allow synchronization of data collected with two different DAT recorders, where each DAT records two of the four channels of the receiver.

Data processing is performed at any convenient time after the real-time data collection session. Each of the two DAT cassettes carrying data from four channels is played back using a Sony DTC – 700 DAT player. A Digital Audio Laboratories Digital Only CardD^{TM} interfaces the DAT player to a PC. The four received signals are phase referenced to each other so the actual array beamforming occurs in the non real time.

4.1.2. HAAT Diversity Combining Software

Offline processing of the measured data allows use of different techniques and algorithms. The measured data is logged so that in the future a new diversity combining technique or beamforming algorithm can be employed and compared to the existing ones.

The raw data from each of the four receiver channels, collected in DAT recorders, is stored on a PC using the Sound Forge XP 4.0 software. The Sony DTC – 700 DAT player plays back one DAT record at a time. Sound Forge XP 4.0 software captures the data played back in stereo mode by the DAT player using the CardD^{TM} interface as two-channel (stereo) audio (.wav) file. Data is stored in Microsoft .wav file format, using a sampling rate of 32 KHz with 16 bits per sample.

Diversity combining software consists of a Matlab program 'divproc4' that reads the .wav file and processes the data to calculate the mean branch powers, normalized branch envelopes, and envelope correlations. These statistics of the measured data are stored in '.div' processed data file as shown in Fig 4.1.5. Another Matlab program 'divdisplay4' reads the data from the '.div' file and calculates the mean absolute branch power imbalance, level crossing rates, and the diversity gain for maximal ratio and switched diversity techniques as shown in Fig 4.1.6. Diversity gain was calculated from the envelopes of the combined signal and the branch signals. The relative power information is preserved by normalizing the received signal envelope to some reference, which is chosen as the mean of the strongest signal.

To retain the power balance information, the envelope of each of the four channels is normalized by the mean of the strongest branch. Diversity gain is determined as described in Section 2.4. The CDF of signal envelope of each branch and the combined signal is normalized by the time average of the strongest branch.

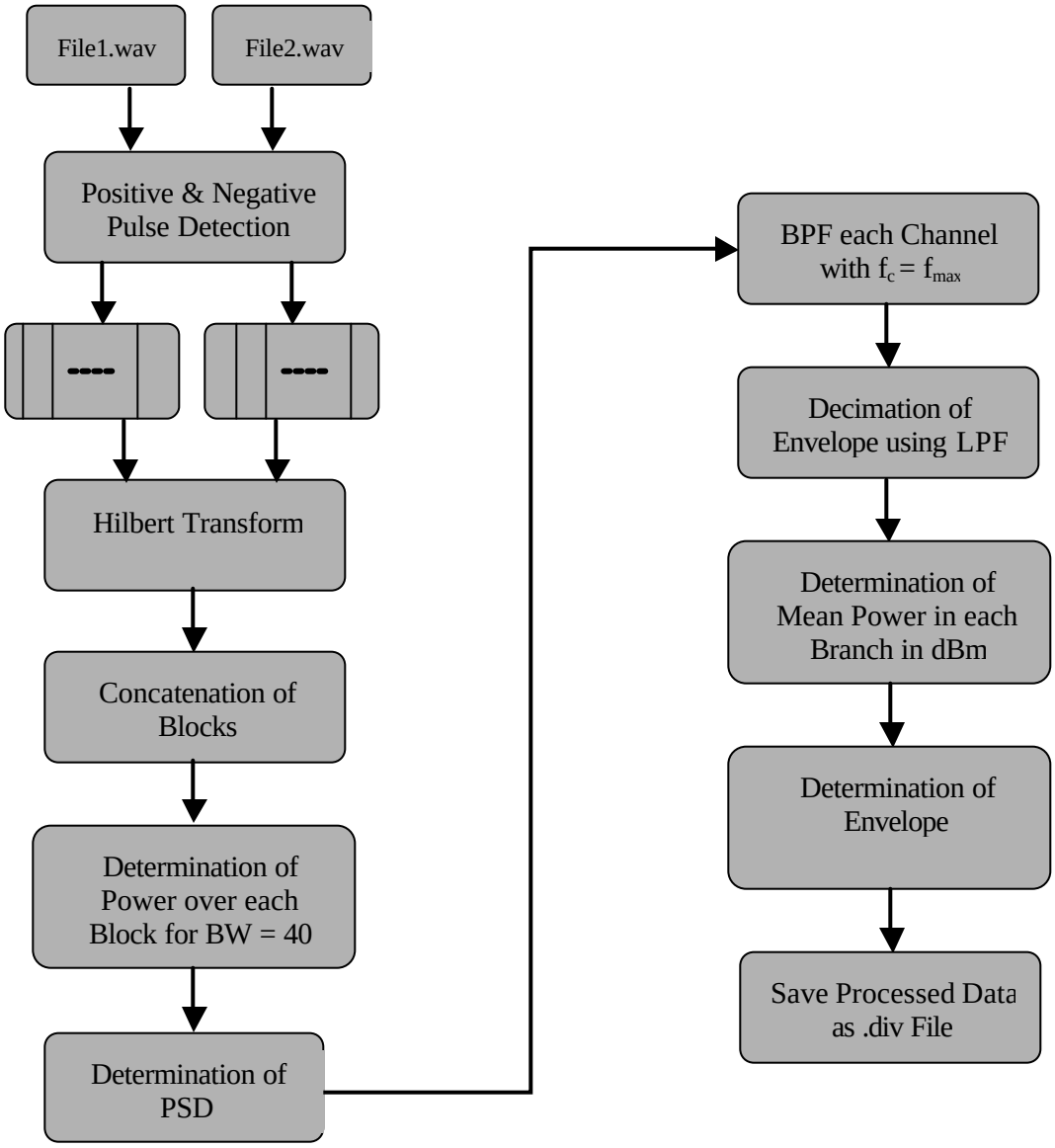

Figure 4.1.5 'divproc4.m' Software Overview for use in data collection and diversity combining with the HAAT system
(Data divided into blocks of 1 sec duration equivalent to 32000 samples)

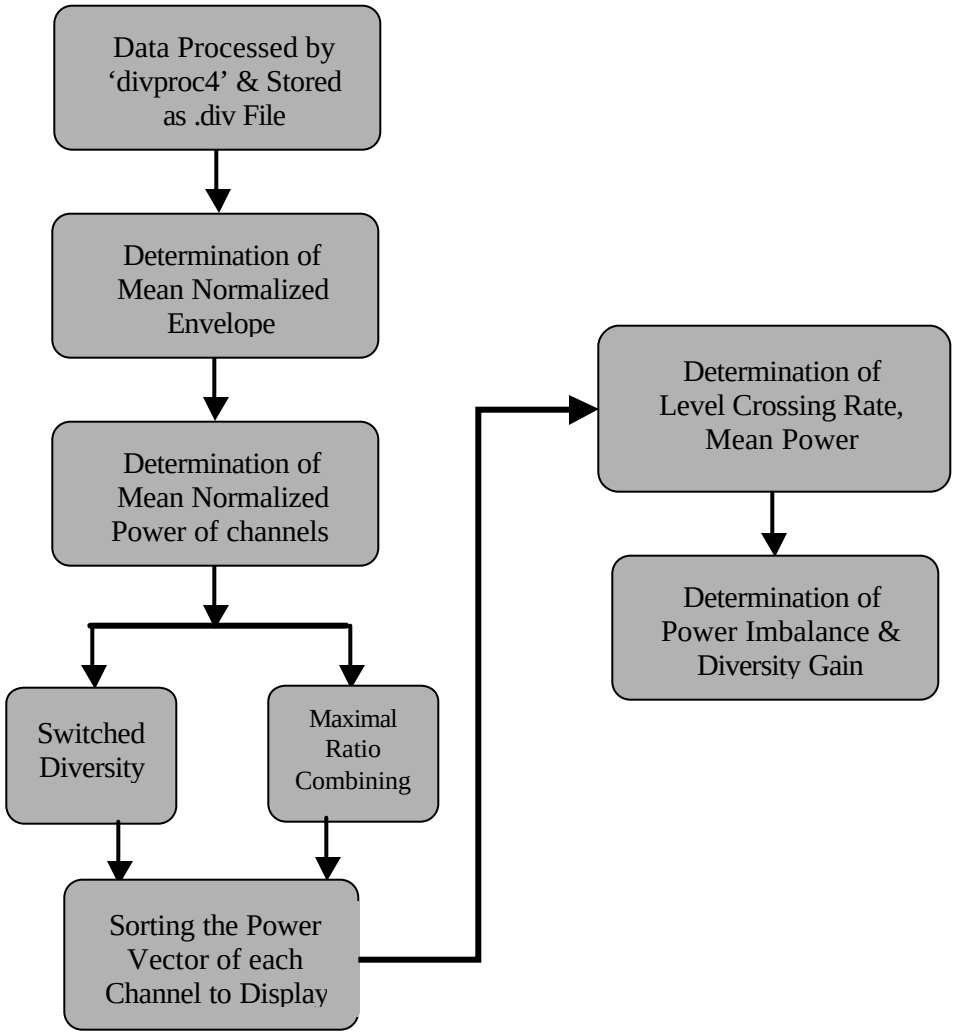

Figure 4.1.6 'divdisplay4.m' Software Overview, used to extract statistical information of level crossing rate, power imbalance and diversity gain at 1% outage probability from the '.div' file created by 'divproc4' software.

4.1.3 HAAT Beamforming Software

Interference rejection measurement data were processed using a Multi Target Least Squares Constant Modulus Algorithm (MT-LSCMA). This algorithm is a variation of more general LSCMA, which is an efficient blind adaptive beamforming algorithm. Blind beamforming algorithms do not require any prior information on the reference signal to update the weights. The reference signal in this case is chosen as $d(t) = \frac{r(t)}{|r(t)|}$, exploiting the constant modulus property of the received signal. As explained in Section 3.4.3, MT-LSCMA is used to generate two sets of weights for each of the two transmitted signals. Each set of weights selects one of the two transmitted signals, rejecting the other.

The measured signal data from four channels is stored in two .wav files. Adaptive beamforming software consists of a Matlab program 'cmaproc4' that reads the .wav file and processes the data to calculate the mean signal-to-noise ratio (SNR) and signal-to-interference-plus-noise ratio (SINR) before and after beamforming. These statistics of the measured data are stored in '.cma' processed data file as shown in Fig 4.1.7. The parameter block length determines the update interval for the beamforming weights. Another Matlab program 'cmadisplay4' reads the data from the '. cma' file and calculates the mean absolute branch power imbalance, level crossing rates, and the diversity gain for maximal ratio and switched diversity techniques as shown in Fig 4.1.8. The relative power information is preserved by normalizing the received signal envelope to some reference, which is chosen as the mean of the strongest signal.

In the four-channel HAAT system, each of the two mutually orthogonal weight vectors, which contain weights for every individual antenna array element is updated independently. The weights are calculated by direct matrix inversion of the received signal covariance matrix R_{rr}

$$w_i = R_{rr}^{-1} C_{rd} \tag{4.1}$$

where $R_{rr} = r(t)\, r(t)^H$ is the received signal covariance matrix and $C_{rd} = r(t)\, d(t)^*$ is the cross correlation between the received signal and the desired reference signal. The Matlab program cmaproc4.m divides the received signal samples into blocks of 320. LS-CMA beamforming

algorithm is operated on these blocks to update the complex weights iteratively. The number of iterations is chosen to be two, after which no significant improvement was observed. To optimize each of the two signals transmitted, two mutually orthogonal sets of weights are calculated.

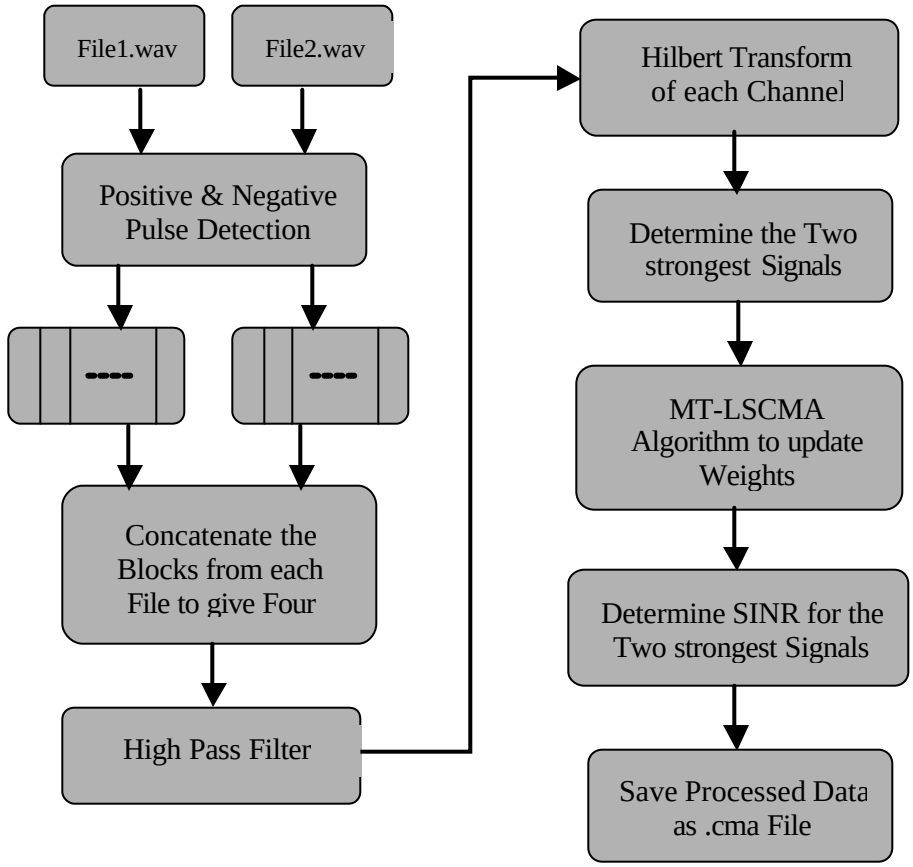

Figure 4.1.7 'cmaproc4.m' Software Overview, used for data collection from the audio (.wav) files and for adaptive beamforming using MT-LSCMA blind algorithm

Another Matlab program cmadisplay4.m processes the .cma file generated by the cmaproc4.m to calculate SNR and SINR before and after beamforming. A bandwidth of 100 Hz is chosen centered on the two down converted signals at intermediate frequency of 7 kHz to determine the noise power as well as the signal power. The SNR thus calculated is used to estimate an upper limit to the achievable SINR after beamforming.

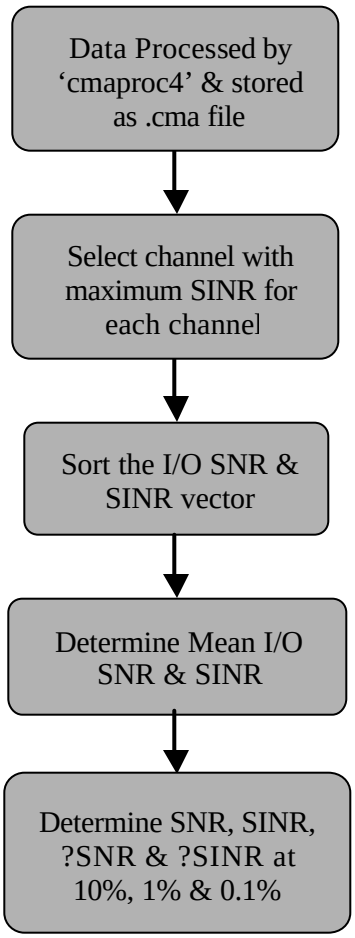

Figure 4.1.8 'cmadisplay4.m' Software Overview, used for reading processed data from .cma file and determining mean signal-to-interference-plus-noise ratio and SINR improvement at 10%, 1% and 0.1% CDF

4.2 Antennas

Antennas play a significant role in wireless communications by extending range, increasing the quality of service, power efficiency, and most importantly, capacity. Antenna arrays used for diversity combining and adaptive beamforming at portable and mobile wireless terminals must be compact and low profile. Low-profile four-element arrays for portable and vehicular terminals are investigated. The four-element antenna arrays used for diversity combining and interference rejection measurements are summarized in Table 4.1. Arrays play an important role in improving system reliability, as mobile radio systems employ higher frequencies, it is becoming possible to use compact antenna arrays at mobile and handheld terminals for diversity combining and adaptive beam forming.

Table 4.1
Summary of four-element antenna arrays used in the diversity and beamforming experiments

NUMBER	NAME	GEOMETRY AND DESCRIPTION
Array 1	Linear array of monopole elements	Linear configuration of four capacitive loaded monopole elements spaced apart by ?/2 at 2.05 GHz, fed against a ground plane, shown in Fig 4.2.1 (a) and 4.2.3 (a)
Array 2	Square array of monopole elements	Four monopoles fed against a ground plane with adjacent element spacing of ?/2, shown in 4.2.1 (b) and Fig. 4.2.3 (b)
Array 3	Sectored square array of monopole elements backed by corner reflectors	Four monopole elements in square configuration are backed by corner reflectors. Adjacent element separation is ?/2 at 2.05 GHz, shown in Fig. 4.2.1 (c) and 4.2.3 (d)
Array 4	Four wire antenna on high impedance plane	Half-wavelength wires mounted close to high impedance plane with electromagnetic band-gap structure in square configuration, shown in Fig. 4.2.2 (a) and 4.2.3 (d)
Array 5	Four wire linear array	Half wavelength wires mounted on high impedance planes are arranged in linear configuration with variable spacing, shown in Fig. 4.2.2 (b)
Array 6	Square array of co-axial dipoles	Dipoles elements are mounted in square configuration with adjacent element separation of 0.4?, shown in Fig. 4.2.3 (e)

Linear, square and sectored square array of low-profile broadband monopole elements, summarized in Table 4.1 as array 1, 2 and 3, respectively, are designed by Foltz, et al [Fol98]. These arrays are shown in Fig. 4.2.1 (a), (b) and (c) respectively. Fig. 4.2.1 (c) shows a square sectored array of four monopole elements that are backed by corner reflectors to generate directional patterns.

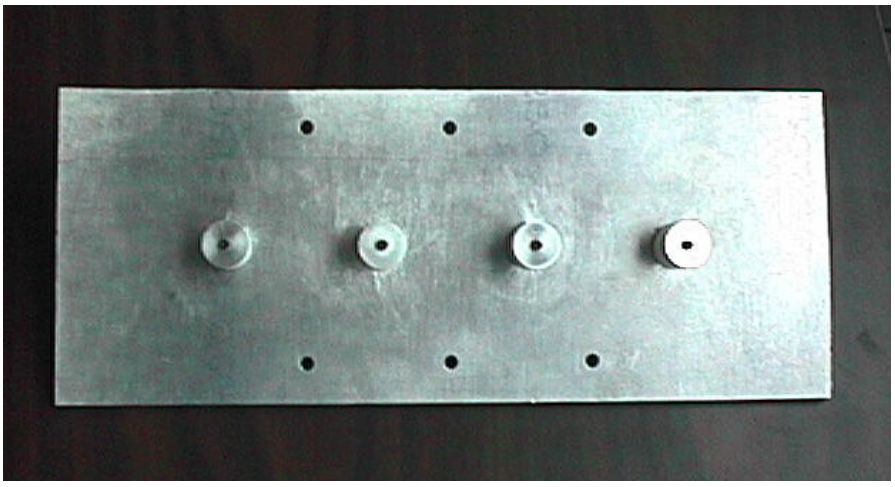

(a) Linear array of four-monopole elements (Array 1 as shown in Table 4.1)

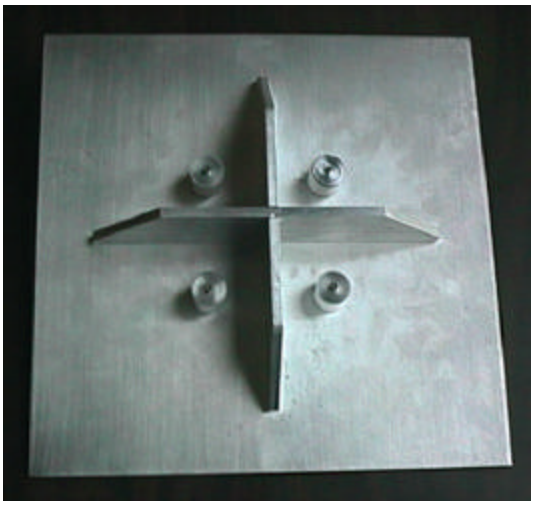

(b) Square array of monopoles (Array 2) (c) Sectored square (Array 3)

Figure 4.2.1 Linear, square and sectored square arrays [Fol98]

Antenna arrays with low-profile wire antenna elements mounted over a high-impedance electromagnetic band gap structure were also used to investigate their performance in adaptive beamforming and diversity combining. Fig. 4.2.2 shows wire antennas mounted on high impedance surface with linear and square configuration, similar to the one described in [Sie00]. These arrays are described in detail in Sections 4.2.1 and 4.2.2.

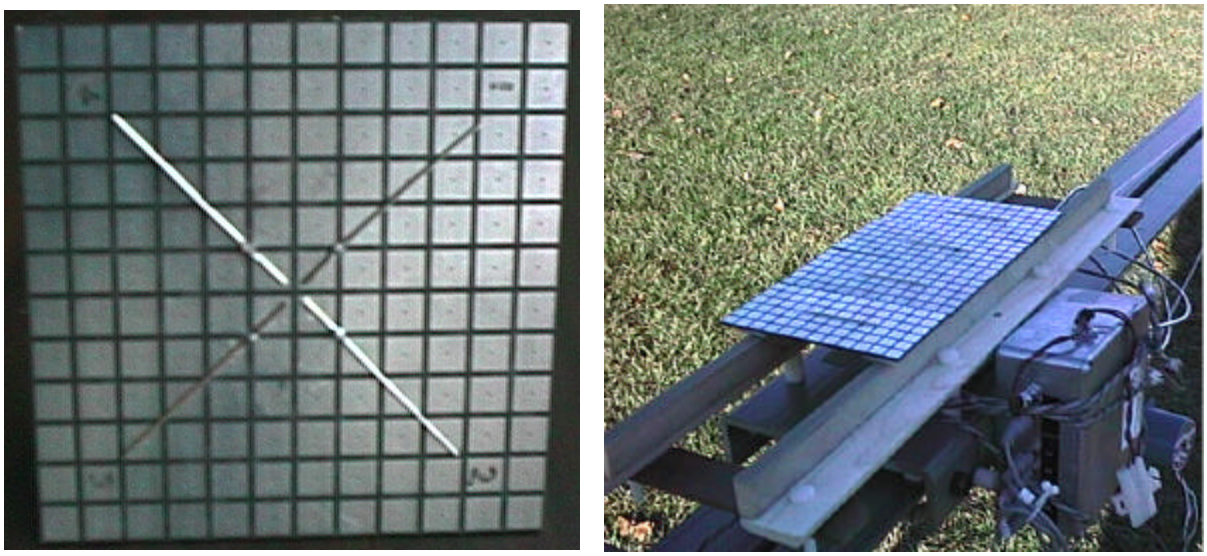

(a) Square Configuration (Array 4) (b) Linear configuration (Array 5)

Figure 4.2.2 Low profile wire antenna mounted over a high impedance band gap structure [Sie00] mounted on HAAT linear positioner.

4.2.1 Antenna Arrays

Antenna arrays investigated for diversity combining and adaptive beamforming are described in Table 4.1. Fig 4.2.3 (a) shows a linear array (Array 1 in Table 4.1) of low-profile broadband omni directional monopoles separated by a distance of $\lambda/2$ at 2.05 GHz. This array of electrically small monopole elements was designed at the University of Texas-Pan American, (Edinburg) using a top loading capacitive disk. Fig 4.2.3 (b) and Fig 4.2.3 (c), respectively, show a square (Array 2) and a square sectored array (Array 3) of four monopole elements that is backed by corner reflectors. These array configurations were tested at the Virginia Tech Antenna Group facilities.

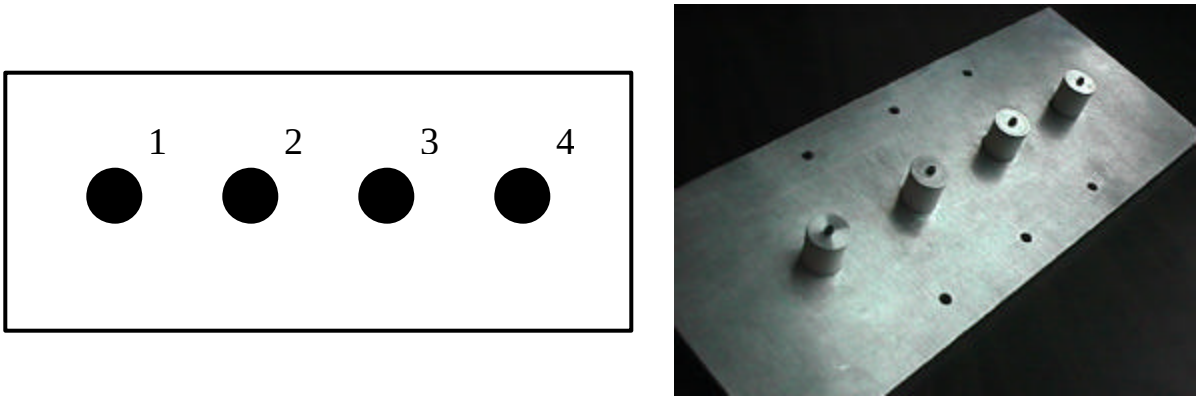

(a) Linear array of broadband monopoles (Array 1)

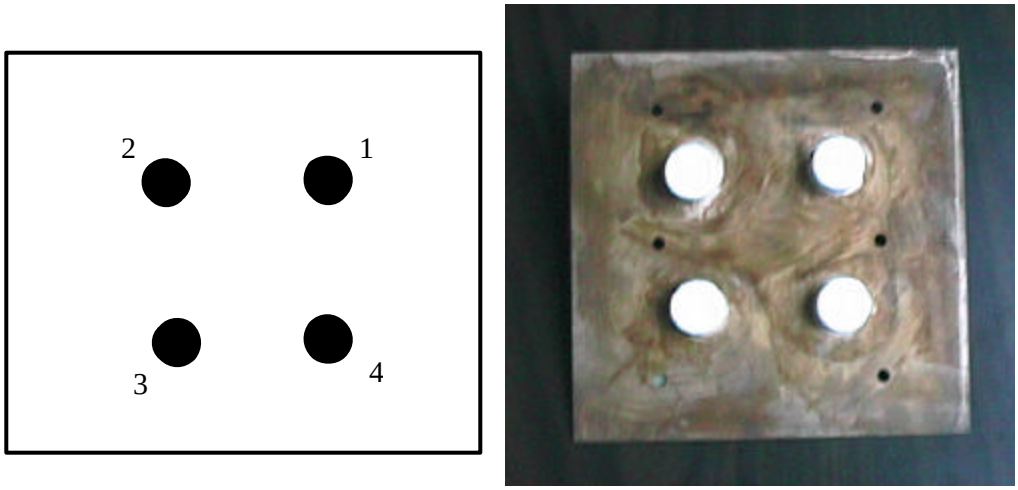

(b) Square array of low profile broadband monopoles (Array 2)

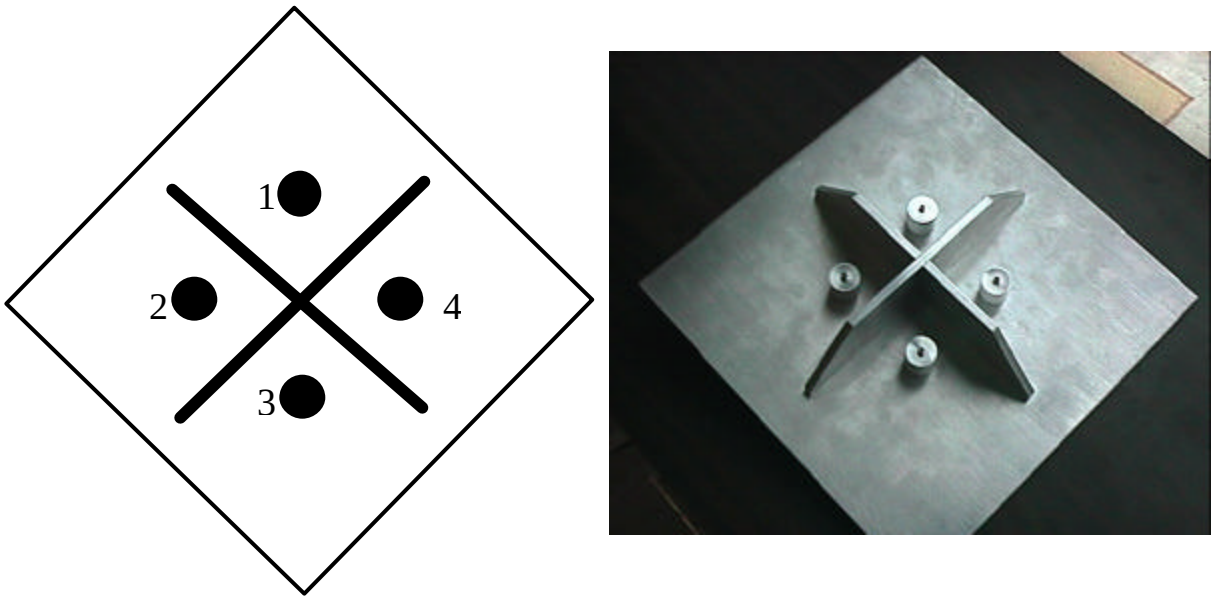

(c) Square Sectored Array with monopoles backed by corner reflectors (Array 3)

Figure 4.2.3 Array configurations, designed by Foltz et al. [Fol98] and used in diversity combining and adaptive beamforming experiments

The four-wire antenna with elements mounted on a high impedance surface (Arrays 4 in Table 4.1) was designed at HRL Laboratories, Malibu, CA for vehicular applications. This low-profile antenna, when fed through a hybrid network, offers directional beams and is shown in Fig. 4.2.3 (d). Unlike other arrays, this antenna array when mounted on a metallic vehicle rooftop does not support surface currents. The high impedance ground plane suppresses surface currents and provides a smooth radiation pattern [Sie99]. The electromagnetic waves are reflected off the high impedance surface without phase reversal and so it allows antennas to be constructed close to the high impedance surface.

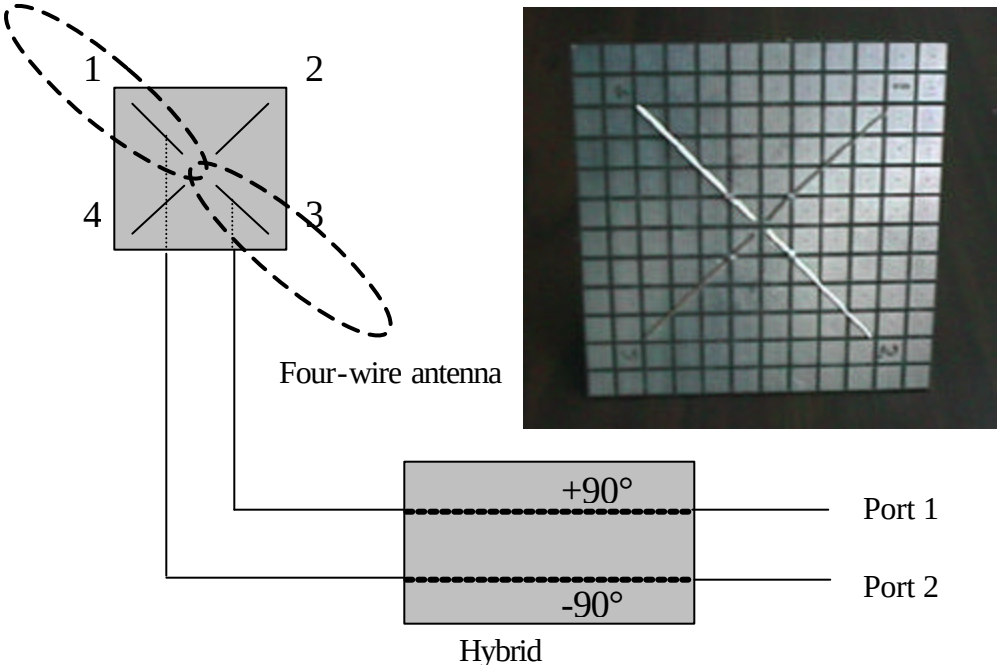

Figure 4.2.3 (d) Four-wire antenna array with the +90°/-90° hybrid (Array 4)

A four element square array of half wave dipole elements (Array 6) was used to provide a baseline for evaluating the diversity and interference rejection performance of different arrays. The half-wavelength dipole elements are co-axial dipoles as shown in Fig. 4.2.3 (e)

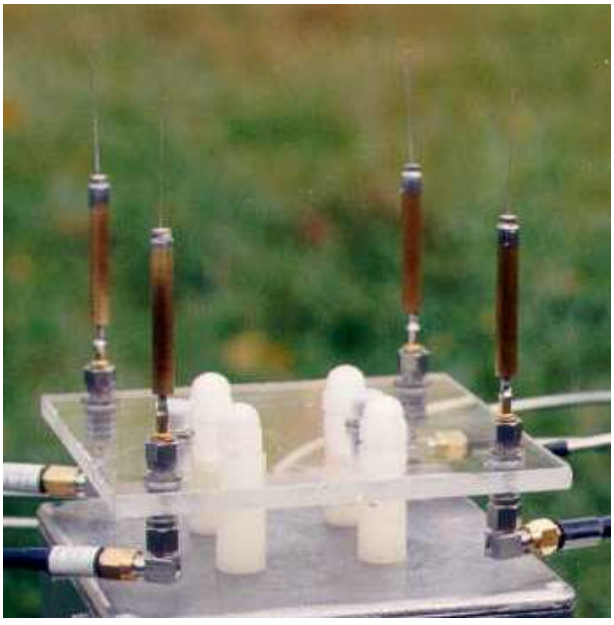

Figure 4.2.3 (e) Four-element square array of coaxial dipoles (Array 6)

4.2.2 Impedance Measurements

The antenna terminal reflection, specified by the voltage reflection coefficient Γ, is specified by the voltage standing wave ratio (VSWR), which is the ratio of the maximum voltage to the minimum voltage on the line.

$$\Gamma = (VSWR - 1) / (VSWR + 1) \tag{4.2}$$

The VSWR measurements were carried out using an HP 8720 Network Analyzer. The VSWR values were recorded at the operating frequency of 2.05 GHz. The first set of measurements was carried out with the linear array of broadband monopoles (Array 1 in Table 4.1). VSWR measurements were performed for end element '1' and center element '2' and were recorded as low as 1.31 and 1.32, respectively. The coupling between various elements was recorded by taking S_{21} on the network analyzer with port 1 of the network analyzer connected to the element '1' of the linear array and port 2 was connected first to the element '2' and then to the element '3' and finally to element '4'. S-parameters between adjacent elements '1' and '2' recorded a coupling of $| S_{12} |$ = –15.2 dB, while measurement between distant elements were recorded as:

$| S_{31} |$ = -26.5 dB

$| S_{41} |$ = -30.0 dB

$| S_{23} |$ = -16.0 dB

$| S_{34} |$ = -15.4 dB

The coupling results for linear array are summarized in Fig. 4.2.4. The values indicated are voltage standing-wave ratio (VSWR).

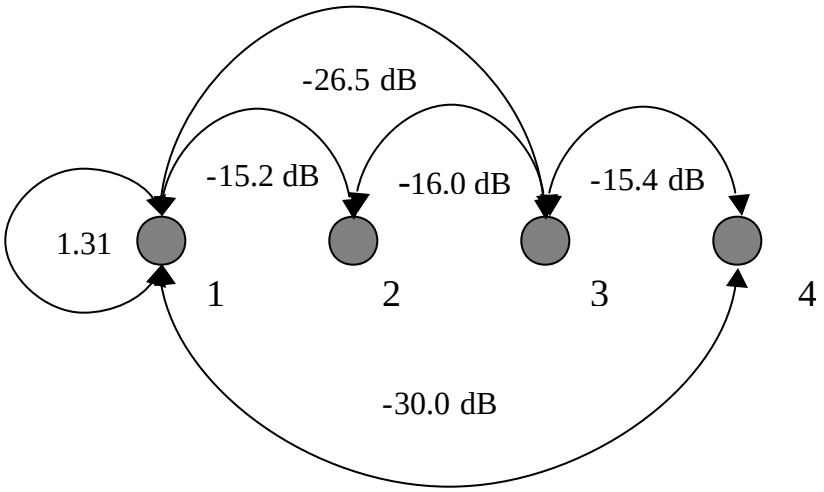

Figure 4.2.4 Measured coupling between elements of the linear array with monopole elements (Array 1 in Table 4.1) for mutual coupling

Note that the couplings between adjacent array elements ($| S_{12} |$, $| S_{23} |$, $| S_{34} |$) are nearly equal for all adjacent elements pairs. Moreover, as the separation increases the isolation improves. Measurements for mutual coupling between the array elements were carried out by terminating the other array elements in a 50 O impedance

The second set of measurements involved recording VSWR readings from the network analyzer for the square array of monopole elements (Array 2) shown in Fig 4.2.5. The measured VSWR for element '1' was 1.72. From the symmetry of square array we can assume same VSWR for the other array elements. Isolation measurements were taken to determine mutual coupling between the elements in the square array. The measured mutual coupling between adjacent elements '1' and '2' and between diagonally opposite elements '1' and '3' with other terminals terminated in a 50-ohm impedance are:

$| S_{21} |$ = -12.2 dB

$| S_{31} |$ = -19.4 dB

The coupling results for the square array with monopole elements are summarized in Fig. 4.2.5. The values indicated are voltage standing-wave ratio (VSWR).

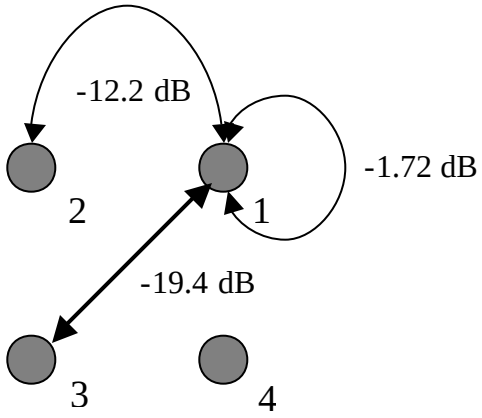

Figure 4.2.5 Measured coupling of square array of four monopole elements (Array 2) for mutual coupling

The third set of measurements involved recording VSWR readings from the network analyzer for the sectored square array of four monopole elements (Array 3). Similar to the square array, the VSWR for element '1', was measured as 1.04. From the symmetry of sectored square array, just as with the square array we can assume same VSWR for the other array elements. Isolation measurements were taken to determine mutual coupling between the elements in the sectored square array. The measured value of mutual coupling between adjacent elements '1' and '2' and between diagonally opposite elements '1' and '3' are:

$| S_{21} |$ = -22.6 dB

$| S_{31} |$ = -38.5 dB

The coupling results for the sectored square array with monopole elements (Array 3) are summarized in Fig. 4.2.6. The values indicated are voltage standing-wave ratio (VSWR).

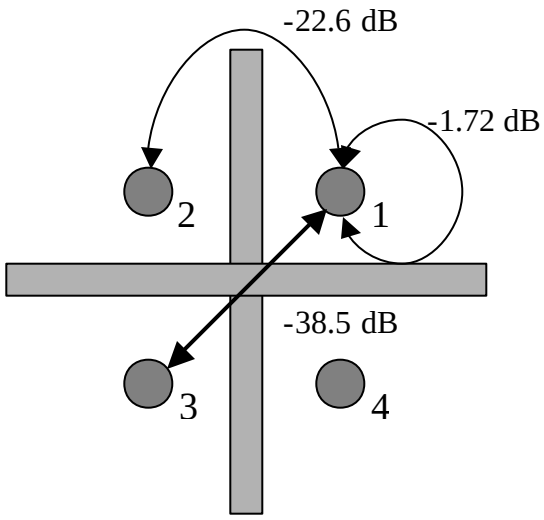

Figure 4.2.6 Measured coupling of sectored square array with monopole elements (Array 3) for mutual coupling

The final set of VSWR measurements were recorded with the terminals of the four-wire antenna with high impedance ground plane, connected to the hybrids (Array 4). Elements '1' and '3' of the antenna were connected to the hybrid, which introduces 90º-phase shift, while elements '2' and '4' are terminated in 50-ohm impedance.

The VSWR for the 'port 1' shown in Fig 4.2.3 (d) was recorded as 1.52, with other channels terminated in 50-ohm impedance. The same measurement was repeated for all four elements of the four-wire antenna. The measured VSWR values for channels 2, 3 and 4 were 1.59, 1.66 and 1.58, respectively.

A second set of measurements was performed on the four-wire antenna (Array 4) with the hybrids removed. The VSWR for 'port 1', with other terminals terminated in 50 ohm impedance was recorded as 2.6. Measurement was repeated for all four elements of the four-wire antenna. The measured VSWR for channels 2, 3 and 4 were 2.8, 3.0 and 1.94, respectively. These results indicate a slight increase in the VSWR value in the absence of hybrid.

The four-wire antenna (Array 4) consists of four wires close to the high impedance ground plane. In practice, the antenna elements may get shorted to the high impedance ground plane. To account for such a case the VSWR measurements were recorded for the just one

element (‘1’) shorted at the tip while the others were kept as they were. This caused the VSWR to rise sharply to 4.4. However, when the same element was shorted all along its length then its VSWR value remained about 1.43 which, interestingly, is lower than then what the recorded in the second set of measurements with the elements not touching the high impedance plane. One more measurement was carried out to account for all four elements shorted to the plane, in which case the VSWR value for element ‘1’ was recorded as 1.78.

4.2.3. Pattern Measurements

The far field pattern measurements of the linear, square and sectored square arrays were carried out on the outdoor antenna range at Virginia Tech. A standard horn antenna was used as the transmitting antenna and the array elements were used as the receiving antennas. The azimuth antenna patterns were recorded with the test antenna rotated over a positioner. The pattern was measured using a co-polarized horn antenna as the source antenna.

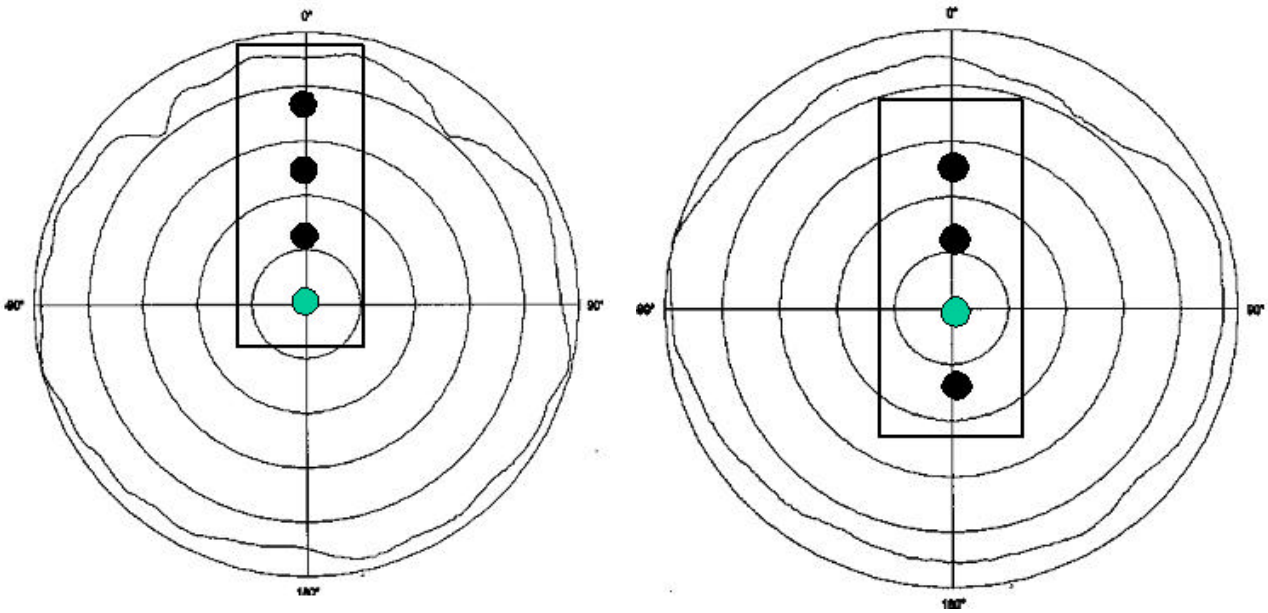

(a) end element (b) center element

Figure 4.2.7 Measured azimuth radiation pattern of an active element in the linear array (Array 1 in Table 4.1) shown in Fig. 4.2.2 (a). The scale is 10 dB/div.

The azimuth pattern for the end element of the linear array provided by the University of Texas Pan – Am (Array 1) is shown in Fig. 4.2.7 (a). The maximum gain corresponds to an

absolute signal with 9-10 dB nulls at approximately 45° from the broadside and this would explain its good performance in rejecting interference coming from 45° in azimuth. The maximum radiation is approximately broadside to the array. The pattern characteristics in Fig 4.2.7 (b) for an active center element are quite similar to the one obtained by exciting the end element of the linear array. However, the maximum gain in this case corresponds to a level of about –14.44 dB, which is 0.64 higher than the first case because of the element gain. Both patterns show similar null at 45° from broadside in azimuth.

The measured far field pattern in the horizontal plane for the four element square array (Array 2) is shown in Fig 4.2.8 (a). Only one element is excited and the other elements are terminated in 50 O load. The reference level that corresponds to maximum gain is about –17.48 dB, which is 3 dB lower than that of the linear array of monopoles (Array 1). The pattern is omni-directional pattern, with a pattern minimum about 6 dB below the maximum.

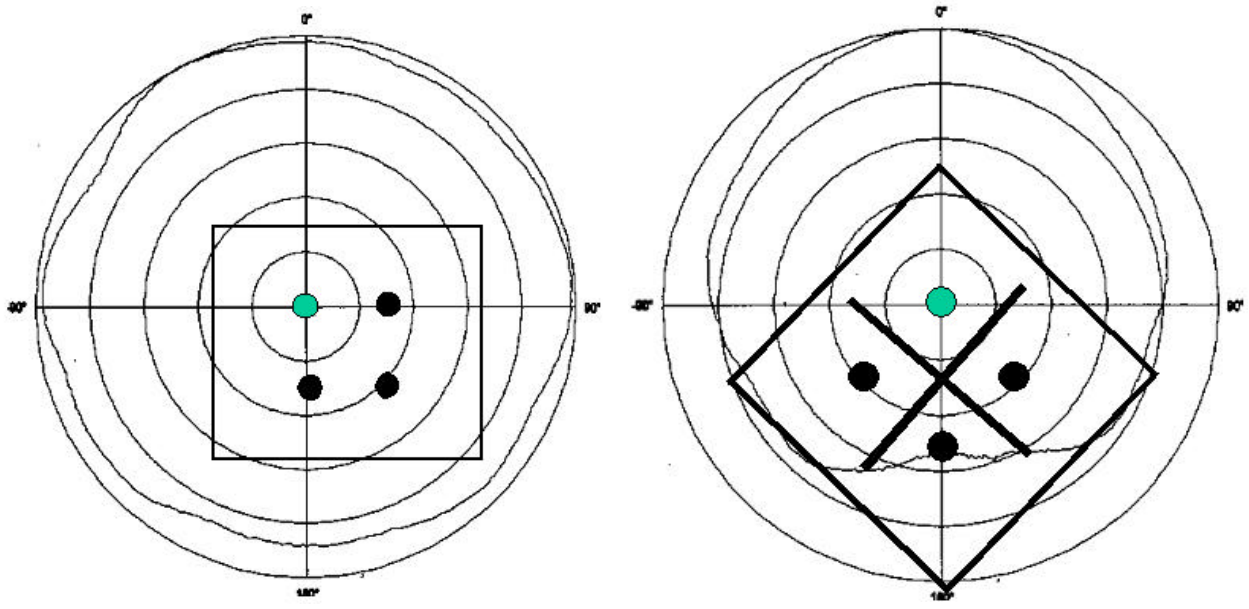

(a) Square Array (Array 2) (b) Sectored Square Array (Array 3)

Figure 4.2.8 Measured active element azimuth radiation pattern of the square and sectored square arrays of four monopole elements. The scale is 10 dB/div

The active element pattern of the sectored square array (Array 3) is shown in Fig. 4.2.8 (b). The sectored square array element has a gain that corresponds to a reference level of –10.73

dB. This is approximately 4 dB to 7 dB higher than the gains of the elements of the other two arrays. The sectored square array element also has a front-to-back ratio of over 20 dB.

The pattern measurements of the four-wire antenna with high impedance ground plane (Array 4) were carried out in the anechoic chamber built at Virginia Tech. Each pair of elements ('1' & '3' and '2' & '4') was fed through the hybrid, providing equal amplitude and 90° relative phase shift. The active element pattern with elements '1' and '3' through the hybrid is shown in Fig 4.2.9.

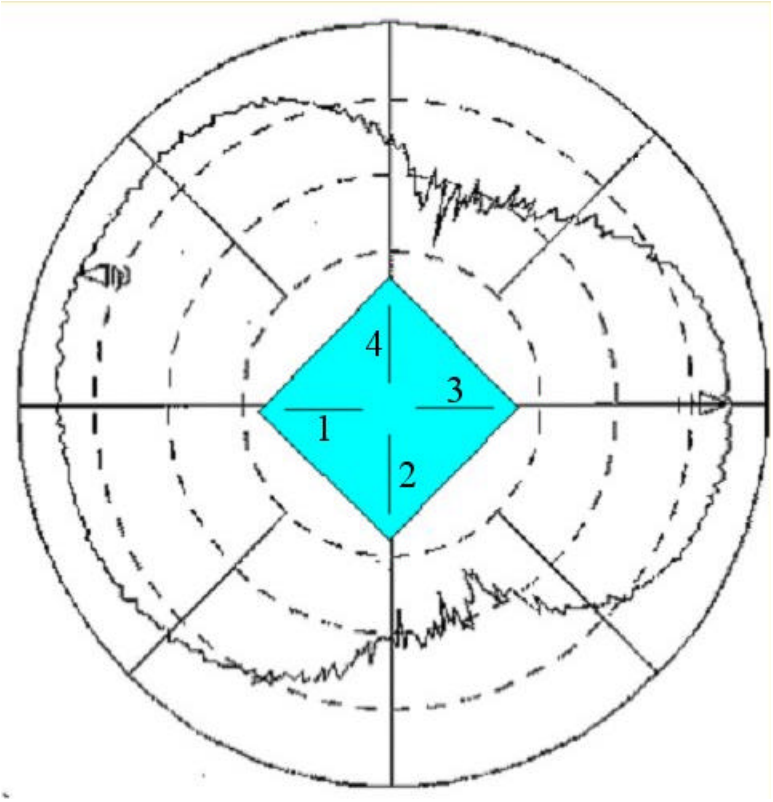

Figure 4.2.9 Measured azimuth radiation pattern of the four-wire antenna array (Array 4 in Table 4.1 and shown in Fig. 4.2.1) with elements '1' and '3' fed through a hybrid with 90° phase shift. The measurement indicates the directional pattern useful in interference rejection. Scale is 10 dB/div.

The marker in Fig. 4.2.9 shows the maximum pattern gain with elements '1' and '3' of the four-wire antenna fed with the hybrids and the corresponding unnormalized signal level is –54.3 dB. Under similar conditions at 2.05 GHz, the pattern gain of coaxial dipole was measured to be -49.4 dB. It shows that the four-wire antenna achieves about –4.9 dBd (as compared to

dipole) which is about –2.7 dBi. Observe that the marker '1' shown in the figure gives the back lobe gain and it is seen to be nearly equal to the main lobe at about –54.6 dB which is about –2.9 dBi.

References

[Car00] Dietrich Carl B. Jr., *"Adaptive Arrays and Diversity Antenna Configurations for Handheld Wireless Communications Terminals"*, Ph.D. Dissertation, Virginia Tech, 2000.

[Car01] Dietrich C. B. Jr., Dietze K., Nealy J. R., Stutzman W. L., *"Spatial, polarization, and pattern diversity for wireless handheld terminals"*, Antennas and Propagation, IEEE Transactions on, Volume: 49 Issue: 9, Sept.2001.

[Stu98] Stutzman W. L. and Thiele G. A., *Antenna Theory and Design*, Second Edition, Wiley.

[Sie99] Sievenpiper D., Broas R., and Yablonovitch E., *"Antennas on high-impedance ground plane"*, Microwave Symposium Digest, 1999 IEEE MTT-S International, Volume: 3,1999. Page(s): 1245 –1248.

[Sie00] Sievenpiper D., Hsu H. P., Schaffner J., Tangonan G., Garcia R., Ontiveros S., *'Low-profile, four-sector diversity antenna on high-impedance ground plane'*, Electronics Letters, Vol. 36 Issue: 16, Aug. 3, 2000.

[Fol98] Foltz H. D., McLean J. S., Crook G., *'Disk-loaded monopoles with parallel strip elements'*, Antennas and Propagation, IEEE Transactions on, Vol. 46 Issue: 12, Dec. 1998. Page(s): 1894-1896.

Chapter 5
Diversity Experiments

Diversity combining at the mobile terminal has been shown to improve reliability [Vau93]. Also, Dietrich [Die00] investigated mitigation of multipath fading using two-element and four-element handheld antenna arrays. This chapter reports on an investigation into the diversity performance of the four-element linear, square and sectored square arrays for mobile (vehicular speed) and portable (pedestrian speed) terminals.

The chapter begins with a brief discussion on the experiment objective. The urban and suburban, line-of-sight and obstructed channel environments are described in Section 5.1. Measurement results using a linear positioner as well as vehicle-mounted arrays are presented in Section 5.2. The performance of the antenna arrays in diversity combining was evaluated in urban and suburban environments; with line-of-sight and non line-of-sight scenarios. The chapter concludes with a brief summary of measurement results.

Data collected from diversity experiments were processed using two basic diversity-combining techniques. The first technique is *switched diversity* in which the branch having the highest instantaneous power level is selected until its power drops below an acceptable level, after which the next branch is selected. The second technique is *maximal ratio combining*, which involves weighting the branch signal outputs proportional to their signal-to-noise ratio (SNR) or simply the envelope power (under similar noise environment) before combining. This is the optimum combining method because it maximizes the SNR of the combined signal.

Diversity combining performance is quantified by the *diversity gain*, which is the improvement in the signal strength at a given level of reliability (say 99%) compared to the case when no diversity combining is employed, as explained in Section 2.3. The four-wire antenna array with elements mounted on a high impedance surface showed improved signal reception through mitigation of fading due to multipath. Measured results showed a diversity gain of about 8 dB to 10 dB with maximal ratio combining at 99% reliability with envelope correlation of 0.3. This permits to an 8 dB to 10 dB decrease in the required base station transmit power on the downlink to overcome multipath fading in operational systems.

Experiments showed that the linear array of Fig. 4.2.3 (a) performed about 2.0 dB to 3.8 dB better than the square array with monopole elements of Fig. 4.2.3 (b). The sectored square array of monopole elements backed by corner reflectors of Fig. 4.2.3 (c) offered high diversity gain because of its high active element gain. Also, with the increasing separation between the adjacent wire elements in the linear configuration of wire elements mounted on high impedance band gap structure (Array 5 in Table 4.1), shown in Fig. 4.2.2 (b), diversity gain was observed to increase. For arrays mounted on a vehicle rooftop, diversity gain of 11 dB to 14 dB was observed.

5.1 Experiment Objectives and Scenario

Extensive diversity measurements were performed in urban and suburban environments for both line-of-sight (LOS) and obstructed multipath channels. The objective was to analyze and compare the performance of the array configurations in different multipath environments. To meet this objective, controlled experiments were conducted using the HAAT system shown in Fig. 4.1.1. The six arrays explained in Table 4.1 were used in the measurement campaign. The arrays used were linear, square and square sectorized arrays of low-profile broadband omni-directional monopoles (Arrays 1, 2 & 3 respectively). Since a four-wire antenna array and a linear array configuration of single wire elements with variable spacings mounted on a high impedance surface are low profile antenna arrays, these were also used (Array 4),. A half-wavelength spaced square array of four half-wave dipole elements (Array 6), shown in Fig. 4.2.3 (e) was used to provide a baseline for evaluating and comparing diversity performance of arrays

given in Table 4.1. The effect of omni-directional active element azimuth radiation pattern shown in Fig. 4.2.7 and Fig. 4.2.8 (a) on diversity combining are analyzed. The effect of the directional radiation pattern of the sectored square array shown in Fig. 4.2.8 (b) and of the four-wire antenna over high impedance surface using the hybrids, shown in Fig. 4.2.9, over diversity combining is also evaluated. Results of diversity combining for vehicular measurements with the arrays mounted on a ground plane suspended above a vehicle rooftop are also reported.

The range arrival of the incoming signal directions at the receiver determines the decorrelation distance of the array elements [Lee82][Nor01]. Since the mobile usually moves in an environment surrounded by scatterers, the direction of arrival of the signals is uniformly distributed in the azimuth plane. Decorrelation distance is the separation between sufficiently uncorrelated array elements and is small for large angle spread such as that seen at the mobile terminals. The four elements of the arrays were numbered from 1 to 4 sequentially for linear arrays (Arrays 1 & 5) and counterclockwise with correspondence to the quadrants for square arrays (Arrays 2, 3, 4 & 6) as shown in Fig. 4.2.3 (b), (c), (d) & (e). Measurements were taken with the element marked '1' on the linear array moved towards and in the direction perpendicular to the transmitter. For the square arrays, the side bordering the elements marked '1' & '2' is moved towards and in the direction perpendicular to the transmitter as shown in Fig. 5.1.1.

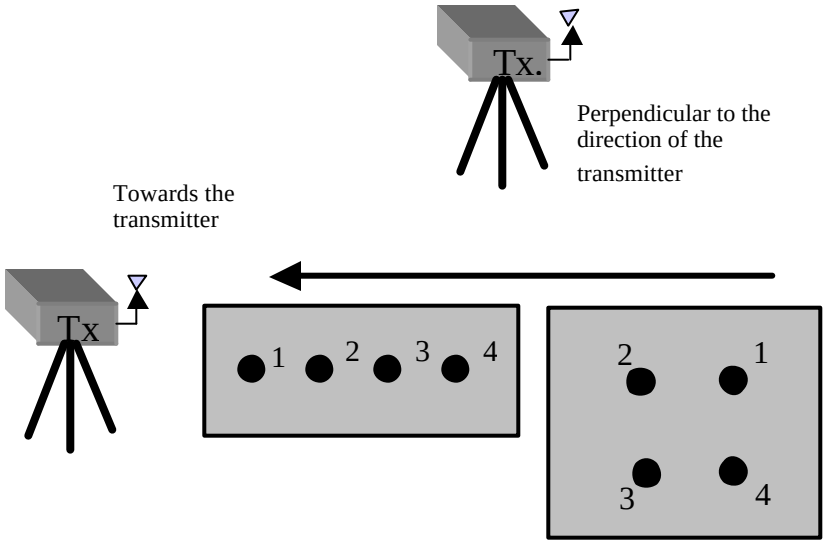

Figure 5.1.1 Illustration of how receiving antenna arrays move on the linear positioner at a speed of 0.115 m/sec relative to the transmitter for the two cases of motion towards and in the direction perpendicular to the transmitter.

Notations for different orientations of the receiver arrays relative to the transmitter are summarized in Table 5.1.

Table 5.1
Notation for receiver array orientations relative to the transmitter

Receiver Array orientation relative to the transmitter	Scenario	Notation
Element '1' for linear array (#1) and elements '1' and '2' for square array (# 2) moves towards the transmitter	Urban line-of-sight	$U_{\|}$ LOS
	Urban non-line-of-sight	$U_{\|}$ NLOS
	Suburban line-of-sight	$S_{\|}$ LOS
	Urban non-line-of-sight	$S_{\|}$ NLOS
Element '1' for linear array (#1) and elements '1' and '2' for square array (# 2) moves perpendicular to the transmitter	Urban line-of-sight	U$_{\perp}$ LOS
	Urban non-line-of-sight	U$_{\perp}$ NLOS
	Suburban line-of-sight	S$_{\perp}$ LOS
	Urban non-line-of-sight	S$_{\perp}$ NLOS

Diversity measurements in urban scenario were performed with the transmitter mounted at a fixed location and the receiving antenna arrays were moved in line-of-sight and in non-line-of-sight. For suburban environment, measurements were taken with the transmitter mounted on a building in a fixed location and the arrays mounted on the linear positioner or on a vehicle rooftop were moved in LOS and in N-LOS. Table 5.2 summarizes the measurement scenarios.

Table 5.2

Diversity Measurement Scenarios

Scenario No.	Measurement Scenario*	Transmitter	Measurement Location	Comments
1 (a)	Urban (pedestrian)	LOS**	Pathway between Whittemore Hall, Randolph Hall and Hancock Hall, at Virginia Tech campus	Receiving arrays are moved on the linear positioner and shown in Fig. 5.1.2
1 (b)		NLOS***		
1 (c)	Urban (vehicular)	NLOS	Draper Road	Transmitter mounted on the balcony of Squires Center
2 (a)	Suburban (pedestrian)	NLOS	South-west end of Drillfield, Virginia Tech	Transmitter uses vertically polarized dipole antennas
2 (b)	Suburban (vehicular)	LOS	Parking Lot 'B', west end, Virginia Tech	Transmitter was mounted on the third floor balcony of Whittemore Hall (Fig. 5.1.3)
2 (c)	Suburban (vehicular)	NLOS	Parking Lot 'L', on Stenger Street, Virginia Tech	Durham Hall and Whittemore Hall obstruct the direct line-of-sight

* In all the scenarios, measurements were taken with the element '1' for linear array and elements '1' & '2' for the square arrays, pointing towards/perpendicular to the transmitter as shown in Fig. 5.1.1

** line-of-sight

*** non-line-of-sight

Measurements were taken for different experiment scenarios corresponding to different combinations of urban/suburban, LOS/N-LOS and element '1' for linear and '1' & '2' for square array pointing towards/perpendicular to the transmitter, summarized in Table 5.2. An 'urban' measurement environment consisted of a flat grass-covered area surrounded by buildings on three sides as shown in Fig. 5.1.2. The receiver is mounted on the linear positioner at an approximate height of 1 m above ground. The transmitting antenna is mounted on the third floor balcony of Whittemore Hall at Virginia Tech.

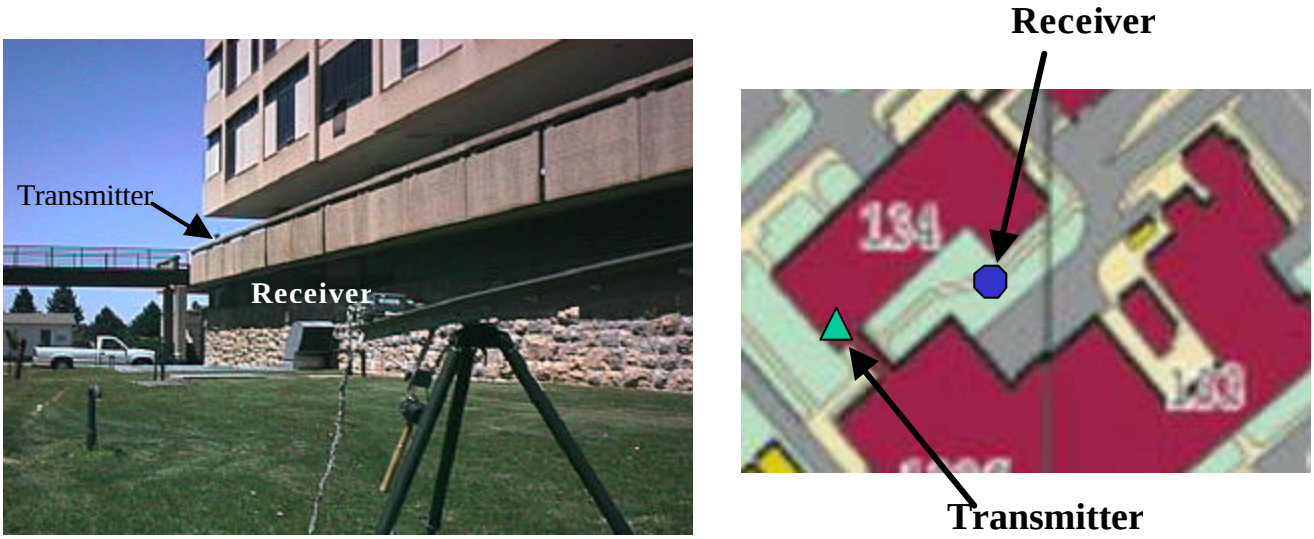

Figure 5.1.2 The 'urban' measurement scenario (Scenario 1 in Table 5.2). The photo on the left shows the HAAT positioner with the Whittemore Hall in the background. The right photo is an aerial view showing the Whittemore Hall (134), Randolph Hall (132) and Hancock Hall **(**133)

Suburban measurements with arrays mounted on the linear positioner were conducted on the southwest end of the Drill field on the Virginia Tech campus (not shown). Experiments in an sub-urban scenario with arrays mounted on a vehicle rooftop were conducted in Lot 'B' parking, Virginia Tech campus as shown in Fig. 5.1.3.

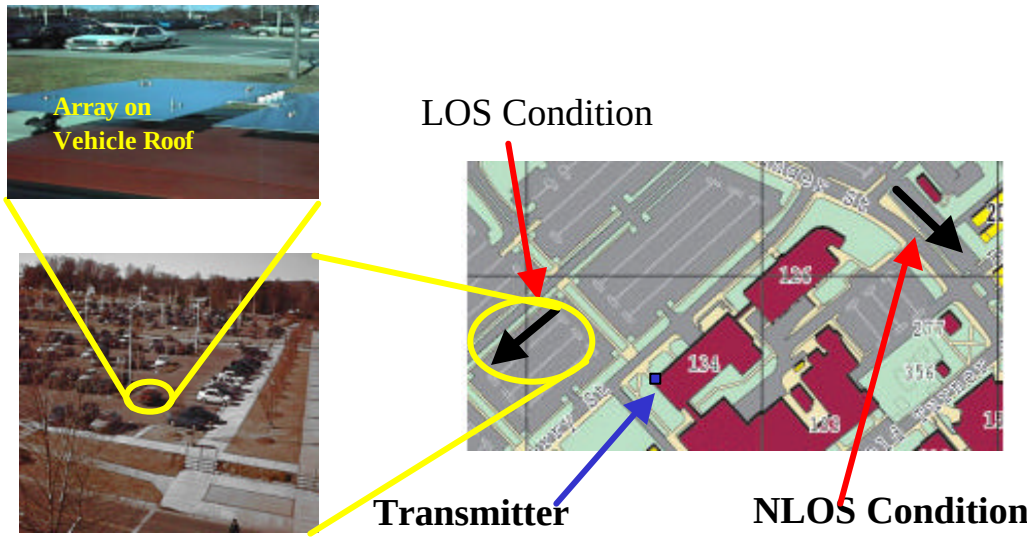

Figure 5.1.3 Suburban scenario with LOS and N-LOS conditions (Scenario 2 (b) & (c)) for vehicular measurements. The right photo shows an aerial view of the suburban measurement scenario with the transmitter mounted on Whittemore Hall (134). The left bottom photo shows the parking Lot B, where measurements were taken with the arrays mounted on the vehicle rooftop, shown in top left photo

5.2 Measured Results

5.2.1 Experiments with the Linear Positioner

Measurements were divided into two main categories: the urban channel and the suburban channel. Measurements were further subdivided to account for line-of-sight and non-line-of-sight channels. The diversity results for the four element linear array of Fig. 4.2.3 (a) are shown in Table 5.3. The envelope correlation between first and the second branch $?_{e12}$ was evaluated. The power imbalance $?P_{avg}$, which is the imbalance in average power between the channels '1' and '2' was also found from the data. The diversity gain G_{div} at 10% and 1% cumulative probabilities was calculated for maximal ratio combining. The values for all these quantities are listed in Table 5.3.

Table 5.3

Measured Results for Four-Element Linear Array (Array 1 in Table 4.1) with Monopole elements of Fig. 4.2.3 (a) in urban and suburban scenarios described in Table 5.2

	Urban (Scenario 1 (a) & (b))				Suburban (Scenario 2 (a))	
	$U_{\|}$		U_{-}		$S_{\|}$	S_{-}
	LOS	N-LOS	LOS	N-LOS	N-LOS	N-LOS
$?_{e12}$	0.8	0.6	0.04	0.1	0.5	0.4
$? P_{avg}$ dB	0.3	2.5	0.8	0.3	2.1	-1.1
$G_{div}(10\%)$ dB	6.8	4.8	4.7	9.5	7.2	9.0
$G_{div}(1\%)$ dB	11.3	7.2	8.0	13.2	14.1	12.0

Note from Table 5.3 that the linear array of broadband monopole elements (Array 1 in Table 4.1) offers 11.3 dB of diversity gain at 1% outage probability in urban line-of-sight scenario (Scenario 1 (a) in Table 5.2) with the transmitter in the endfire direction of the array. In comparison, 8.0 dB of diversity gain at 1% outage probability is achieved for the transmitter in broadside direction of the array for scenario 1 (a). Note that the suburban line-of-sight

measurements with arrays mounted on the linear positioner were not taken because in this case the transmitter saturated the receiver in clear unobstructed environment, thus resulting in high power imbalance at the receiver branch outputs, offering negligible diversity gain.

Table 5.4 shows diversity measurement results for square array (Array 2) of monopole elements in Fig. 4.2.3 (b) urban and suburban environments (Scenarios 1 & 2 (a) in Table 5.1). Because of symmetry in the azimuth plane, square array of monopole elements offers near similar diversity combining results in all directions. That is for urban LOS case with $U_{\|}$ and $U_{\perp}$, similar diversity gain values at 10% and 1% cumulative probabilities are observed.

Table 5.4

Measured Results for Four-Element Square Array (Array 2 in Table 4.1) with Monopole elements of Fig. 4.2.3 (b) in urban and suburban scenarios described in Table 5.2

	URBAN				SUBURBAN	
	$U_{\|}$		$U_{\perp}$		$S_{\|}$	$S_{\perp}$
	LOS	N-LOS	LOS	N-LOS	N-LOS	N-LOS
ρ_{e12}	0.4	0.2	0.6	0.6	0.3	0.8
ΔP_{avg} dB	0.7	2.7	0.4	-4.4	-3.6	0.7
$G_{div}(10\%)$ dB	6.3	6.3	5.7	7.2	7.8	8.1
$G_{div}(1\%)$ dB	10.7	8.6	9.8	10.3	13.8	7.3

Table 5.5 shows envelope correlation, power imbalance and diversity gain available at 10% and 1% outage probabilities for the sectored square array (Array 3) with monopole elements backed by corner reflectors in Fig. 4.2.3 (c). Note from Table 5.5 that 3.5 dB of diversity gain at 99% reliability is achieved in urban line-of-sight environment (Scenario 1(a) in Table 5.2) for the case of the edge with elements '1' & '2' moved towards the transmitter ($S_{\|}$) on the linear positioner. Low diversity gain is achieved because of severe power imbalance as all branches do not contribute to combined signal.

Table 5.5

Measured Results for Four-Element Sectored Square Array (Array 3 in Table 4.1) with Monopole elements of Fig. 4.2.3 (c) in urban and suburban scenarios described in Table 5.2

	URBAN				SUBURBAN	
	$U_{\|\|}$		$U_{\perp}$		$S_{\|\|}$	$S_{\perp}$
	LOS	N-LOS	LOS	N-LOS	N-LOS	N-LOS
$?_{e12}$	-0.4	-0.01	0.2	-0.2	0.5	0.2
$? P_{avg}$ dB	1.4	-2.5	-7.2	-7.4	-7.8	-9.3
$G_{div}(10\%)$ dB	4.0	6.1	2.6	6.1	8.3	4.8
$G_{div}(1\%)$ dB	4.2	4.5	3.5	10.5	11.9	7.2

The results for diversity reception using the four-wire antenna elements mounted on a high impedance surface (Array 4 in Table 4.1) and moved at approximately 0.115 m/sec are shown in the Table 5.6. The envelope correlation $?_{eij}$ (Section 2.3.2) between different branches was calculated from the data.

Table 5.6

Measured Results for Four-Wire Antenna (Array 4 in Table 4.1) with elements mounted on high impedance surface, shown in Fig. 4.2.3 (d) in urban and suburban scenarios (Table 5.2)

	URBAN				SUBURBAN			
	$U_{\|}$		U_{-}		$S_{\|}$		S_{-}	
	LOS	N-LOS	LOS	N-LOS	LOS	N-LOS	LOS	N-LOS
$?_{e12}$	0.04	-0.1	0.3	0.3	-0.1	0.2	-0.02	0.8
$?_{e13}$	0.5	0.7	-0.02	0.4	0.7	0.8	-0.1	0.03
$?_{e14}$	-0.2	0.1	0.2	0.3	0.3	0.5	0.2	0.8
$?_{e23}$	0.4	0.03	0.2	0.4	-0.2	0.1	0.03	-0.1
$?_{e24}$	0.2	0.05	0.5	0.8	-0.04	0.2	0.6	0.9
$?_{e34}$	-0.3	0.3	0.4	0.6	0.5	0.8	-0.04	-0.3
$? P_{avg}$ dB	10.1	7.1	-7.8	2.6	10.0	-0.7	10.4	-6.5
G_{div}(10%) dB	3.8	6.4	2.2	4.1	2.6	5.3	2.0	4.0
G_{div}(1%) dB	8.1	11.0	2.7	9.2	2.8	11.1	2.1	6.3

Note: $?_{eij}$ is the envelope correlation between the i^{th} and j^{th} branch, and $? P_{avg}$ is the average power imbalance between the first and the second branch in dB as explained in Section 2.3.2.

Note from Table 5.6 that 11 dB of diversity gain at 1% cumulative probability is achieved in urban non-line-of-sight obstructed environment (Scenario 1 (b)) as compared to 8.1 dB for line-of-sight environment (Scenario 1 (a)) for the case of element '1' moved towards ($U_{\|}$) the transmitter on the linear positioner. Also, the four-wire antenna (Array 4) performs better in the urban environment with severe multipath fading compared to the suburban environment because severe multipath fading increases the achievable diversity gain.

Switched diversity is the simplest way to achieve diversity gain but is not optimum and this can be seen by examining outage probability plot of Fig. 5.2.1, which shows the diversity

gain achieved using switched diversity with a threshold of 5 dB below mean signal power, using a four-element linear array (Array 1) of broadband monopoles.

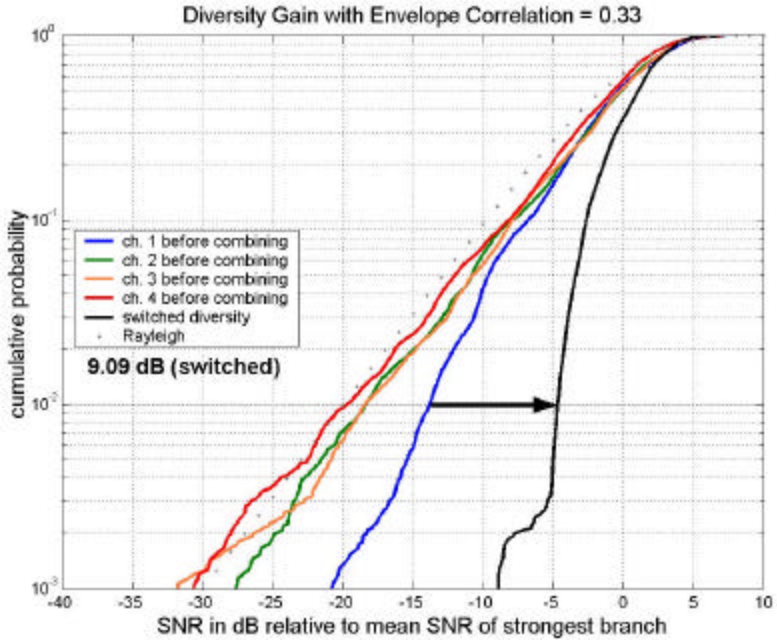

(a) Cumulative distribution plots of measured signals and signal combined using switched diversity in urban obstructed environment using four-element linear array of monopoles

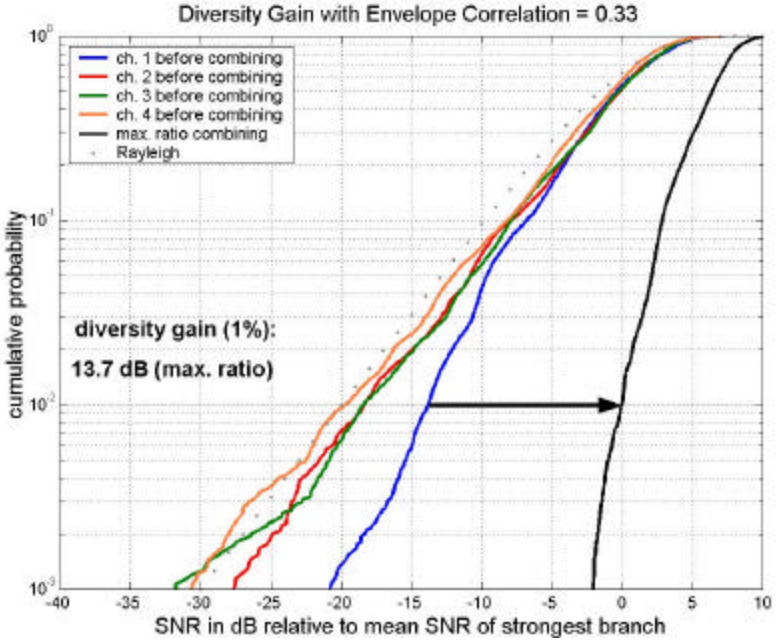

(b) Cumulative Distribution plots of measured signals and signal combined using maximal ratio combining in urban obstructed environment using four-element linear array of monopoles

Figure 5.2.1 Performance comparison of switched diversity technique and maximal ratio combining in urban non-line-of-sight scenario (Scenario 1(b)) using four-monopole linear array (Array 1 as in Table 4.1)

The diversity gain is about 9.1 dB at 99% reliability as compared to 13.7 dB gain achieved by the maximal ratio combining for the experiment scenario of non line-of –sight in the urban environment (Scenario 1(b)) is shown in Fig 5.2.1. Switched diversity performs about 3 to 4 dB worse than maximal ratio combining because switched diversity uses information from only one branch at a time. Thus, even though there may be a branch having better SNR, switched diversity does not select this signal so long as the currently selected channel does not drop below the acceptable level. This can be seen in the fading envelopes of the branches shown in Fig 5.2.2 (a) for switched diversity and Fig. 5.2.2 (b) for maximal ratio combining. Switched diversity is the simplest and the least expensive to implement, but does not give the optimum result. However, in maximal ratio combining the signals from various branches are combined after they are weighted proportional to their signal strength. This maximizes the SNR of the combined signal.

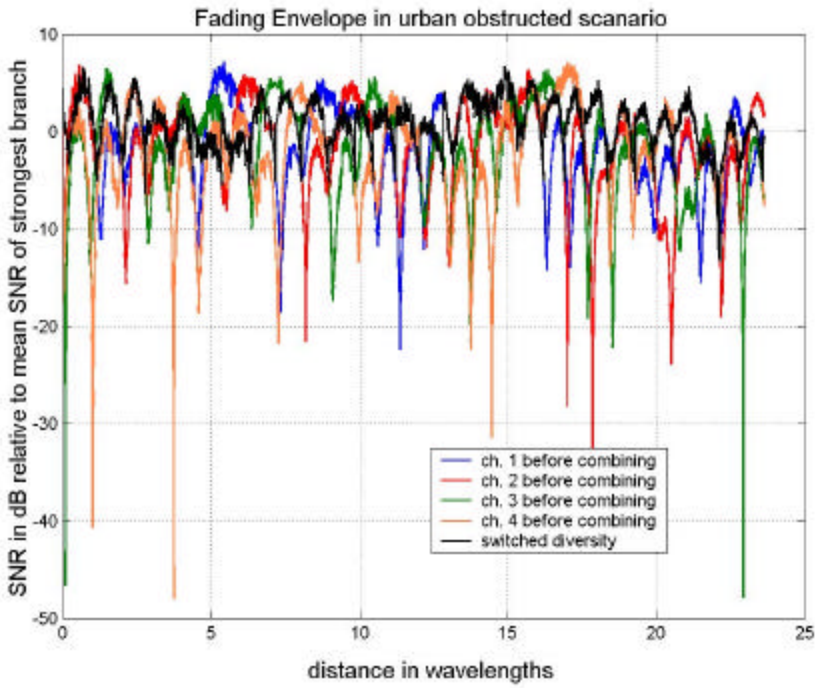

(a) Fading envelope of switched diversity combined signal in urban obstructed environment (Scenario 1(b)) using four-element linear array of monopoles (Array 1) with switching threshold of -5dB

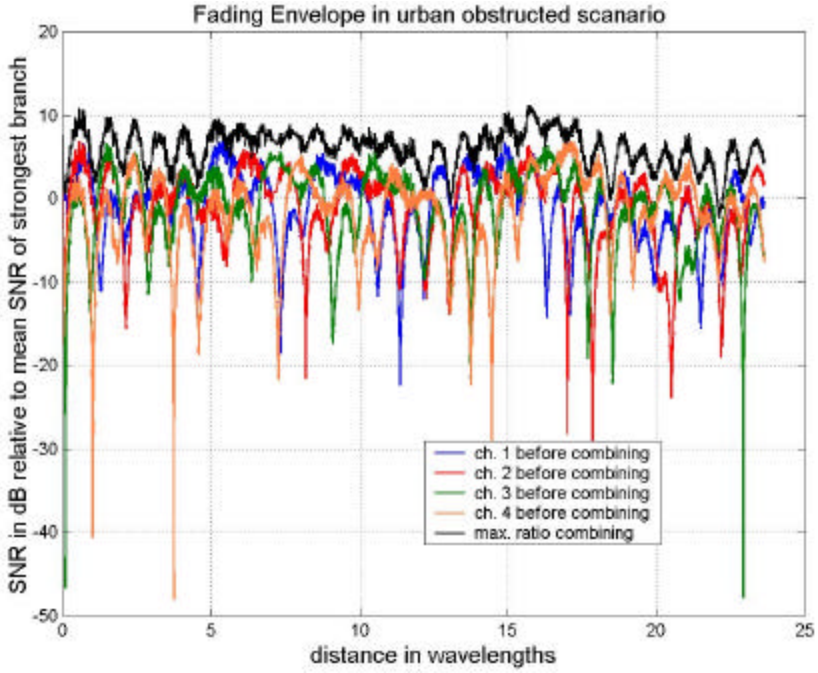

(b) Fading envelope of maximal ratio combined signal in urban obstructed environment (Scenario 1(b)) using four-element linear array of monopoles (Array 1)

Figure 5.2.2 Fading envelope plots of measured individual signals and combined signal using switched diversity technique and maximal ratio combining in urban obstructed environment (Scenario 1(b)) using four-element linear array of monopoles (Array 1)

Data plots for the experiments with the four-wire antenna (Array 4) in line-of-sight and non line-of-sight urban scenario (Scenarios 1(a) & (b)) are shown in Fig. 5.2.3. Note that as previously mentioned in Section 2.3.1, Array 4 offers better gain in the obstructed environment compared to the clear line-of-sight (LOS) condition. This is because in the non line-of-sight channel a wider multipath spread reduces power imbalances between the signals of various branches; this is seen from Table 5.6 where power imbalance values are 10.1 dB and 7.1 dB respectively, for LOS (1(a)) and N-LOS (1(b)) urban scenarios . In the LOS channel there is one direct signal with little fading, causing significant power imbalance.

Figure 5.2.3 compares the diversity gain for the LOS and the N-LOS experimental setup in the urban channel (Scenarios 1(a) & (b)). For envelope correlation of 0.04 in the LOS condition the diversity gain of 8.14 dB with power imbalance of 10.1 dB was recorded, shown in Fig 5.2.4 (a). In comparison, diversity gain of 11.0 dB with power imbalance of 7.16 dB for obstructed scenario, is shown in Fig. 5.2.4 (b). In the LOS case there is little severe fading and this reduces the achievable diversity gain.

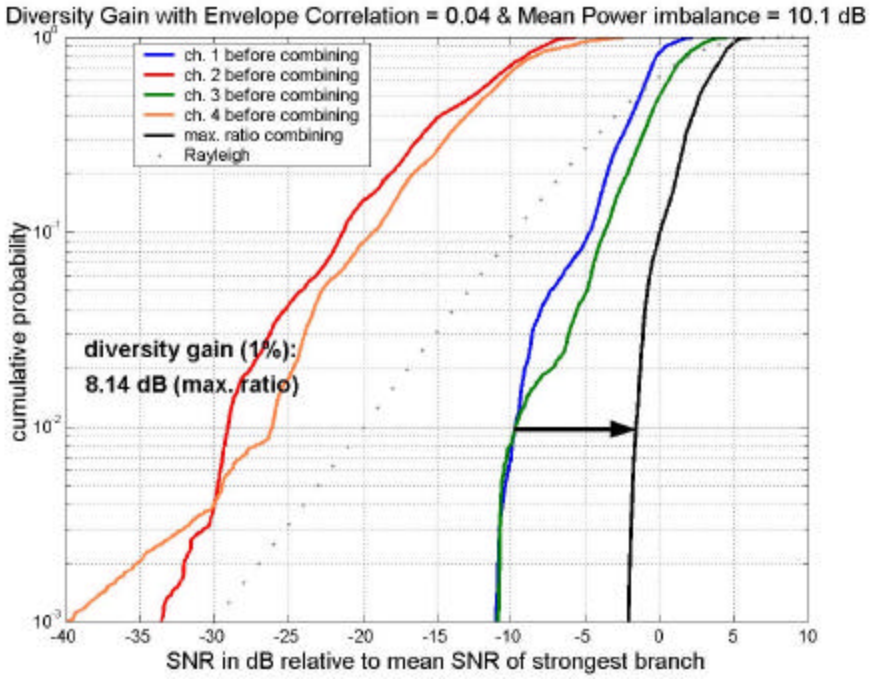

(a) CDF plot of the measured signals and MRC combined signal in Urban Line-of-Sight (LOS) scenario (1(a)) with 10.1 dB power imbalance

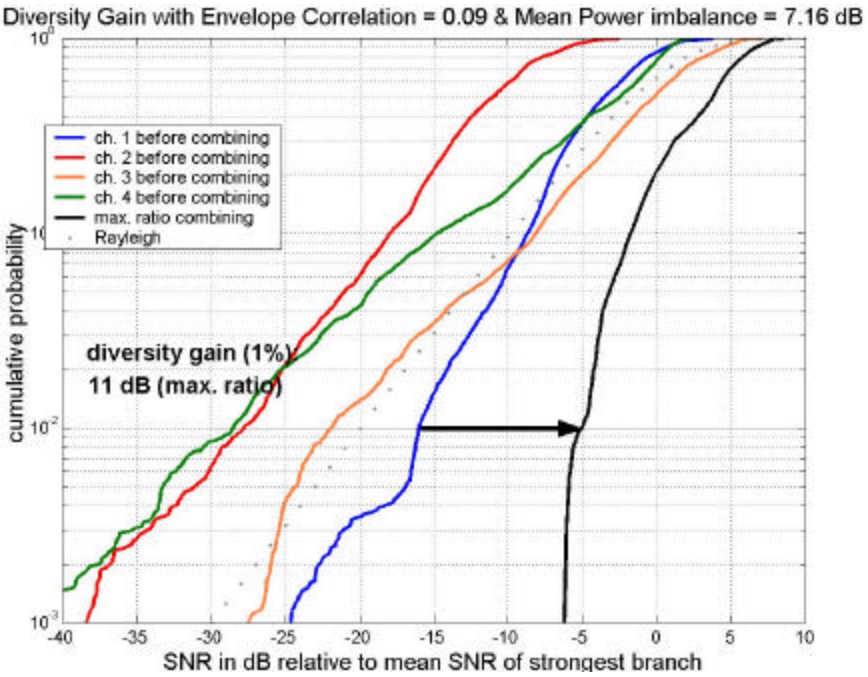

(b) CDF plot of the measured signals and MRC combined signal in Urban Non-Line-of-Sight (NLOS) (1(b)) obstructed scenario with 7.16 dB power imbalance

Figure 5.2.3 CDF plots recording the effect of power imbalance on achievable diversity gain in urban environment using the four-wire antenna array (Array 4)

It is interesting to compare the performance of different arrays in suburban and urban line-of-sight and obstructed conditions. This was done by comparing performances for the four-wire antenna array (Array 4), four-element linear array (Array 5) with elements mounted on a high impedance surface, square (Array 2) and sectorized square array (Array 3) with broadband monopoles to the strongest signal of the linear array with monopole elements. Table 5.7 compares diversity performance in urban direct line-of-sight condition. Similarly, Table 5.8 compares the diversity performance in urban obstructed non line-of-sight condition.

Table 5.7

Measured Envelope Correlation, Average Power of the Strongest Signal, Power of the Strongest Signal, Combined Signal and Diversity Gain at 1% CDF Results for Arrays described in Table 4.1 in Urban Line-of-sight Scenario (Scenario 1(a)) with Arrays mounted on the linear positioner

Array Name (number)	$?_{e12}$	$P_{s,avr}$ dBm	P_s (1%) dBm	P_c (1%) dBm	G_{div} (1%) dB	G_{div} (1%) dB relative to linear array (Array 1) monopoles
Linear Array (1)	0.79	-23.6	-35.6	-26.7	8.9	8.9
Square Array (2)	0.06	-23.5	-34.5	-23.5	11.0	12.1
Sectored-Square Array (3)	0.93	-24.3	-47.4	-36.6	10.7	-1
Four-wire Antenna (4)	0.08	-26.4	-30.6	-25.5	5.1	10.1
d = 0.4? four element Linear array (5)	0.41	-33.0	-53.1	--37.9	15.2	-2.3
d = 0.6? four element Linear array (5)	0.31	-33.1	-49.2	-34.9	14.3	0.7
d = 0.8? four element Linear array (5)	0.31	-33.2	-48.2	-34.6	13.6	1.0
d = 1.0? four element Linear array (5)	-0.21	-32.7	-45.7	-35.1	10.6	0.5

Note 1: $?_{e12}$ is the envelope correlation between branches 1 and 2, $P_{s,avr}$ is the average signal strength of the strongest branch, P_s is the average signal strength at 1% reliability level and P_c is the average strength of the combined signal at 1% reliability.
Note 2: Diversity gain is given by $G_{div}\ (1\%)\ [dB] = P_c\ [dB] - P_s\ [dB]$
Note 3: Diversity gain with respect to the common reference as the strongest signal received by the linear array is given by $G_{div,r}\ (1\%)\ [dB] = P_c\ [dB] - P_{s,lin}\ [dB]$

Table 5.8

Measured Envelope Correlation, Average Power of the Strongest Signal, Power of the Strongest Signal, Combined Signal and Diversity Gain at 1% CDF Results for Arrays described in Table 4.1 in Urban Obstructed Non-line-of-sight (Scenario 1(b)) with Arrays mounted on the Linear Positioner

Array Name (number)	$?_{e12}$	$P_{s,avr}$ dBm	P_s (1%) dBm	P_c (1%) dBm	G_{div} (1%) dB	G_{div} (1%) dB relative to linear array (Array 1) monopoles
Linear Array (1)	0.32	-36.4	-50.2	-36.5	13.7	13.7
Square Array (2)	-0.26	-35.4	-49.4	-35.0	14.4	15.2
Sectored-Square Array (3)	-0.13	-32.5	-42.5	-34.8	7.7	15.4
Four-wire Antenna (4)	-0.2	-32.6	-36.3	-32.6	3.7	17.6
d = 0.4? four element Linear array (5)	0.07	-46.0	-58.5	-46.3	12.2	3.9
d = 0.6? four element Linear array (5)	-0.04	-46.2	-63.6	-46.3	17.3	3.9
d = 0.8? four element Linear array (5)	-0.07	-45.1	-63.1	-43.8	19.3	6.4
d = 1.0? four element Linear array (5)	0.05	-44.7	-60.2	-46.6	13.6	3.6

5.2.2 Vehicular Measurement Results

In mobile communications at vehicular speeds, the rapidly changing channel introduces significant fast multipath fading at the receiving antenna. In this section, results from diversity measurements demonstrate that roof-mounted four element arrays of low-profile monopole antennas perform better than a single monopole. The four-element arrays described in Section 4.2 (Arrays 1 to 5) are low profile, easy to mount, compact structures with an electrical separation between elements on the order of half a wavelength. The vehicular measurements were made with vehicular speeds of 20 to 25 M.P.H. at Scenarios 2 (b) and 2 (c) as explained in Table 5.2, whereas the handheld measurements were made at Scenarios 1 (a) and 1 (b). It was not possible to use the same measurement sites for the vehicular measurements as the handheld measurements. The different measurement locations for vehicular and pedestrian speeds obviate direct comparison of results.

Since optimum performance is available by combining signals from all possible branches simultaneously, results from maximal ratio combining (MRC) are presented in Table 5.9 for arrays described in Table 4.1 in suburban line-of-sight (LOS) channel (Scenario 2(c)). Note that the linear array of monopole elements (Array 1) offers a diversity gain of 1.3 dB more than the square array of monopoles (Array 2). If the element gain is taken into consideration then the linear array offers 5.3 dB more gain than the square array. The sectored square array (Array 3) offers high diversity gain because of its high element gain. Moreover, as the separation is increased between the adjacent elements in the four-wire linear array with elements mounted on high impedance surface (Array 5) , the diversity gain increased.

Table 5.9
Measured Envelope Correlation, Average Power of the Strongest Signal, Power of the Strongest Signal, Combined Signal and Diversity Gain at 1% CDF for Arrays described in Table 4.1 in Suburban Line-of-Sight (Scenario 2(b)) with Arrays mounted on Vehicle Rooftop

Array Name (number)	$?_{e12}$	$P_{s,avr}$ dBm	P_s (1%) dBm	P_c (1%) dBm	G_{div} (1%) dB	G_{div} (1%) dB relative to linear array (Array 1) monopoles
Square Array of dipoles (6)	0.52	-32.1	-49.1	-37.5	11.6	11.6
Linear Array (1)	0.76	-28.6	-40.8	-29.9	10.9	19.2
Square Array (2)	0.63	-32.7	-44.8	-35.2	9.6	13.9
Sectored-Square Array (3)	0.10	-29.6	-47.6	-30.8	16.8	18.3
Four-wire Antenna (4)	0.85	-37.0	-54.8	-43.8	11.0	5.3
d = 0.4? four element Linear array (5)	0.82	-37.1	-54.6	-43.6	11.0	5.5
d = 0.6? four element Linear array (5)	0.19	-35.6	-55.3	-41.6	13.7	7.5
d = 0.8? four element Linear array (5)	0.69	-35.5	-56.3	-40.3	16.0	8.8
d = 1.0? four element Linear array (5)	0.44	-36.4	-54.1	-41.7	12.4	7.4

Measured results from diversity combining in suburban obstructed scenario with the arrays mounted on a vehicle rooftop are summarized in Table 5.10. Note that unlike the line-of-sight scenario (2(b)), the linear array of monopole elements (Array 1) offers less diversity gain than the square array of monopoles (Array 1). This is because the advantage of larger dimensional length of the linear array in line-of-sight case is no longer applicable in this case. The sectored square array (Array 3) offers best performance in terms of the available diversity

gain. As in the LOS case, the increase in the separation between the adjacent elements in the four-wire linear array with elements mounted on high impedance surface in the obstructed scenario resulted in increased diversity gain except for the case of 1 ? separation, which offers a diversity gain of 2.2 dB at 1% cumulative probability.

Table 5.10

Measured Envelope Correlation, Average Power of the Strongest Signal, Power of the Strongest Signal, Combined Signal and Diversity Gain at 1% CDF for Arrays described in Table 4.1 in Suburban Non-Line-of-Sight (Scenario 2(c)) with Arrays mounted on Vehicle Rooftop

Array Name (number)	$?_{e12}$	$P_{s,avr}$ dBm	P_s (1%) dBm	P_c (1%) dBm	G_{div} (1%) dB	G_{div} (1%) dB relative to linear array (Array 1) monopoles
Square Array of dipoles (6)	0.52	-53.8	-73.3	-58.3	15.0	15.0
Linear Array (1)	0.74	-54.2	-75.2	-61.4	13.8	11.9
Square Array (2)	0.41	-53.8	-74.3	-59.7	14.6	13.6
Sectored-Square Array (3)	0.16	-49.5	-70.8	-56.7	14.1	16.6
d = 0.4? four element Linear array (5)	0.32	-55.9	-77.7	-68.8	8.9	4.5
d = 0.6? four element Linear array (5)	0.55	-58.1	-80.1	-65.8	14.3	7.5
d = 0.8? four element Linear array (5)	0.57	-59.7	-79.2	-65.6	13.6	7.7
d = 1.0? four element Linear array (5)	0.61	-63.1	-82.8	-71.1	11.7	2.2

An important observation from the results given in Table 5.5 is the drop in envelope cross-correlation and increase in diversity gain with increasing separation from 0.4 ? to 0.8 ?. The envelope strength of the combined signal is nearly equal for different spacings. Results from

non-line-of-sight (N-LOS) suburban channel measurements for maximal ratio combining measurements for different arrays in Table 5.10 clearly show that diversity gain increases with increasing element separation and the corresponding envelop correlation coefficient drops. This may be expected, as mutual coupling is high for compact antennas and is shown in Fig 5.2.4.

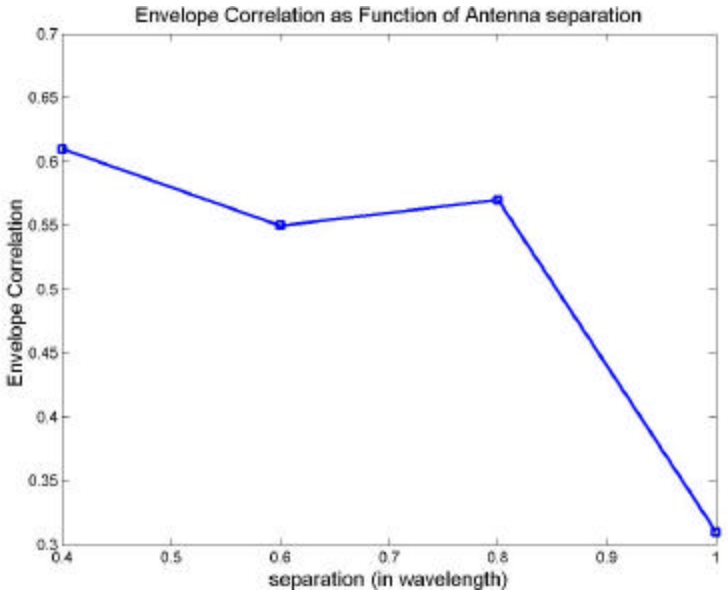

(a) Envelope Cross-Correlation Coefficient

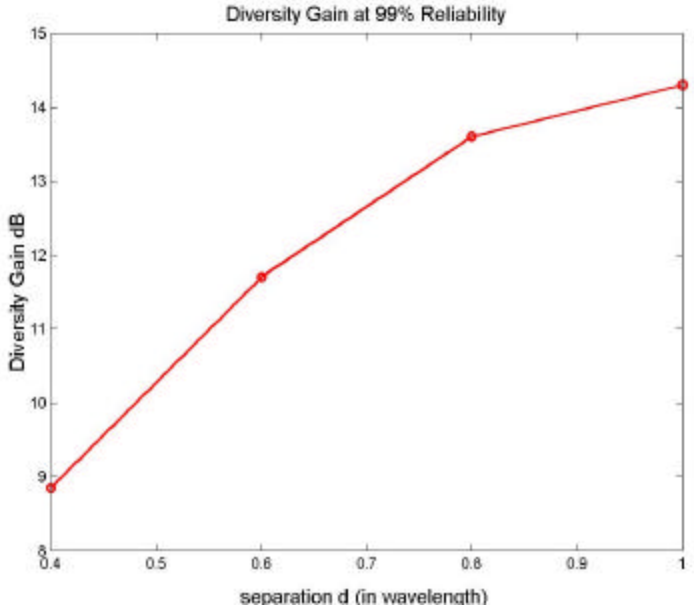

(b) Diversity Gain in dB

Figure 5.2.4 Measured dependence of envelope correlation and diversity gain on antenna element separation for four-wire antenna in linear configuration (Array 5 described in Table 4.1) in Suburban Non-line-of-sight (Scenario 2(c)) with arrays mounted on vehicle rooftop

Measurements taken with square sectored array (Array 3) of low-profile broadband omni-directional monopoles in urban obstructed scenario (Scenario 1 (c)) are compared to the measurements performed for the sectored square array in suburban line-of-sight (LOS) measurement scenario (2 (b)) with the array mounted on the vehicle rooftop. Obstructed channel measurements collected on a nearby urban scenario on Draper Road, Blacksburg, showed substantial signal fading, as expected. Hence, the achievable diversity gain is also substantial. A suburban LOS scenario offers best possible link conditions and so with little fade, there is little scope of improvement. However, obstructed non-line-of-sight scenario offers severe fading and also the possibility of achieving high diversity gain. The diversity performance of the sectored square array with monopole elements backed by corner reflector is shown in Fig. 5.2.5. Note that 12.6 dB of diversity gain is achieved in urban obstructed channel as compared to 6.6 dB of diversity gain achieved in suburban LOS condition for the square sectored array mounted on vehicle rooftop.

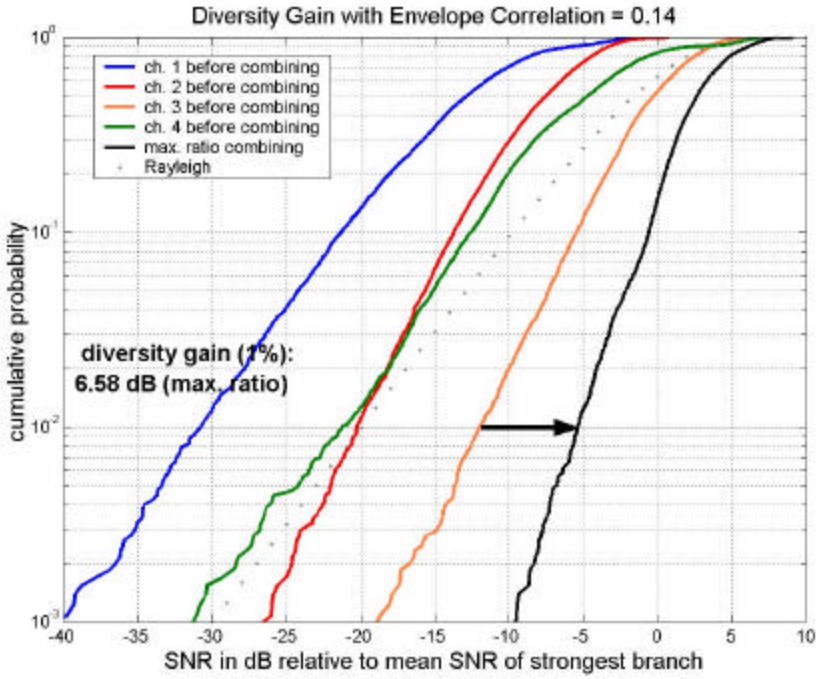

(a) Measured diversity gain for sectored square array (Array 3) in suburban line-of-sight (Scenario 2(b))

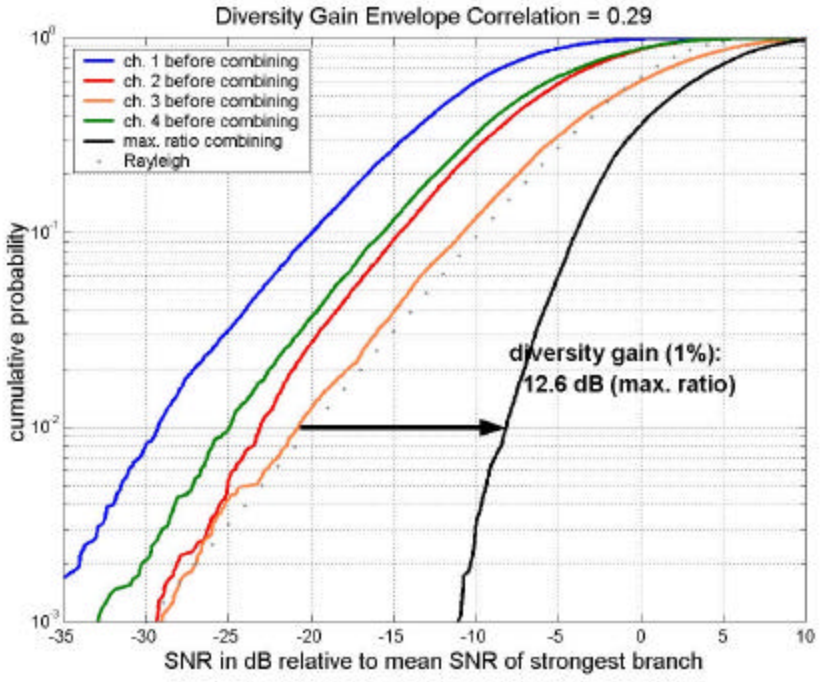

(b) Measured diversity gain for in urban non-line-of-sight (Scenario 1(c))

Figure 5.2.5 Measured diversity gain for sectored square array (Array 3 in Table 4.1) mounted on vehicle rooftop in suburban line-of-sight (Scenario 2 (b) in Table 5.2) and in an obstructed urban channel (Scenario 1 (c)).

Diversity measurements performed for different vehicular speeds with a square array of four dipoles (Array 6) are Fig. 5.2.6. Note that the square array with dipole elements at 20 M.P.H. offered a gain of 9.6 dB at 1% of fading outage probability. It was observed that as the vehicular speed was decreased to 5 M.P.H. the gain increased by a couple of decibels to 12.7 dB as shown in Fig. 5.2.6 (b) because the fading was not severe at lower vehicular speeds.

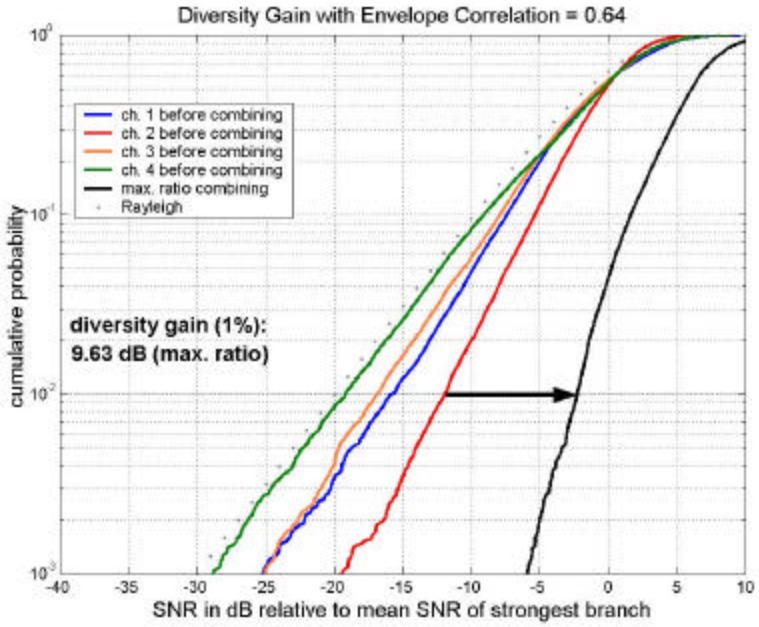

(a) Speed = 20 M.P.H.

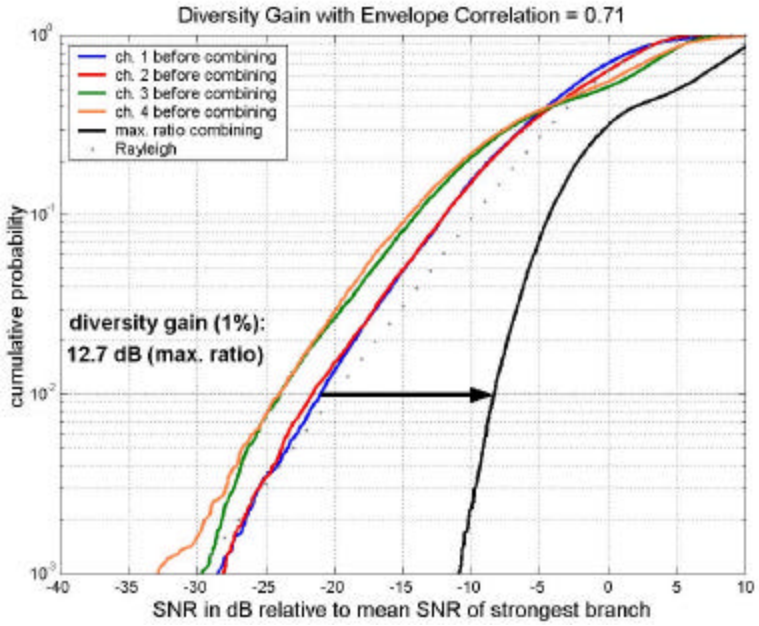

(b) Speed = 5 M.P.H.

Figure 5.2.6 Measured diversity gain of square array with vertical dipoles (Array 6 in Table 4.1) in suburban line-of-sight channel (Scenario 2 (b)) for different vehicular speeds

5.3 Comparison of Array Performances

The arrays that were used in measurements performed differently in different experimental scenarios. The linear with broadband monopoles (Array 1) showed significant improvement in line-of-sight and obstructed suburban scenarios over the square array of monopoles (Array 2). However, the sectored square array offered maximum diversity gain because the its active element gain is 3.7 dB high than the active element gain of the linear array. Measurements showed that the arrays offered high diversity gain even though the elements are correlated in the range of 0.1 to 0.7, making the antennas with omni-directional active element radiation pattern suitable for diversity combining. The performances of different arrays in the urban line-of-sight environment are summarized in Table 5.11. We observe from this comparison that the linear array with monopole elements performs about 3 dB better than the square array.

Table 5.11

Measured Envelope Correlation, Average SNR of the Strongest Signal, SNR of the Strongest Signal, Combined Signal and Diversity Gain at 1% CDF for Arrays 1, 2, 3 & 6 described in Table 4.1 in Suburban Line-of-Sight (Scenario 2(b)) with Arrays mounted on Vehicle Rooftop

Array Name (number)	$?_{e12}$	$P_{s,avr}$ dBm	SNR_s (1%) dB	SNR_c (1%) dB	G_{div} (1%) dB	$G_{r,div}$ (1%) dB
Square Array of dipoles (6)	0.52	-32.1	72.9	84.5	11.6	11.6
Linear Array (1)	0.76	-28.6	81.2	92.1	10.9	19.2
Square Array (2)	0.63	-32.7	77.2	86.8	9.6	13.9
Sectored-Square Array (3)	0.10	-29.6	74.4	91.2	16.8	18.3

The four-wire antenna array with elements mounted on a high impedance surface showed improved signal reception through mitigation of fading in the urban environment. The four-wire antenna achieves about 14.3 dB relative gain with elements mounted on the high impedance surface. Similarly for the diversity performance of different arrays compared in Table 5.12 for urban obstructed non-line-of-sight scenario (1 (c)), it can be observed that the linear array performs about 2 dB to 3 dB better than the square array.

Table 5.12

Measured Envelope Correlation, Average SNR of the Strongest Signal, SNR of the Strongest Signal, Combined Signal and Diversity Gain at 1% CDF for Arrays 1, 2, 3, 4 & 6 described in Table 4.1 in Urban Non-Line-of-Sight (Scenario 1(c)) with Arrays mounted on Vehicle Rooftop

Array Name (number)	$?_{e12}$	$P_{s,avr}$ dBm	SNR_s (1%) dB	SNR_c (1%) dB	G_{div} (1%) dB	$G_{r,div}$ (1%) dB
Square Array of dipoles (6)	0.61	-53.8	48.7	63.7	15.0	15.0
Linear Array (1)	0.41	-53.8	47.7	62.3	14.6	13.6
Square Array (2)	0.74	-54.2	46.8	60.6	13.8	11.9
Sectored-Square Array (3)	0.16	-49.5	51.2	65.3	14.1	16.7
Four-wire antenna Array (4)	0.32	-55.9	56.1	63.2	7.1	14.5

The experiments showed that out of all the antennas listed in Table 4.1, the four-element linear array of monopoles (Array 1) and four-wire antenna with elements mounted on high impedance surface (Array 4) performed well in the urban non line-of-sight obstructed environment and provides substantial diversity gain from 9.6 dB to 13.0 dB at a reliability level of 99%. The sectored square array with directional active element radiation pattern offered high SNR at 1% cumulative probability offering diversity gain in the range of 11.0 dB to 16.7 dB.

Measured results from Table 5.11 and 5.12 indicate that the linear array with omni-directional active element pattern (Array 1) and sectored square array with directional radiation pattern (Array 3) offers best diversity combining results closely followed by the four-wire antenna array (Array 4). However, when the arrays are mounted on the vehicle rooftop and driven at vehicular speeds, the sectored square array showed considerable power imbalance in its branches and didn't offer diversity gain as good as the linear or square array. But as we shall see in Chapter 6, this array performs very well in the presence of interference using adaptive beamforming.

5.4 Conclusion of Diversity Results

For suburban channels we observe that the surrounding buildings and other scatterers widen the angle spread, reducing the envelope correlation and leading to increased diversity gain. Moreover, if the angle of signal arrival of the signal is not uniform pattern, distortion due to mutual coupling between array elements lowers envelope correlation and increases power imbalance. Power imbalance compared to high envelope correlation significantly lowers the diversity gain.

The array performance in different experimental scenarios was examined was analyzed and compared in Section 5.3. Measured results presented in Fig. 5.2.5 indicate the effect of power imbalance in different scenario on diversity combining. Diversity gains calculated using Maximal Ratio Combining showed substantial improvement of 4 to 6 dB over the switched diversity technique for all array configurations. The antenna arrays performed well in the urban non line-of-sight obstructed environment and gives substantial diversity gain of 9.6 to 13.0 dB at reliability of 99%.

References

[Vau93] Vaughan R. G. and Scott N. L., "*Antennas for FPLMTS*," in PIMRCC '93 Proceedings, Sept. 1993.

[Lee82] Lee W. C. Y., *Mobile Communications Engineering*, New York: McGraw – Hill, 1982.

[Jak93] Jakes W. C., "*Microwave Mobile Communications*", New York, IEEE Press 1993.

[Car01] Dietrich C. B. Jr., Dietze K., Nealy J. R., Stutzman W. L., "*Spatial, polarization, and pattern diversity for wireless handheld terminals*", Antennas and Propagation, IEEE Transactions on, Volume: 49 Issue: 9, Sept.2001.

[Vau92] Vaughan R., Scott N., "*Closely spaced terminated monopoles for vehicular diversity antennas*", APS International Symposium, 1992, AP-S, 1992 Digest. Vol. 2; pp: 1093-1096.

[Nor01] Norklit O., Teal P. D., Vaughan R. G., "*Measurement and evaluation of multi-antenna handsets in indoor mobile communication*", Antennas and Propagation, IEEE Transactions on, March 2001, vol.: 49.

Chapter 6

Interference Rejection Measurements

Mobile antenna arrays show tremendous potential for improving the coverage and capacity of wireless mobile communication systems. Using adaptive beamforming techniques, mobile antenna arrays can be used to cancel interfering signals that have spatial characteristics different from the desired signal [Lit96]. Adaptive beamforming techniques dynamically steer the beam to place the maximum possible pattern gain in the direction of the incoming desired signal while it simultaneously places a null in the direction of the interfering signal [Hud81]. Interference rejection using adaptive beamforming increases the system capacity and, thus, revenue for the service provider.

Adaptive beamforming techniques aim to achieve optimum beamforming [Lib99]. The received signals from the array elements are appropriately weighted before combining, with the objective to optimize a performance parameter (normally the signal-to-interference-and-noise ratio) of the combined signal. Agee [Age93] reported simulation results that demonstrated superior interference rejection performance for different arrays when evaluated using Least-Squares Constant Modulus Algorithm (LS-CMA). In this chapter, adaptive beamforming performance of the four-element arrays for mobile (vehicular speed) and portable (pedestrian speed) terminals is investigated. The capability of the four-element arrays in rejecting interference in different directions using a blind adaptive algorithm is also investigated. Interference rejection measurement results using LSCMA with linear, square, and sectorized square four-element array configurations as described in Section 4.2 are analyzed and compared.

The chapter begins with a brief description of the experiment scenario and objectives in Section 6.1, followed by measurement results obtained in suburban and urban environments in Section 6.2. Interference rejection performance of four element arrays is investigated for pedestrian and vehicular speeds and results are analyzed and compared in Section 6.3.

6.1 Experiment Objective and Scenario

Reliable mobile radio communication is hampered by two types of interference: 1) Co-channel interference due to users operating in the co-channel cell and 2) Adjacent-channel interference due to the energy spill over in spectrum from adjacent channels [Rap99]. Co-channel interference rejection depends on the separation in distance between the co-channel cells, while the adjacent channel interference can be mitigated using bandpass filters that have sharp roll off. Interference rejection measured data were collected and processed using the Handheld Antenna Array Testbed (HAAT) system, which is described in Chapter 4.

Interference rejection measurements were undertaken in urban and suburban environments for both line-of-sight (LOS) and obstructed non-line-of-sight (N-LOS) multipath channels, with the objective to analyze and compare the performance of adaptive beamforming with the array configurations listed in Table 4.1 in measurement scenarios listed in Table 6.1. To meet our objective, controlled experiments were conducted using the HAAT system. Linear (Array 1), square (Array 2) and square sectored arrays (Array 3) of low profile, broadband omni-directional monopoles were used. A four-wire antenna array (Array 4) and a linear array configuration of single wire elements mounted on a high impedance surface (Array 5) were also used. A square array of four half-wave dipole elements (Array 6) was used as a baseline to evaluate and compare the interference rejection performance of different arrays,

As mentioned earlier in Section 5.1 for diversity measurements, the four elements of the arrays in Table 4.1 were numbered from 1 to 4 sequentially for linear arrays (Arrays 1 & 5) and counterclockwise with correspondence to the quadrants for square arrays (Arrays 2, 3 & 4). The measurements were taken with the element marked ‘1’ on the linear array and the side of the array bordering the elements marked 1 & 2 on the square and the sectored square arrays pointing

towards and pointing in the direction perpendicular to the transmitter, shown in Fig.5.1.1. Measurements were taken for the urban scenario with the interfering transmitter in line-of-sight and in non-line-of-sight. For suburban and rural environment measurements were taken with both the transmitter in LOS and the interfering transmitter was moved in azimuth to evaluate the interference rejection performance of the arrays in azimuth. Table 6.1 summarizes the measurement scenarios.

Table 6.1

Interference Rejection Measurement Scenarios

Measurement Scenario*	No.	Desired Tx	Interfering Tx	Measurement Location	Comments
Urban	1 (a)	LOS**	LOS	Pathway surrounded by Pamplin Hall, Burruss Hall and Johnson Student Center on three sides, at Virginia Tech campus	Each transmitter uses vertically polarized dipole antennas
	1 (b)	LOS	NLOS***		
	1 (c)	NLOS	LOS		
Suburban (pedestrian)	2 (a)	LOS	LOS	South-west end of Drillfield, Virginia Tech	Interfering Transmitter was moved in azimuth
Suburban (vehicular)	2 (b)	LOS	LOS	Parking Lot 'B', west end, Virginia Tech	Interfering Transmitter was kept at fixed Location
Suburban (vehicular)	2 (c)	NLOS	NLOS	Parking Lot 'L', on Stenger Street, Virginia Tech	Both the desired & the interfering Tx. are fixed
Rural	3	LOS	LOS	Bolley Fields, Montgomery County	Interfering Transmitter was moved in azimuth

* In all the scenarios, measurements were taken with the element '1' for linear and elements '1' & '2' for the square arrays, pointing towards/perpendicular to the transmitter as shown in Fig. 5.1.1

** line-of-sight

*** non-line-of-sight

Experiments in suburban and rural environments were conducted with two co-polarized transmitters named ‘A’ and ‘B’, also co-polarized to the receiver. Linearity is assumed in these measurements, i.e. the interfering signal is not strong enough to overload the receiver, as it might be in a military jamming scenario. Initially the transmitters were separated by 10° in azimuth. The four-element antenna arrays were moved on a 3 m linear positioner with the element 1 in the direction towards and then in the direction tangential to Transmitter ‘A’. Transmitter ‘B’ was then relocated to about 45° in azimuth and similar measurements were recorded. In all experiments, the antenna arrays were oriented horizontally so that the elements were vertically polarized, except for the four-wire antenna with elements mounted horizontally on the high impedance surface.

The testbed uses two transmitters for interference rejection measurements. Either transmitter can be considered to be the desired transmitter and the other to be transmitting an interfering signal. Both the transmitters transmit continuous wave (CW) signals separated by 1 kHz for identification [Die00]. The HAAT configuration for interference measurement is similar to the set up used for the diversity measurements. Data are collected using a four-channel portable receiver system, shown in Fig. 4.1.1. The data collected are analyzed off line to allow comparison of different adaptive beamforming techniques. A portable positioning system having a length of approximately 3 m was used for controlled measurements at pedestrian speeds. A vehicle with a false rooftop was used to mount arrays for measurements at vehicular speeds. Each antenna is connected directly to a mixer and the received RF signal at 2.05 GHz is mixed down directly to baseband. Two stereo DAT recorders are used and each DAT records two of the four channels of the receiver.

A suburban measurement location at Drill Field, Virginia Tech campus is shown in Fig 6.1.1. The left picture shows the two transmitters separated by 10° in azimuth and the figure in right shows the aerial view of Drillfield, Virginia Tech. Both the transmitters have clear LOS to the receiver.

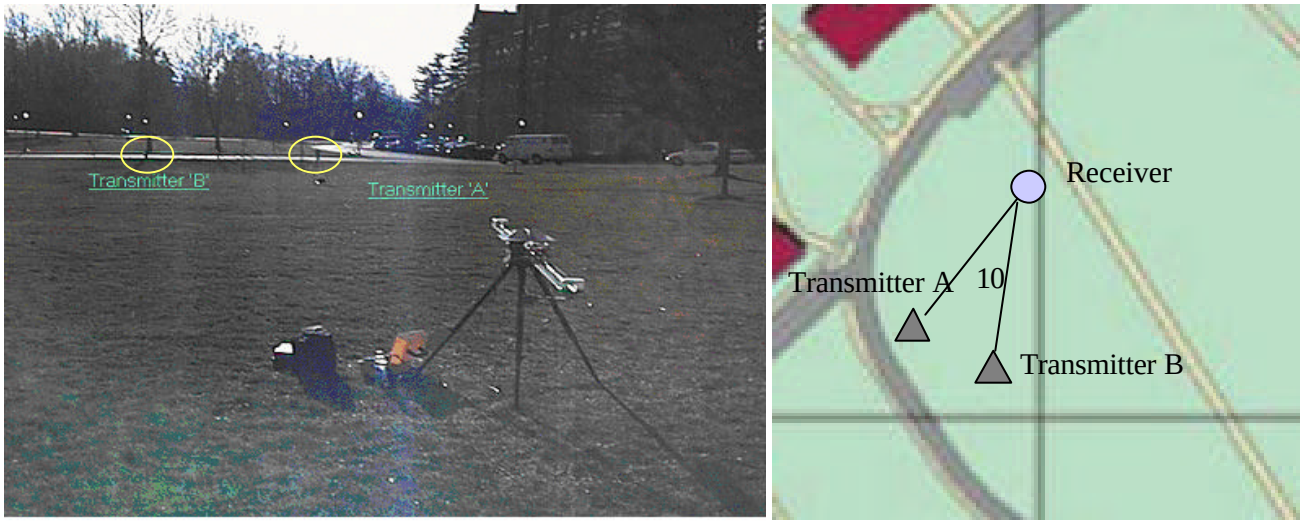

Figure 6.1.1 Interference rejection measurement setup shown on Drill Field, Virginia Tech campus, (suburban scenario 2(a))

Measurements in the urban environment were conducted with transmitter 'A' in line of sight while transmitter 'B' was manually relocated from LOS to N-LOS situations. An 'urban' measurement environment consisted of a pathway surrounded by Pamplin Hall, Burruss Hall and Johnson Student Center on three sides, at Virginia Tech campus.

A suburban scenario for arrays mounted on a vehicle rooftop was achieved in Lot 'B' parking, Virginia Tech campus as shown in Fig. 6.1.2. One transmitter was mounted on the west corner of the third floor balcony, Whittemore Hall, Virginia Tech and a second transmitter was mounted near the north corner on the second floor balcony.

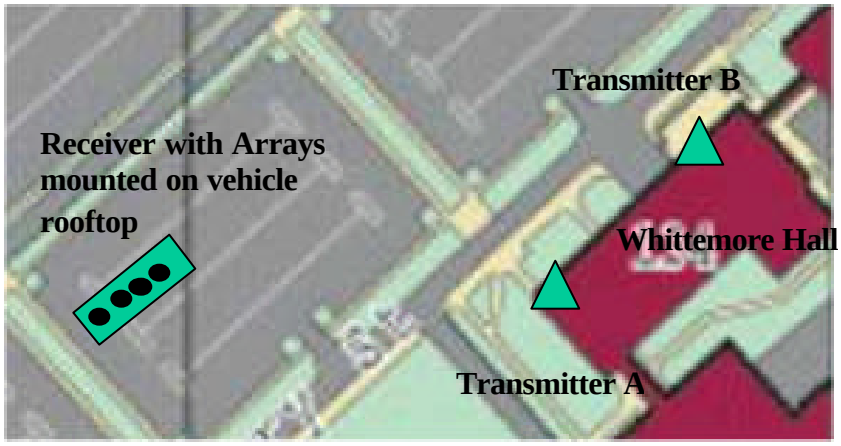

Figure 6.1.2 Interference rejection measurement setup shown in Lot B parking, Virginia Tech campus, (suburban scenario 2(b))

Beamforming was accomplished by processing the data with a multi-target least-squares constant modulus algorithm (MT-LSCMA). This algorithm used a block length of 320 samples (10 ms). The four-channel, two-target LS-CMA algorithm adaptively calculated and updated two weight vectors, one to optimize reception of each signal. SNR and SINR were measured before and after beamforming for each signal and for each channel by comparing the levels in appropriate frequency bins of the discrete Fourier transform of the signal.

The four-wire antenna (Array 4 in Table 4.1) with elements mounted on high impedance surface [Sie00], elements '1' and '3' and elements '2' & '4' were connected in pairs using the two 90° hybrids as shown in Fig. 4.2.3 (d). This results in four different patterns. Each beam has a maximum in the direction of one array element.

6.2 Experiment Results from Interference Rejection Measurements

6.2.1 Experiments with Linear Positioner

Adaptive beamforming experiments were divided into two main categories: the urban channel and the suburban channel. For the urban radio channel the measurements were further divided to account for the line of sight channel and the non-line of sight channel. The results for the four-wire antenna with elements mounted on a high impedance surface, in different measurement environments are summarized in the Table 6.1. Similarly, Tables 6.2, 6.3 and 6.4, respectively, illustrate the performance of the linear, square and sectored square arrays with broadband monopole elements. The performance of element spacing is demonstrated in Table 6.5, for linear arrays of elements mounted on high impedance surface. Mean signal-to-interference-plus-noise ratio (SINR) for two channels is compared with the mean SINR after LS-CMA beamforming. Mean SINR and improvement in SINR at 1% outage probability is also shown in the Tables 6.1 to 6.4. Signal-to-noise (SNR) ratio puts an upper limit on SINR. Mean SNR before and after beamforming are also reported.

For the suburban channel, measurements were conducted by fixing the position of the transmitter 'A' in LOS and various locations for transmitter 'B' to give azimuth separation angles of 10º, 30º, 45º, 60º, 90º and 180º. The first set of results analyze the response of the four-wire antenna array with elements mounted on a high impedance surface in a suburban channel with element '1' as listed Array 4 in Table 4.1 moved towards transmitter 'A' to its response when element '1' is moved tangentially to the direction pointing towards transmitter 'A'. The desired transmitter and the interfering transmitters are separated by 90º in azimuth. A plot is shown in Figure 6.2.1, which compares the signal strength of all branches for these two different conditions. Note that 24 dB of interference rejection as measured from SINR improvement is achieved in the first case when the element '1' is moved towards the desired transmitter (shown in Fig. 5.1.1) compared to 15 dB in the latter case when the element '1' is moved in the direction perpendicular to the desired transmitter at 1% cumulative probability of signal-to-interference-plus-noise ratio. However, beamforming works equally well in both the cases and gives nearly equal SINR of about 32 dB measured at 1% cumulative probability after adaptive beamforming. This is because of the symmetry of the four-wire antenna in azimuth.

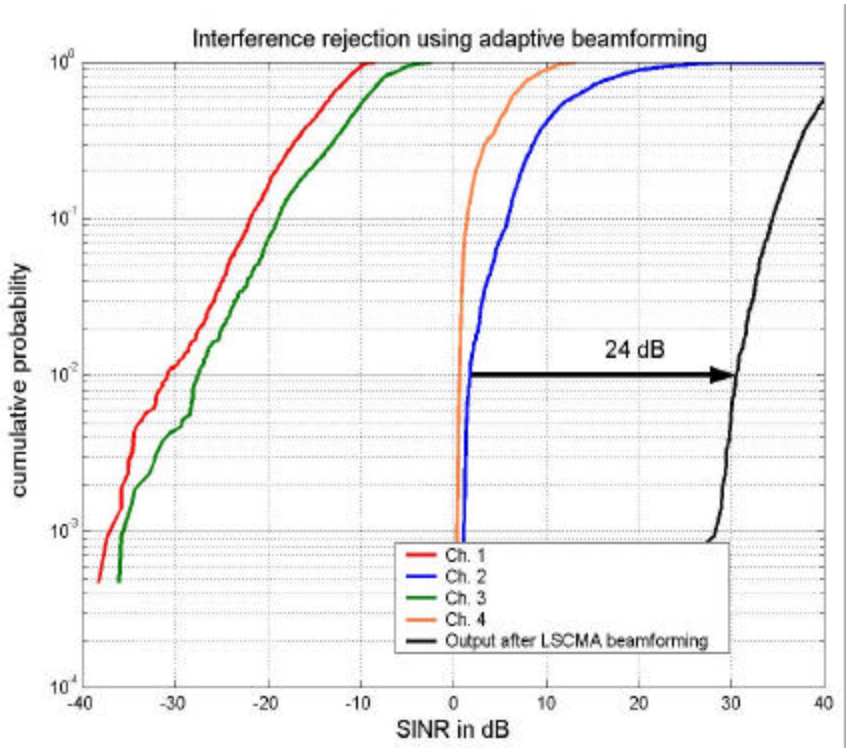

(a) Element '1' moving towards Tx. 'A' ($S_{\|}$)

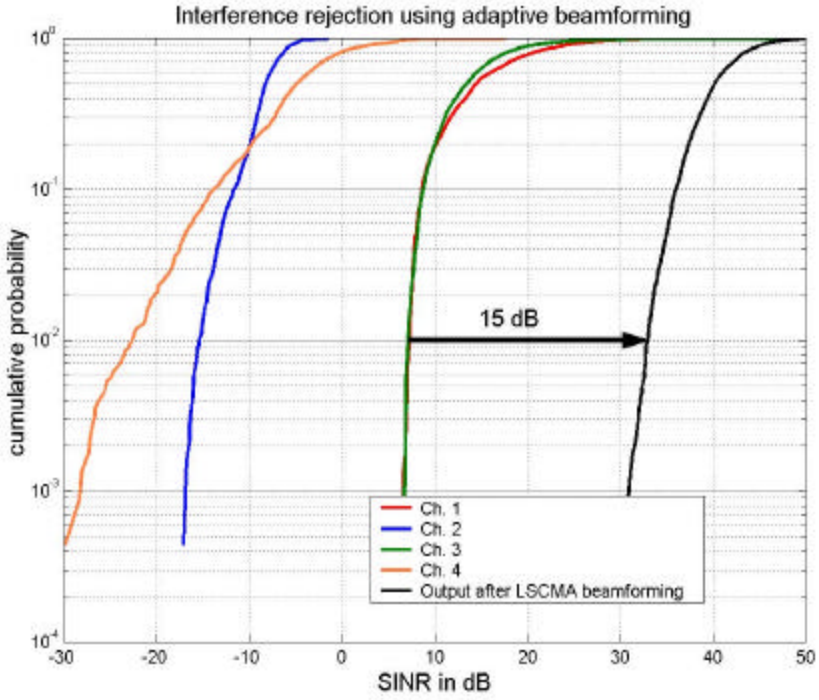

(b) Element '1' moving in the direction perpendicular to Tx. 'A'(S.)

Figure 6.2.1 Measured SINR Cumulative probability plots for four-wire antenna (Array 4) with elements mounted on high impedance surface in suburban line-of-sight (Scenario 2 (a) in Table 6.1) with (a) receiving antennas moved towards and (b) perpendicular to the transmitter while mounted on the linear positioner

Table 6.1
Interference Rejection Measurement Results using four-wire antenna (Array 4) mounted on high impedance surface in suburban line-of-sight scenario at Drillfield, Virginia Tech (Scenario 2 (a))

Measured Results in dB	Suburban						Urban			
	$S_{\|\|}$			S_{-}			$U_{\|\|}$		U_{-}	
	10°	45°	90°	10°	45°	90°	Tx. 'B' in LOS	Tx. 'B' in NLOS	Tx. 'B' in LOS	Tx. 'B' in NLOS
Mean I/P SINR on Ch. '2' dB	0.3	5.2	12.4	-4.9	-8.5	-8.3	-5.9	-3.0	-7.1	-3.9
Mean I/P SINR on Ch. '3' dB	-0.8	-4.2	-11.5	0.7	8.7	14.3	-12.8	-9.8	-11.2	-3.1
Mean O/P SINR dB	26.8	35.0	39.4	26.5	35.5	40.5	39.4	39.5	39.4	37.4
O/P SINR at 1% CDF dB	22.5	20.4	30.5	17.2	27.3	32.9	29.5	21.7	29.5	20.0
?SINR at 1% CDF dB	26.8	22.8	28.7	20.5	26.1	25.6	38.8	27.3	43.3	28.3
Mean I/P SNR on Ch. '2' dB	41.3	42.7	42.4	37.7	32.9	34.1	39.5	38.1	37.9	36.0
Mean I/P SNR on Ch. '3' dB	40.3	34.7	28.9	40.0	42.8	44.3	31.1	31.7	34.8	38.1
Mean O/P SNR dB	49.0	47.0	48.1	44.7	50.9	53.1	46.6	47.1	44.9	45.5

Table 6.2
Interference Rejection Measurement Results using linear array with broadband low-profile monopole elements (Array 1) in rural line-of-sight scenario at Bolley Fields (Scenario 3)

Parameters	Suburban										Urban			
	$S_{\|\|}$					S_{-}					$U_{\|\|}$		U_{-}	
	0°	30°	60°	90°	180°	0°	30°	60°	90°	180°	Tx. B LOS	Tx. B NLOS	Tx. B LOS	Tx. B NLOS
Mean i/p SINR on Ch. '1' dB	6.0	6.6	-2.4	-2.5	11.9	4.5	5.9	2.5	13.8	13.6	-19.5	12.4	-20.8	7.3
Mean i/p SINR on Ch. '2' dB	7.0	6.3	-5.0	-4.5	12.2	4.7	9.4	4.5	15.1	12.1	-19.8	11.1	-20.9	4.9
Mean i/p SINR on Ch. '3' dB	6.4	4.9	-4.2	-3.4	11.6	4.6	6.7	4.9	17.5	12.1	-20.5	8.8	-21.0	6.1
Mean i/p SINR on Ch. '4' dB	7.9	2.8	-4.1	-4.6	11.6	4.4	8.5	5.5	17.7	13.0	-19.6	6.4	-21.2	5.1
Mean o/p SINR dB	23.9	18.0	23.9	24.9	25.5	25.7	24.3	33.2	26.8	24.7	2.9	33.7	3.8	34.0
o/p SINR at 1% CDF dB	12.9	1.0	7.5	12.3	11.9	12.2	12.8	19.3	12.7	11.6	-12.5	23.2	-11.3	24.2
?SINR at 1% CDF dB	15.6	6.6	24.7	27.1	19.6	12.9	10.6	18.3	8.8	8.4	21.2	37.4	22.7	26.8
Mean i/p SNR on Ch. '1' dB	19.9	15.8	20.2	17.6	22.6	22.0	19.7	25.9	24.2	20.4	1.4	32.0	2.1	32.7
Mean i/p SNR on Ch. '2' dB	20.2	15.9	18.8	15.9	21.9	22.1	22.0	26.7	24.6	19.2	1.3	32.2	2.0	32.4
Mean i/p SNR on Ch. '3' dB	20.1	14.2	19.2	16.6	21.5	22.1	20.2	26.8	24.3	19.2	1.2	31.2	2.1	32.7
Mean i/p SNR on Ch. '4' dB	20.1	12.5	18.8	15.4	21.3	21.9	21.3	26.9	24.4	19.7	1.2	30.6	2.1	32.2
Mean o/p SNR dB	27.3	19.4	26.4	25.1	30.5	27.4	27.7	33.4	27.2	24.9	2.9	38.6	5.4	38.2

Table 6.3
Interference Rejection Measurement Results using square array with broadband low-profile monopole elements (Array 2) in rural line-of-sight scenario at Bolley Fields (Scenario 3)

Parameters	Suburban										Urban			
	$S_{\|\|}$					S_{-}					$U_{\|\|}$		U_{-}	
	0°	30°	60°	90°	180°	0°	30°	60°	90°	180°	Tx. B LOS	Tx. B NLOS	Tx. B LOS	Tx. B NLOS
Mean i/p SINR on Ch. '1' dB	4.3	0.2	6.6	5.3	17.8	6.0	8.5	14.1	15.9	13.6	-20.7	-27.4	-24.8	-27.5
Mean i/p SINR on Ch. '2' dB	5.5	1.7	6.2	-0.7	15.6	5.6	8.1	10.6	14.9	16.4	-21.4	-27.2	-24.8	-27.4
Mean i/p SINR on Ch. '3' dB	6.6	4.8	7.2	1.9	18.4	5.5	4.1	9.6	15.8	14.5	-21.7	-27.3	-20.1	-22.2
Mean i/p SINR on Ch. '4' dB	5.9	3.8	12.7	2.8	20.2	5.9	2.9	13.3	19.9	12.4	-17.9	-27.2	-25.3	-27.6
Mean o/p SINR dB	20.4	24.9	24.1	26.4	27.6	15.5	26.3	25.7	26.6	24.7	2.5	1.5	0.7	-5.2
o/p SINR at 1% CDF dB	5.3	12.5	11.7	13.8	14.8	2.0	14.4	15.1	14.4	12.6	-15.2	-16.6	-15.5	-12.7
?SINR at 1% CDF dB	6.7	17.5	14.8	20.8	13.4	1.6	10.7	11.4	7.2	5.6	21.4	21.9	20.9	26.1
Mean i/p SNR on Ch. '1' dB	22.6	16.3	14.4	21.4	19.2	22.4	24.5	22.5	24.4	19.6	1.6	1.5	1.2	1.6
Mean i/p SNR on Ch. '2' dB	22.3	18.1	13.6	17.6	19.5	22.2	24.4	19.7	24.8	22.1	1.4	1.7	0.9	1.7
Mean i/p SNR on Ch. '3' dB	23.3	20.8	15.5	20.5	22.2	21.9	22.5	18.8	24.8	20.5	1.4	1.4	1.1	1.5
Mean i/p SNR on Ch. '4' dB	22.3	18.8	19.4	20.6	21.1	22.3	21.8	21.8	24.7	18.7	2.2	1.5	1.1	1.5
Mean o/p SNR dB	26.7	25.5	25.8	30.6	31.1	25.8	27.7	27.5	30.4	28.6	5.1	2.8	2.4	5.3

Table 6.4
Interference Rejection Measurement Results using sectored square array with broadband low-profile monopole elements backed by corner reflectors (Array 1) in rural line-of-sight scenario at Bolley Fields (Scenario 3)

Parameters	Suburban										Urban			
	$S_{\|\|}$					S-					$U_{\|\|}$		U-	
	0°	30°	60°	90°	180°	0°	30°	60°	90°	180°	Tx. B LOS	Tx. B NLOS	Tx. B LOS	Tx. B NLOS
Mean i/p SINR on Ch. '1' dB	11.4	10.6	13.9	15.2	20.8	11.7	16.2	14.9	21.8	7.6	-25.3	-23.9	-25.7	-27.3
Mean i/p SINR on Ch. '2' dB	11.2	5.8	7.1	9.5	21.2	11.4	14.7	18.8	25.1	20.4	-25.3	-23.8	-25.4	-27.2
Mean i/p SINR on Ch. '3' dB	11.9	8.0	1.9	2.1	3.5	11.4	7.7	9.0	19.2	19.6	-25.0	-23.9	-25.3	-27.1
Mean i/p SINR on Ch. '4' dB	12.6	11.5	12.8	8.8	4.2	13.6	6.7	2.1	12.1	3.4	-24.4	-23.8	-25.6	-27.2
Mean o/p SINR dB	20.9	24.5	22.3	23.2	26.7	19.1	22.8	22.4	28.7	23.6	2.3	1.7	2.9	-0.1
o/p SINR at 1% CDF dB	7.8	12.7	10.3	10.8	13.7	6.5	10.4	7.7	16.5	11.6	-16.1	-15.7	-13.4	-18.2
?SINR at 1% CDF dB	5.5	15.0	9.6	6.1	3.1	4.1	4.5	0.0	0.9	0.8	20.2	25.5	22.6	20.7
Mean i/p SNR on Ch. '1' dB	20.1	16.1	14.9	19.7	24.2	16.1	21.7	19.3	25.6	12.6	1.2	2.5	1.5	1.5
Mean i/p SNR on Ch. '2' dB	20.4	11.8	12.8	14.9	24.5	16.5	21.8	21.8	27.9	22.9	1.3	2.5	0.9	1.5
Mean i/p SNR on Ch. '3' dB	19.4	12.5	7.2	6.7	10.5	16.5	16.2	14.6	24.0	22.5	0.9	2.3	1.2	1.6
Mean i/p SNR on Ch. '4' dB	18.3	13.9	16.1	12.4	8.7	17.1	14.6	6.9	14.9	8.3	0.8	2.5	1.4	1.5
Mean o/p SNR dB	24.9	27.8	23.6	25.7	27.1	21.3	24.0	22.9	29.3	24.6	6.6	3.4	4.8	0.1

Table 6.5
Interference Rejection Measurement Results using four-wire antenna (Array 4) and linear array with variable spacing (Array 5) mounted on high impedance surface in urban scenario at Virginia Tech (Scenario 1 (a) and (b))

Parameters	Virginia Tech Square Dipole Array.		HRL 4-wire Antenna		HRL 4 element Linear Array							
					Separation 0.4 ?		Separation 0.6 ?		Separation 0.8 ?		Separation 1.0 ?	
	LOS	N-LOS	LOS	N-LOS	LOS	N-LOS	LOS	N-LOS	LOS	N-LOS	LOS	N-LOS
Mean i/p SINR on Ch. ‘1’ dB	-22.4	-25.4	-20.5	-1.5	7.8	12.1	12.0	11.9	-0.4	8.1	-21.4	8.9
Mean i/p SINR on Ch. ‘2’ dB	-22.6	-25.2	-20.3	9.8	4.8	8.4	6.7	9.3	8.4	9.4	-22.2	7.2
Mean i/p SINR on Ch. ‘3’ dB	-22.7	-24.7	-25.7	-0.6	10.3	10.1	12.0	10.8	10.5	11.0	-21.4	8.9
Mean i/p SINR on Ch. ‘4’ dB	-22.7	-25.4	-17.1	6.7	9.7	16.1	7.8	10.4	3.2	15.6	-23.3	5.2
Mean o/p SINR dB	3.4	1.5	-0.4	32.8	31.3	31.0	33.3	32.6	32.6	33.2	4.2	33.3
o/p SINR at 1% CDF dB	-13.7	-15.8	-21.1	21.2	13.4	20.4	23.1	21.3	19.7	22.2	-11.0	22.1
?SINR at 1% CDF dB	25.8	22.4	14.5	28.9	23.9	28.9	24.1	31.1	34.2	34.1	23.9	33.9
Mean i/p SNR on Ch. ‘1’ dB	1.6	1.6	3.5	29.2	26.1	29.7	28.4	31.1	27.2	30.4	1.6	29.9
Mean i/p SNR on Ch. ‘2’ dB	1.7	1.7	3.3	30.4	25.0	28.0	26.6	30.1	29.9	29.3	1.9	30.7
Mean i/p SNR on Ch. ‘3’ dB	1.6	1.7	2.5	30.3	25.0	27.7	28.8	30.3	29.7	29.9	1.6	31.1
Mean i/p SNR on Ch. ‘4’ dB	1.6	1.5	4.9	31.0	25.4	29.2	26.4	30.9	31.3	31.0	1.8	29.2
Mean o/p SNR dB	4.5	2.1	4.4	34.2	30.8	32.7	37.7	33.2	36.4	38.3	4.0	37.0

The second set of results for the four-wire antenna array (Array 4) illustrates interference rejection using beamforming with different locations of interfering transmitter 'B' in azimuth plane as demonstrated in Table 6.1. Note from Fig. 6.2.2 that when the interferer (transmitter 'B') is 10°, 45° and 90° separated from the transmitter 'A' in azimuth, the mean SINR achieved after beamforming is 26.8 dB, 35.0 dB and 39.4 dB respectively, which shows steady increase in the mean output SINR. This is because, up to 90°, the interferer steadily moves into the pattern null of the antenna as shown in Fig. 4.2.9. However, the SINR improvement achieved is nearly the same about 27 dB that further asserts that the four-wire antenna performs equally well to reject interference coming from any direction in the azimuth.

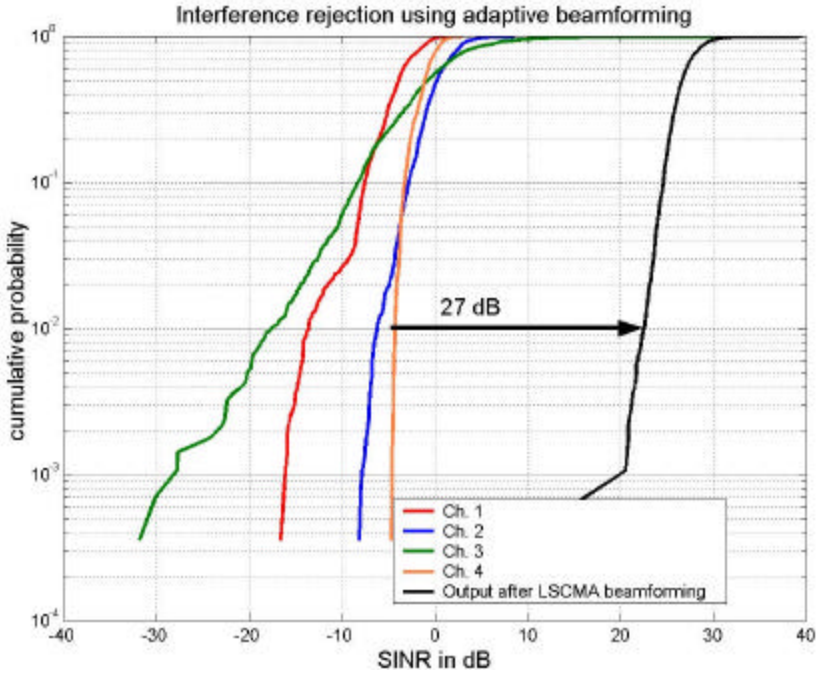

(a) 10° separation

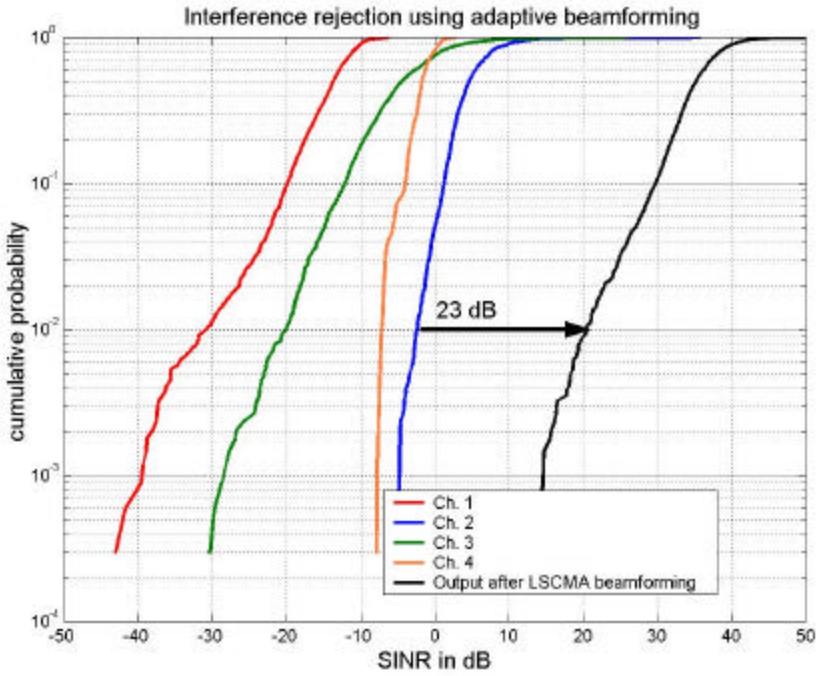

(b) 45° separation

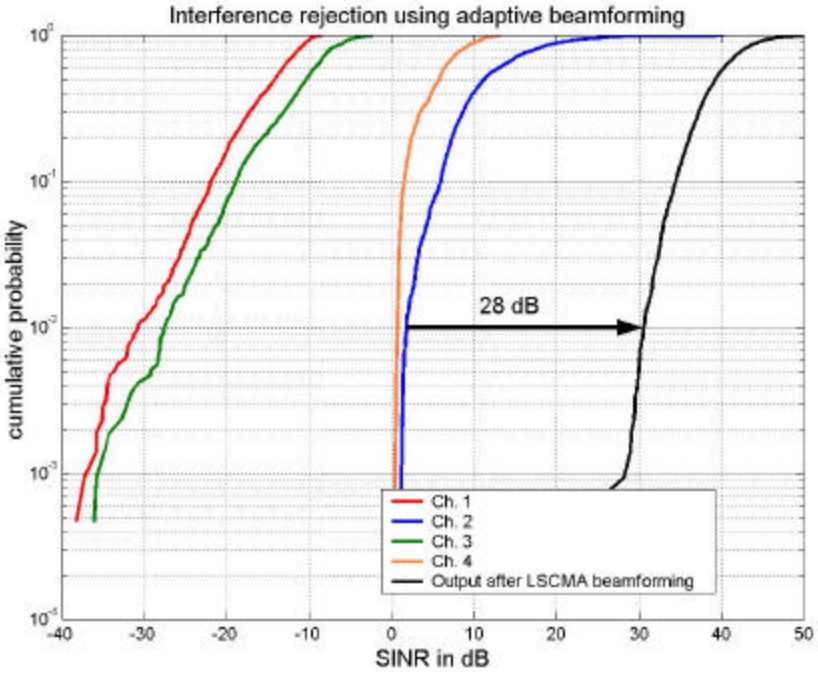

.

(c) 90° separation

Figure 6.2.2 Measured interference rejection in azimuth with four-wire antenna (Array 4) in suburban line-of-sight measurement channel at Drillfield, Virginia Tech (Scenario 2 (a))

The next set of measurements was taken in the urban environment with transmitter ‘B’ placed in LOS and then relocated to non-LOS, keeping the transmitter 'A' in direct LOS. For post processing either of the transmitters can be considered to be transmitting the desired signal and the other to be transmitting the interfering signal. Thus, for a single set of measurements we have two different results. First, consider transmitter 'A' to be the desired signal and is always in LOS. The data for the interferer (transmitter ‘B’) in LOS (Scenario 1(a) in Table 6.1), is shown in Figure 6.2.3 (a), and for the interferer in non-LOS (Scenario 1(b) in Table 6.1), is shown in Figure 6.2.3 (b). Note that the mean output SINR achieved in both cases is the same, about 39 dB, because the desired transmitter is always in LOS. The direct interfering signal strength in LOS and the strongest multipath interfering signal in NLOS were measured to be nearly equal. The improvement in SINR achieved after beamforming at a cumulative probability of 1% is about 38.8 dB in the case when the interferer is in the LOS compared to 27.3 dB when the interferer is in N-LOS. This is because there was negligible variation in the direction of the incoming interfering signal for the interferer in LOS case allowing LS-CMA to place a null in the direction of the interfering transmitter. Note that with the interferer in LOS, the SINR after beamforming at 1% CDF is about 36.6 dB compared to 27.4 dB, for the interferer in N-LOS, indicating that final SINR is greater for the interferer in LOS. This is because, in the N-LOS case (Scenario 1(b)), the interfering signal arrives through multipaths, thus the interfering signal may seem to arrive at the receiver from different directions instantaneously. Since LS-CMA beamforming algorithm uses 10 msec of data to determine the weights in Fig.3.4.1, complete interference cancellation cannot be achieved.

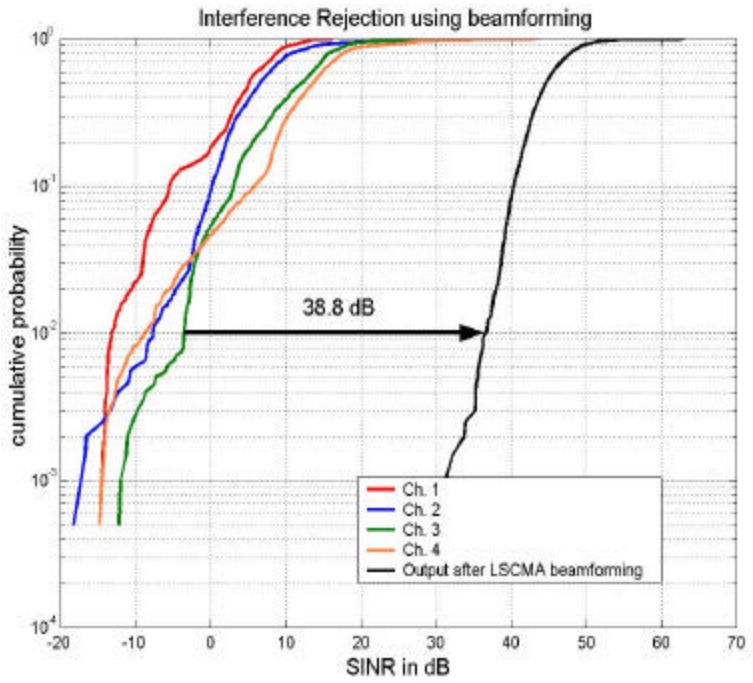

(a) Desired Tx. in LOS, Interfering Tx. in LOS in urban scenario (Scenario 1(a))

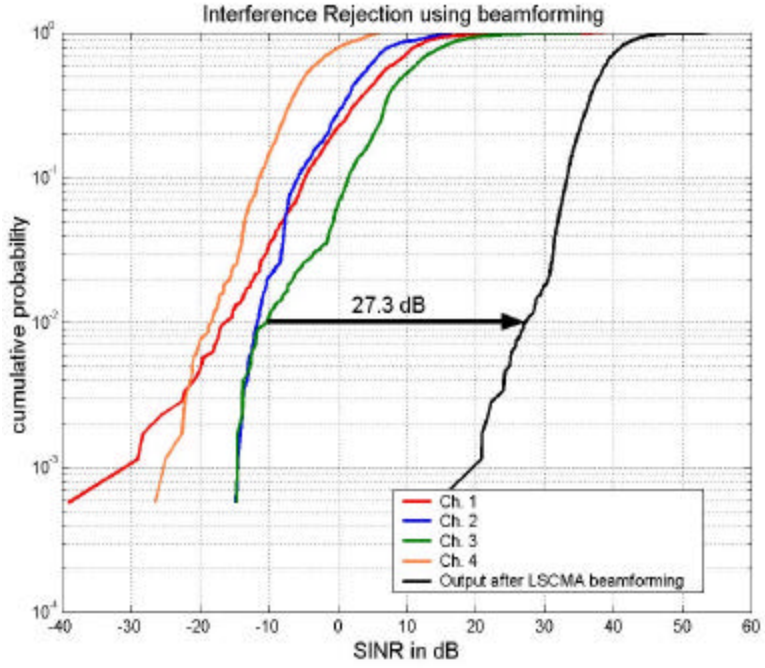

(b) Desired Tx. in LOS, Interfering Tx. in N-LOS in urban scenario (Scenario 1(b))

Figure 6.2.3 Measured interference rejection results for the four-monopole square array (Array 2) mounted on the linear positioner in urban environment, the desired Tx. 'A' is in LOS and the interfering Tx. 'B' is in (a) LOS and (b) relocated to obstructed N-LOS condition

Looking at the same set of measurements from a different perspective, let us consider that transmitter 'A' is now the interferer and is always in LOS, while transmitter 'B' now transmits the desired signal. In the first case transmitter 'B' is in LOS (Scenario 1(a)) and the measured results are shown in Figure 6.2.4 (a). The desired transmitter ('B') is then relocated to N-LOS condition (Scenario 1(c)) and the measured data is shown in Figure 6.2.4 (b). We observe that when both the desired signal and the interfering signal arrive by a direct path, the beamforming algorithm works well to reject the interference and achieve high SINR too. High mean output SINR after beamforming is achieved in both cases due to the interfering signal coming from a direct path and it is about 39.4 dB. SINR improvement of 35 dB at cumulative probability of 1% is achieved when the desired signal also comes along a direct path. However, as the transmitter 'B' transmitting the desired signal moves into the N-LOS condition, its signal strength drops thus increasing the improvement to 37.5 dB.

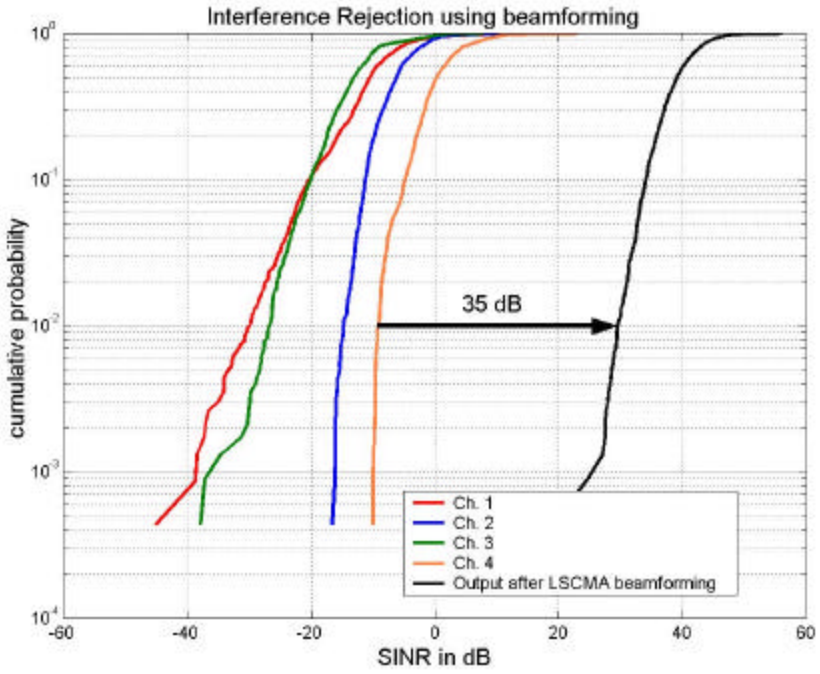

(a) Desired transmitter in LOS and the interfering transmitter is in LOS (Scenario 1(a))

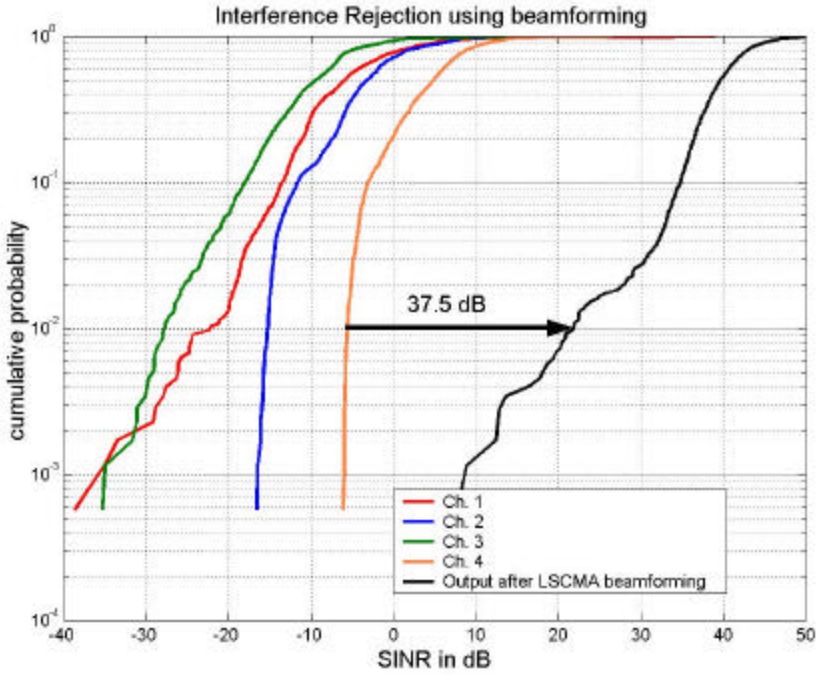

(b) Desired Transmitter in NLOS

Figure 6.2.3 Measured interference rejection results for the four-monopole square array (Array 2) mounted on the linear positioner in urban environment, the interfering Tx. 'B' is in LOS and the desired Tx. 'A' is in (a) LOS (Scenario 1(a)) and (b) relocated to obstructed N-LOS condition (Scenario 1 (c))

The third measurement set of results show how the four-element linear array (Array 1), with wideband low profile monopole elements, performs with broadside orientation to the desired signal to reject interference when the interference (transmitter 'B') is moved in azimuth in suburban scenario 2(a) as explained in Table 6.1. A plot is shown in Figure 6.2.5, which compares the SINR improvement achieved when the interference is separated from the desired signal in azimuth by 10°, 45°, 90° and 180°. Note that when the interferer (transmitter 'B') is 10°, 45°, 90° and 180° separated from the transmitter 'A' in azimuth, the mean SINR achieved after beamforming is 16.6 dB, 19.5 dB, 15.9 dB and 15.9 dB respectively, which shows nearly constant value in the mean output SINR. This is because the desired signal transmitter is fixed. However the SINR improvement achieved for 1% cumulative probability is 10.6 dB, 14.8 dB, 9.7 dB and 7.0 dB for 10°, 45°, 90° and 180° respectively that shows that the linear array functions well when the interfering signal arrives with different spatial characteristics than that of the desired signal. The poor performance when the transmitters are at 0° and 180° is due to the geometry of the array, as a null cannot be formed on only one side of the array.

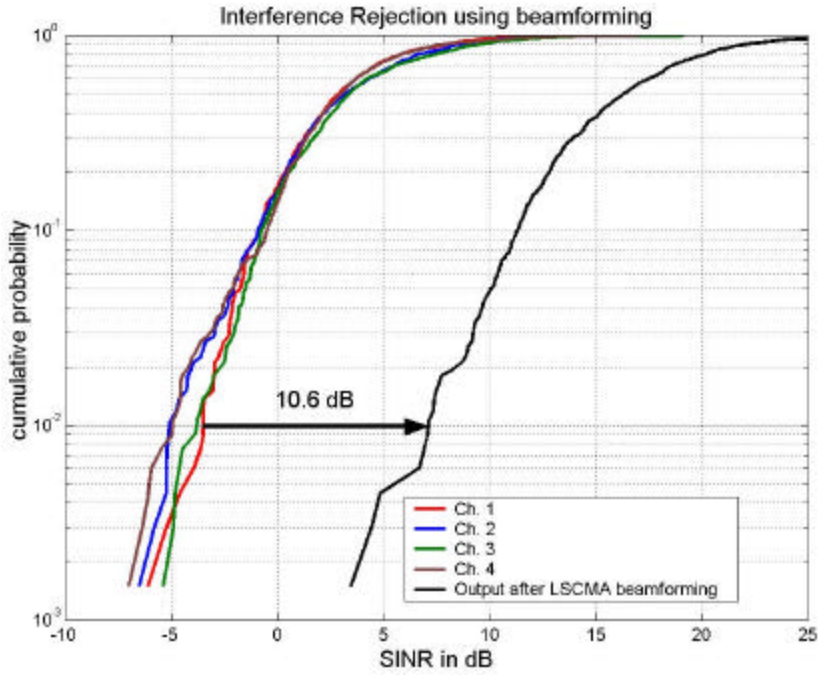

(a) 10° separation in azimuth between the desired and the interfering transmitter in suburban LOS condition

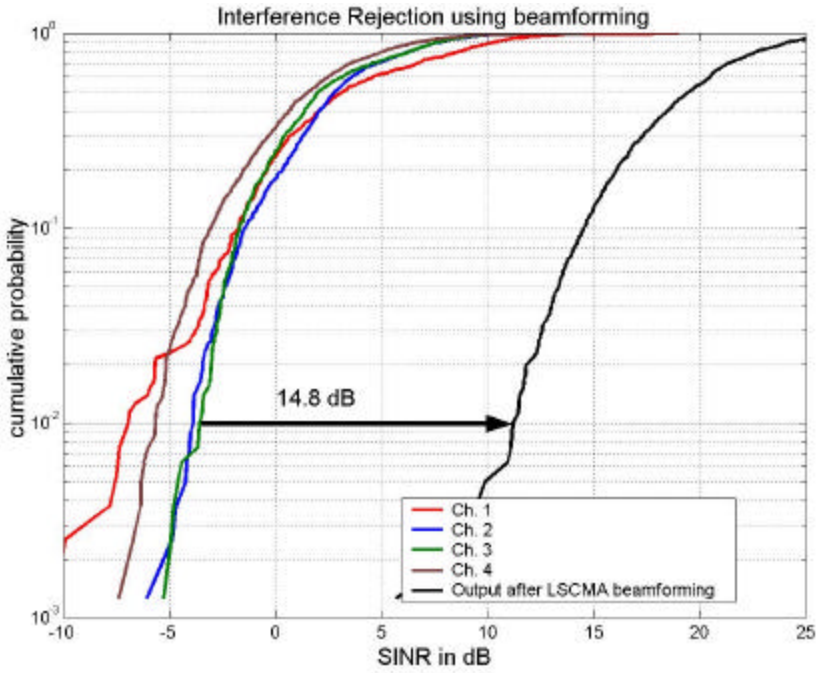

(b) 45° separation in azimuth between the desired and the interfering transmitter in suburban LOS condition

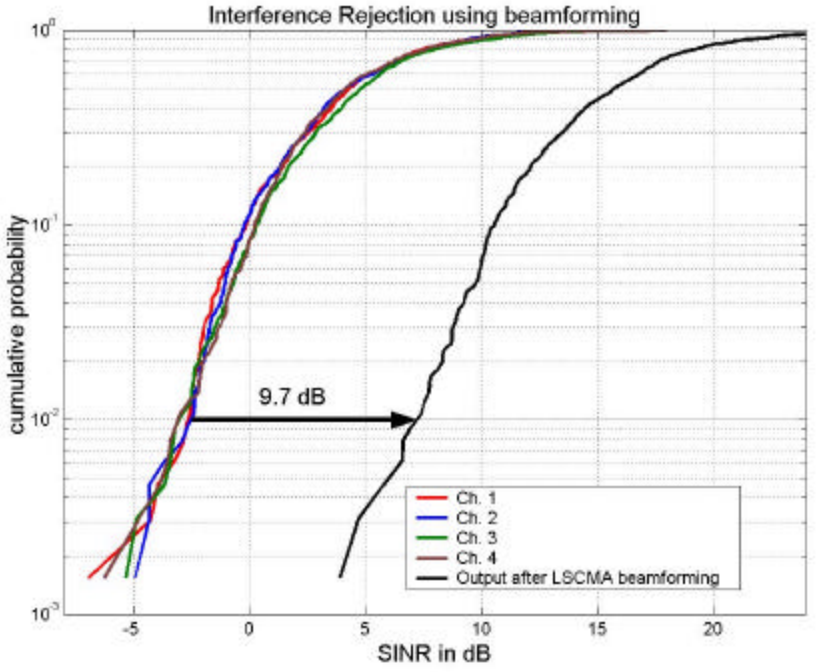

(c) 90° separation in azimuth between the desired and the interfering transmitter in suburban LOS condition

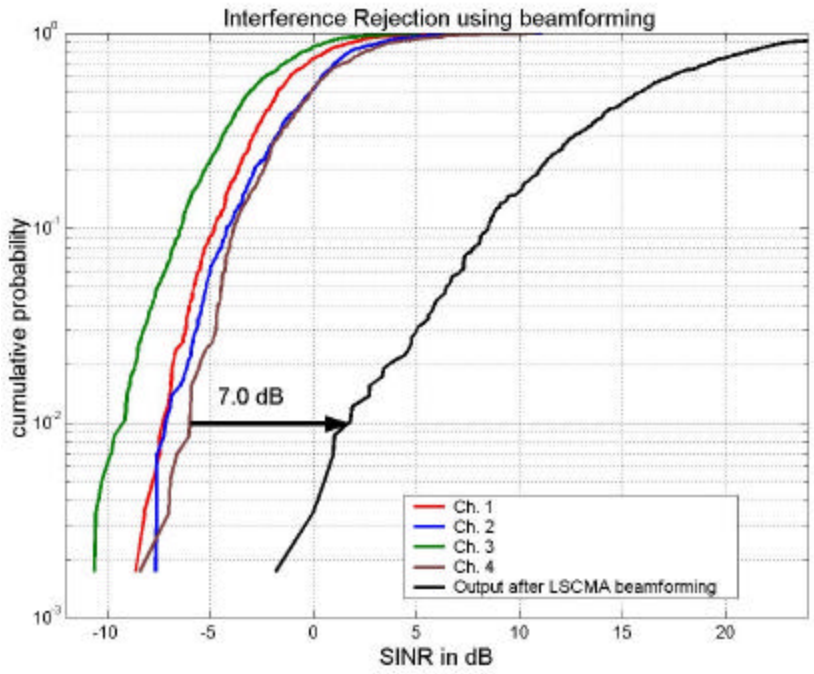

(d) 180° separation in azimuth between the desired and the interfering transmitter in suburban LOS condition

Figure 6.2.5 Measured interference rejection results in suburban line-of-sight channel (Scenario 2(a)) with the desired transmitter in fixed location and the interfering transmitter relocated at 10°, 45°, 90° and 180° in azimuth for the linear array of four monopoles (Array 1)

The fourth set of measurement results show performance of the sectored square array (Array 3 as listed in Table 4.1) in interference rejection when the interference (transmitter 'B') is relocated in azimuth in a suburban line-of-sight (Scenario 2(a)) condition. Figure 6.2.6 compares the SINR improvement achieved when the interference is separated from the desired signal in azimuth by 10°, 30°, 60°, 90° and 180°. Note that when the interferer (transmitter 'B') is 10°, 30°, 60°, 90° and 180° separated from the transmitter 'A' in azimuth, the mean SINR achieved after beamforming is 3.5 dB, 34.7 dB, 39.9 dB, 43.3 and 26.8 dB respectively. This shows that with 10° separation in azimuth, the sectored square array is not capable of rejecting interference with its directional radiation pattern. However, with increasing separation in azimuth up to 90°, the interference rejection capability increases as seen with increased improvement in SINR at 1% CDF. Note that the mean SINR after beamforming shows nearly constant value in the mean output SINR. This is because the desired signal transmitter is fixed in line-of-sight.

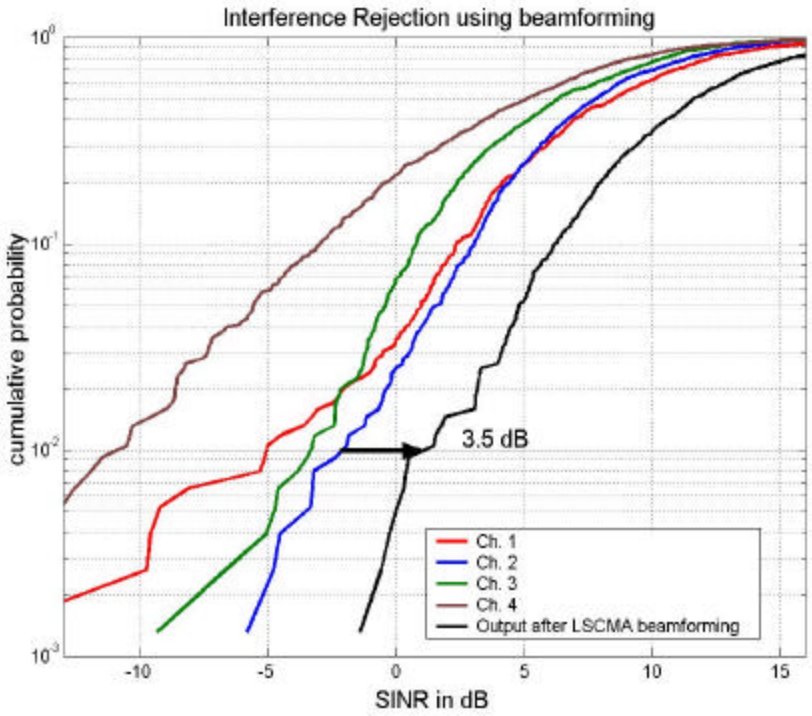

(a) 10° separation in azimuth between the desired and the interfering transmitter in suburban LOS condition

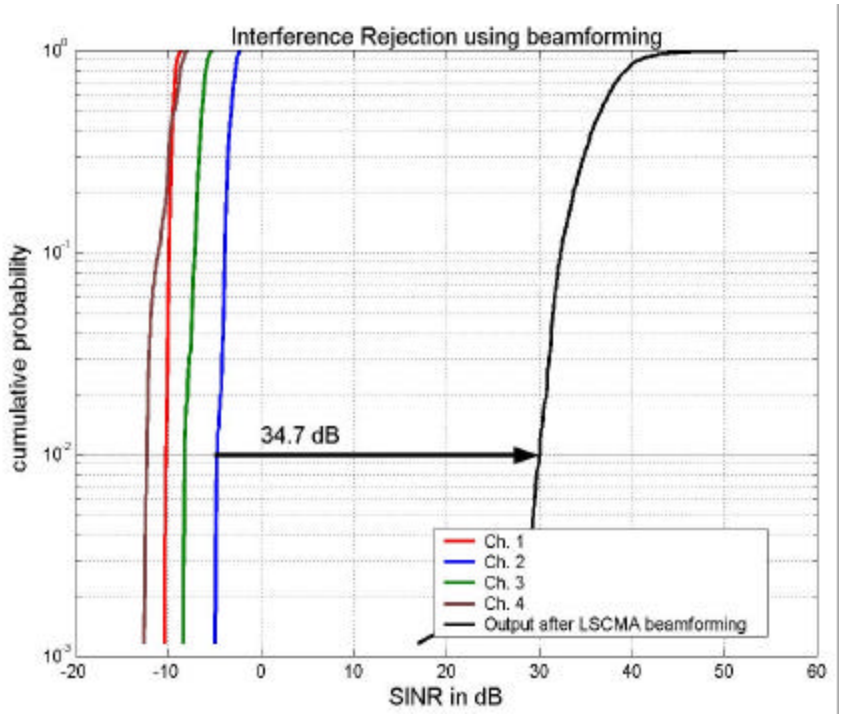

(b) 30° separation in azimuth between the desired and the interfering transmitter in suburban LOS condition

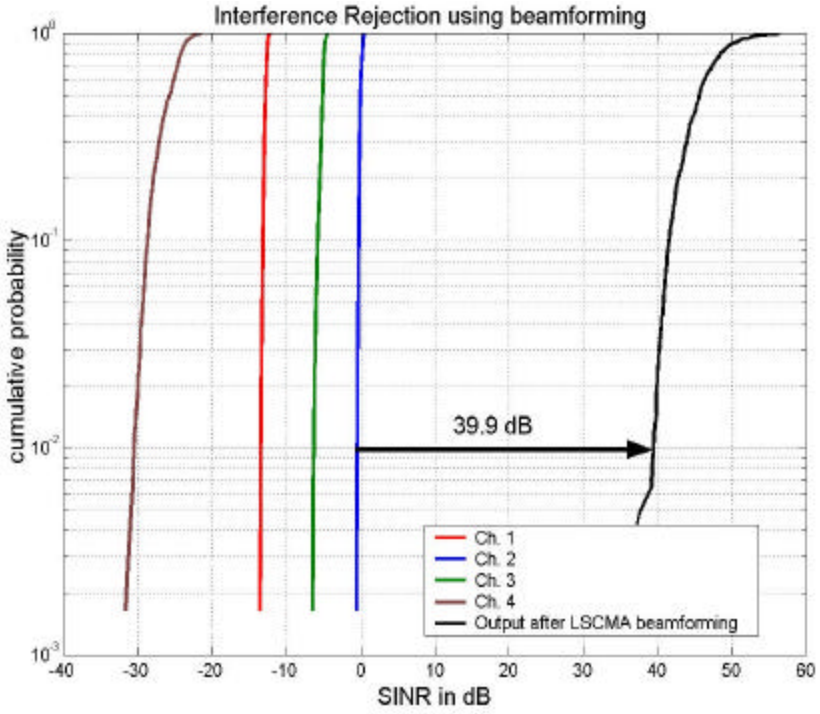

(c) 60° separation in azimuth between the desired and the interfering transmitter in suburban LOS condition

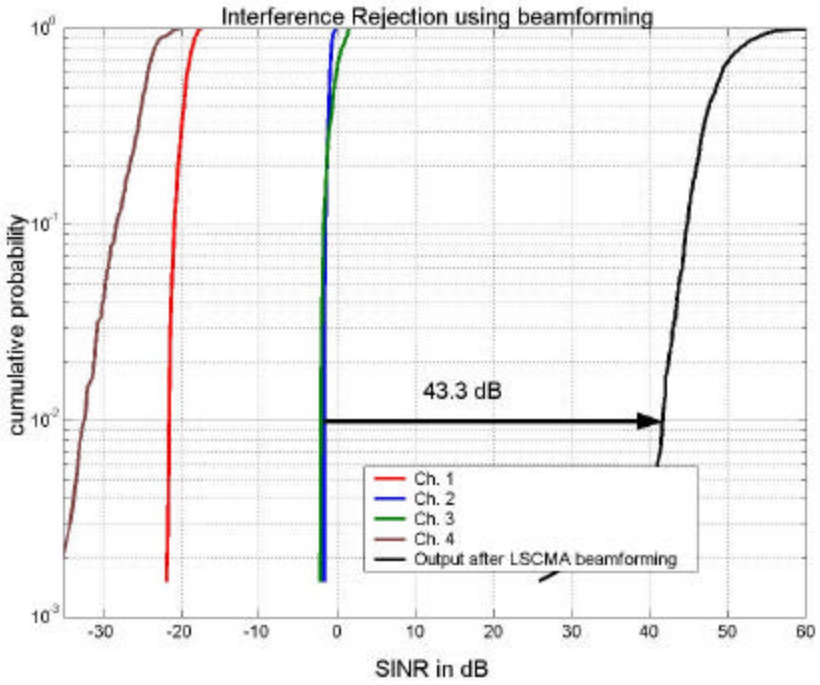

(d) 90° separation in azimuth between the desired and the interfering transmitter in suburban LOS condition

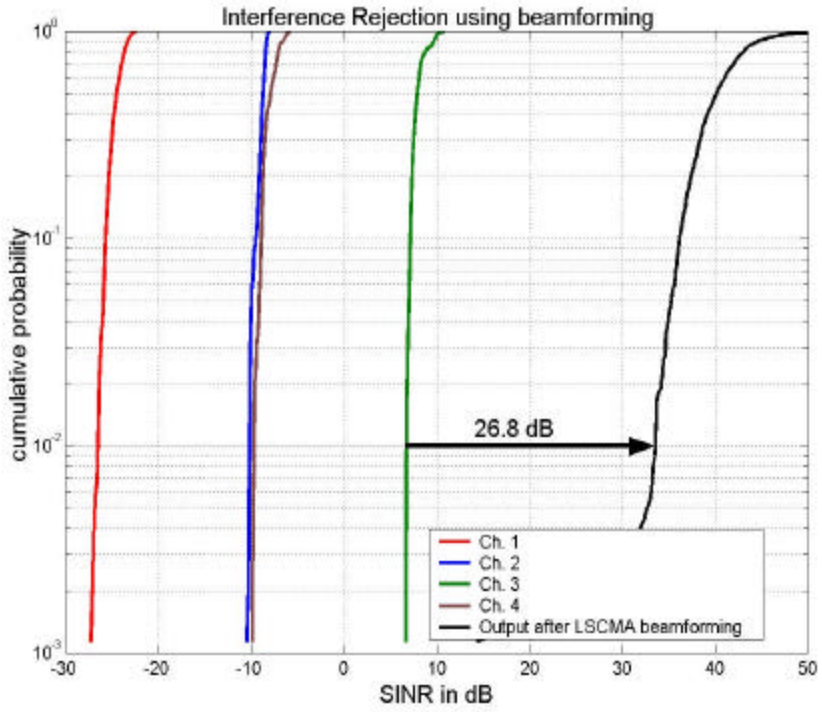

(e) 180° separation

Figure 6.2.6 Measured interference rejection results in suburban line-of-sight channel (Scenario 2(a)) with the desired transmitter in fixed location and the interfering transmitter relocated at 10°, 30°, 60°, 90° and 180° in azimuth for the sectored square array of four monopoles backed by corner reflectors offering directional pattern (Array 3)

Based on the experimental results obtained for the four-element antenna arrays in interference rejection using MT-LSCMA algorithm for adaptive beamforming for suburban (Scenario 2 (a)) and urban channels (Scenarios 1(a), (b) & (c)), we can safely conclude that the sectored square array antenna (Array 3) of four monopole elements backed by corner reflector performed well in the suburban line-of-sight environment and give substantial improvement in SINR of 3.5 dB to 43.3 dB at the cumulative probability level of 1%. Array 3 was observed to perform well in rejecting interference when the desired and the interfering transmitters were separated by 90° in azimuth. Moreover, in the suburban LOS (Scenario 2(a)) environment the four-element linear array of monopoles was observed to reject 45 dB of interference in broadside direction compared to 43 dB interference rejection in endfire case.

6.2.2. Vehicular Measurements

The signals received by multiple array elements are down converted, digitized, weighted and combined to suppress interference. The Multi-Target LS-CMA algorithm dynamically weights the received signals and offers near-optimum performance at pedestrian speeds. Interference rejection experiments conducted with a linear positioner have shown SINR improvement of 32 dB to 35 dB using four-element linear arrays in a suburban LOS scenario.

Weight adaptation performance of the MT – LSCMA algorithm depends on the block length of the data it process. All adaptive beamforming measurements were conducted using a block length of 320. At a vehicular speed of 25 mph, the MT – LSCMA algorithm offered 16 dB interference rejection at 1% outage level, with L = 320 (10 msec) as shown in Figure 6.2.7 (a). Interference suppression of 36 dB was observed with L = 160 (5 msec) as shown in Figure 6.2.7 (b). Note that use of lower block size is required to allow faster adaptation needed at vehicular speeds.

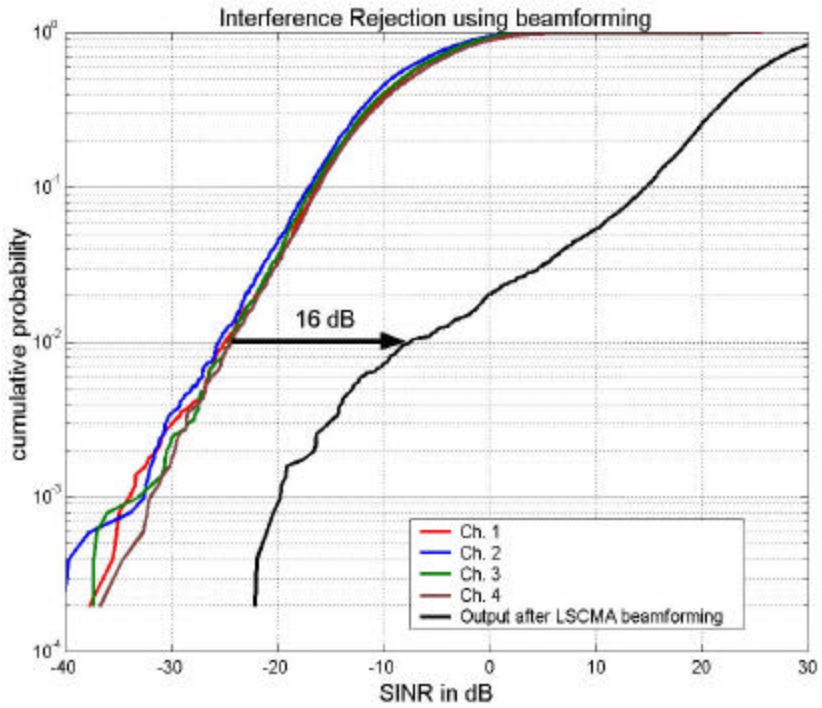

(a) LS-CMA block length: L = 320 (10 msec)

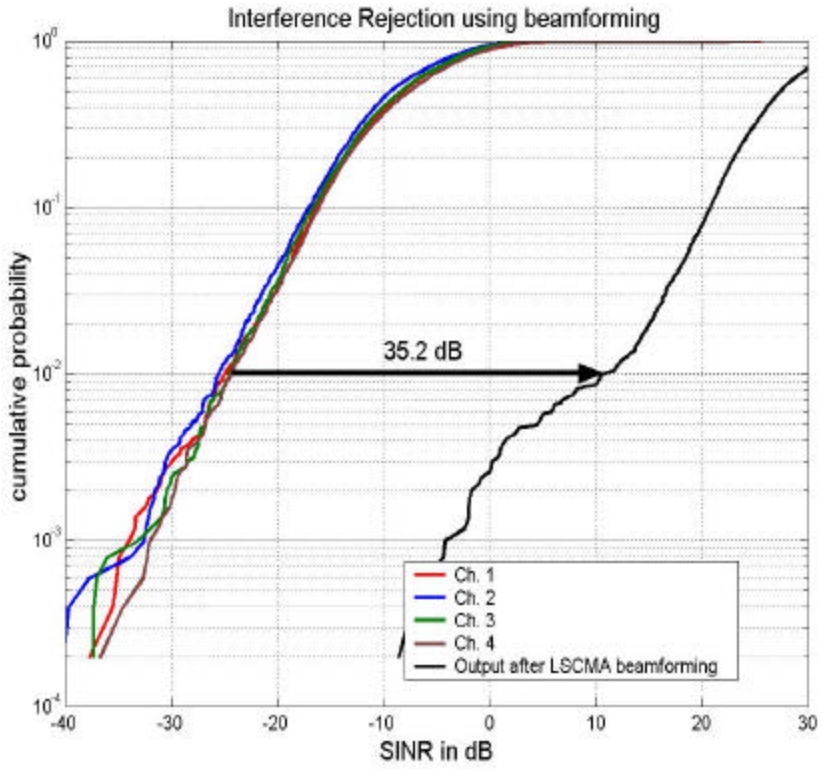

(b) LS-CMA block length: L = 160 (5 msec)

Figure 6.2.7 Weight Adaptation Performance of MT – LSCMA Algorithm for linear array (Array 1) of four monopole elements in suburban line-of-sight channel (Scenario 2 (b))

In a typical line of sight suburban scenario (# 2(b) as listed in Table 6.1) the performance of linear array (Array 1), square array(Array 2), sectorized square array (Array 3) and a square array of vertical dipoles (Array 6) mounted on the vehicle rooftop and run at 20 mph is shown in Figure 6.2.8 (a), (b), (c) and (d) respectively giving interference rejection of 35 dB, 24 dB, 21 dB and 24 dB at 1% cumulative probability of the SINR after using MT-LSCMA blind beamforming algorithm.

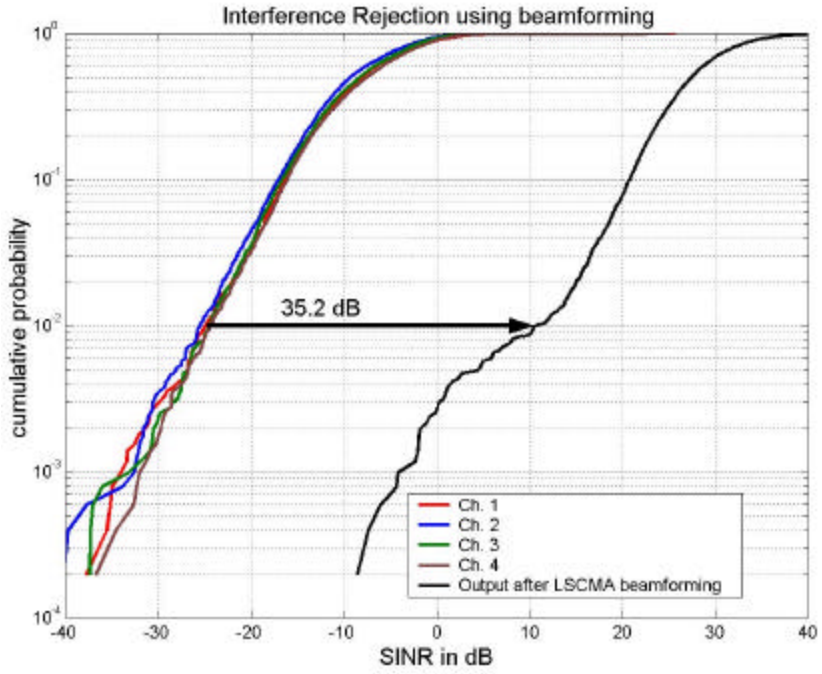

(a) Linear Array (Array 2)

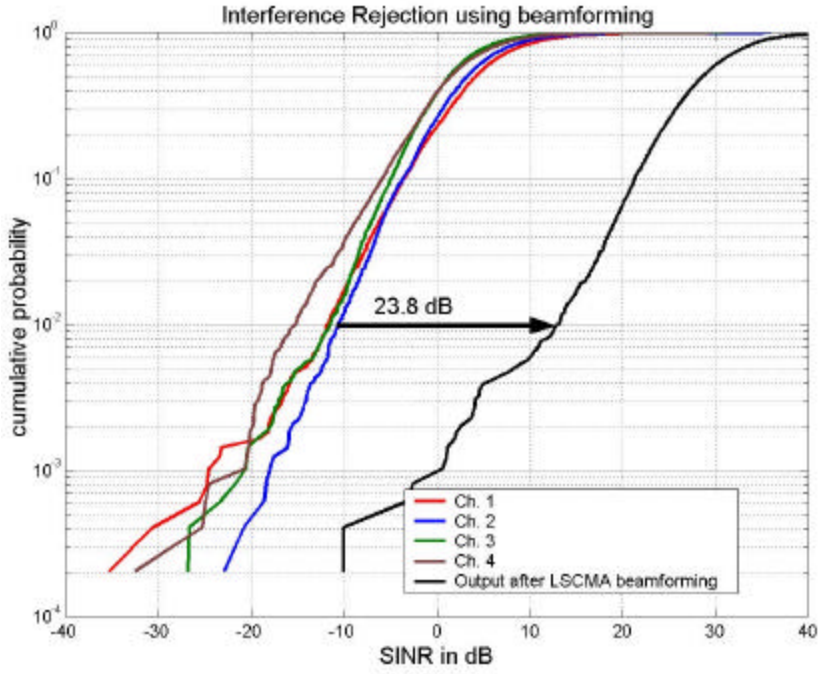

(b) Square array (Array 2)

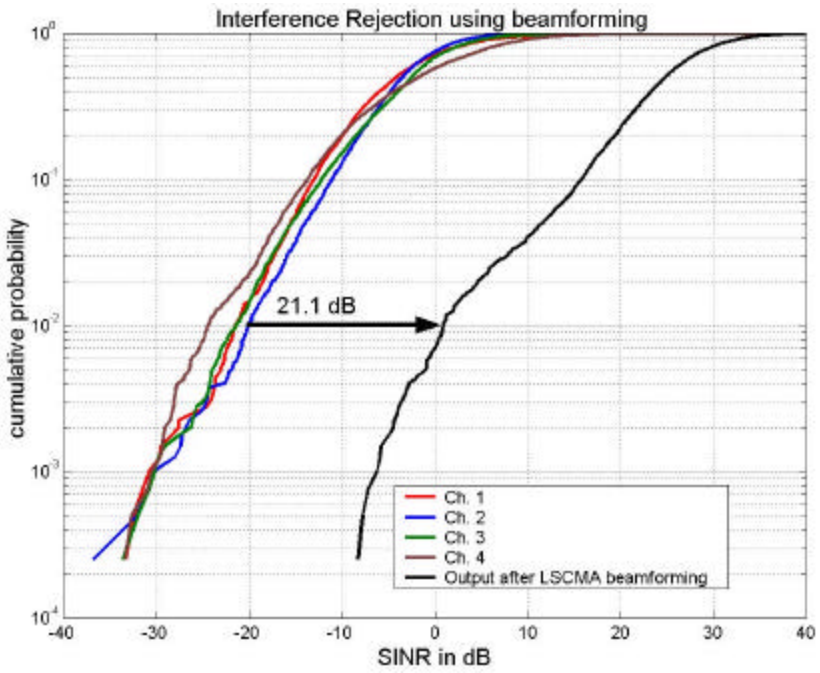

(c) Sectorized square Array (Array 3)

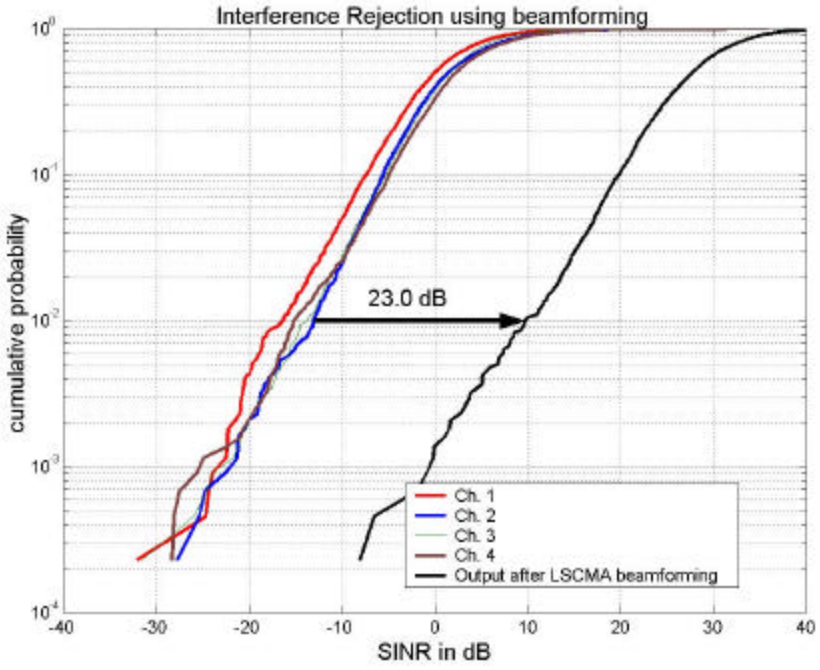

(d) Square array of vertical dipoles (Array 6)

Figure 6.2.8 Measured interference rejection performance in suburban line-of-sight channel (Scenario 2(b)) using Arrays 1, 2, 3 and 6 listed in Table 4.1, mounted on vehicle. The block length used for beamforming is L = 160 (5 msec).

6.3 Comparison of Array Performance

Experimental results from adaptive beamforming measurements showed that the four element array configurations listed in Table 4.1 and shown in Fig. 4.2.3 performed well in rejecting interference in different adaptive beamforming scenarios. In this section performances of linear (Array 1), square (Array 2) and square sectored array (Array 3) of low-profile broadband monopoles, four-wire antenna array (Array 4) and a linear array configuration (Array 5) of single wire elements mounted on a high impedance surface are evaluated and compared. For comparison a square array of four half-wave dipole elements (Array 6) was used as a reference baseline.

The four-wire antenna array with elements mounted on a high impedance surface (Array 4) showed improved signal reception compared to the square array of half-wave dipoles (Array 6) used as reference. The superior performance of the four-wire antenna in rejecting interference from all directions in azimuth is illustrated in Fig. 6.2.2 and summarized in Table 6.1. The linear array performed poorly in rejecting interference coming from two opposite endfire directions as shown in Fig. 6.2.5. However, the geometry of the square array in azimuth makes it suitable to reject interference in any direction. The high mean SINR achieved by the sectored square array shows that it performs better compared to the other arrays in interference rejection and this is demonstrated in Fig. 6.2.6 and summarized in Table 6.4. The performance of various arrays when mounted on vehicle rooftops in a suburban environment with line-of-sight condition is demonstrated in Table 6.6.

We also examined the effect of element spacing in arrays. Table 6.6 shows that as the adjacent element separation between the wire elements (Array 5) in linear configuration is increased from 0.4? to 1.0?, the mean SINR after beamforming drops. Also, note that interference rejection capability as measured by the improvement in SINR after beamforming at 1% CDF also decreases. This is because as the separation between the adjacent wire elements increases the interference rejection capability is limited to a narrow range of angles in broadside direction [Hud81]. The results recorded in Table 6.6 are from the experiments conducted in

suburban line-of-sight scenario with arrays mounted on vehicle rooftop as described by row 2 (b) in Table 6.1.

Table 6.6
Comparison of Measured Interference Rejection performance of arrays listed in Table 4.1 in Suburban LOS (Scenario 2(b))

	Average Mean I/P SINR (dB)	Mean SINR output (dB)	O/P SINR at 1% (dB)	?SINR at 1% CDF (dB)	Mean SNR output (dB)
Linear Array (1)	14.3	31.0	10.4	34.9	33.1
Square Array (2)	3.0	30.8	10.6	26.1	32.2
Sectored-Square Array (3)	35.4	38.0	15.9	20.1	38.9
Four-wire Antenna (4)	11.4	28.0	15.5	18.3	32.1
d = 0.4? four element Linear array (5)	36.9	39.0	18.0	16.9	39.7
d = 0.6? four element Linear array (5)	4.8	32.3	4.4	26.1	35.3
d = 0.8? four element Linear array (5)	5.9	27.8	18.5	17.7	35.2
d = 1.0? four element Linear array (5)	4.7	26.9	1.0	19.8	29.6
Square array of dipoles (6)	4.1	30.5	8.0	23.2	31.8

* for L = 320 (10 msec)

The available interference rejection (increase in SINR) at 1% cumulative probability is limited by the signal-to-noise ratio of the system. Signal-to-noise ratio (SNR) puts an upper limit on the achievable signal-to-interference-plus-noise ratio (SINR). Measurement results indicate

that the square array with monopoles sectorized by corner reflectors (Array 3) offers maximum interference rejection as shown in Table 6.6. Interference rejection performance of different arrays in the suburban non-line-of-sight obstructed environment (Scenario 2(c)) as summarized in Table 6.7.

Table 6.7
Comparison of Measured Performance of arrays listed in Table 4.1 in Suburban N-LOS Obstructed Environment (Scenario 2(c))

	Average Mean I/P SINR (dB)	Mean SINR output (dB)	O/P SINR at 1% (dB)	?SINR at 1% CDF (dB)	Mean SNR output (dB)
Linear Array (1)	5.6	25.5	4.4	15.9	29.2
Square Array (2)	8.9	24.3	2.3	13.6	28.7
Sectored-Square Array (3)	9.8	28.1	1.7	15.5	31.0
Four-wire Antenna (4)	4.6	23.1	12.5	15.2	24.4
d = 0.4? four element Linear array (5)	8.2	14.3	7.7	7.0	26.1
d = 0.6? four element Linear array (5)	8.2	14.7	7.3	6.1	28.0
d = 0.8? four element Linear array (5)	8.7	17.2	5.2	8.9	27.7
d = 1.0? four element Linear array (5)	8.3	13.5	13.3	6.2	28.3
Square array of dipoles (6)	10.8	24.7	1.9	13.0	31.2

* for L = 160 (5 msec)

The experimental results recorded in Table 6.7 are from the suburban NLOS scenario given by row 2 (c) in Table 6.1. Note that because both the desired and the interfering transmitter are in obstructed condition the interference and the desired signal come through multipaths. This reduces the mean SINR after beamforming and the interference rejection is also noted to be less than the results recorded in Table 6.6 for line-of-sight scenario.

6.4 Conclusions

A complete experimental investigation was conducted to evaluate the performance of the four-element array listed in Table 4.1 including linear, square, sectored square and four-wire antenna with elements mounted on a high impedance plan. The antenna profile of the four-element arrays (Array 4) makes them suitable for vehicular use.

The results from interference rejection measurements indicate that the low-profile arrays described in Fig. 4.2.3 perform satisfactorily in rejecting interference, especially the sectored square array (Array 3) having directional radiation active element pattern in suburban line-of-sight (Scenario 2(a)) environment. The arrays under discussion provided a substantial improvement in SINR of 15 dB to 28 dB at cumulative probability of 1% in the urban non line-of-sight environment using adaptive beamforming techniques. If it were not for a severe unavoidable broadband interference, even greater SINR improvement could have been achieved. Moreover, in the suburban environment the four element square arrays (Array 2) can reject interference equally well in all directions in the azimuth plane, with the sectored square array (Array 3) performing slightly better. Based on the experimental results obtained for these arrays in interference rejection we can safely infer that the arrays listed in Table 4.1 perform well in the sub-urban line-of-sight environment and give substantial improvement in SINR of 25 dB – 35 dB at cumulative probability of 1%.

References

[Lit96] Litva J. and Lo T. K., *Digital Beamforming in Wireless Communication*, Artech House Publishers, 1996,

[Hud81] Hudson J. E., *Adaptive Array Principles*, Institution of Electrical Engineers, London, 1981.

[Age93] Agee B. G.; Reed J. H.; Cohen K.; Hsia T. C., *"Simulation performance of a blind adaptive array for a realistic mobile channel"*, 43rd IEEE Vehicular Technology Conference, 1993.

[Lib99] Liberti, J.C., Rappaport T.S., *"Smart Antennas for Wireless Communications: CDMA Applications"*, Prentice Hall, 1999.

[Rap99] Rappaport T. S., *"Wireless Communications; Principles & Practice"*, Prentice Hall, NJ 1999.

[Die00] Dietrich Carl B. Jr., *"Adaptive Arrays and Diversity Antenna Configurations for Handheld Wireless Communications Terminals"*, Ph.D. Dissertation, Virginia Tech, 2000.

[Sie00] Sievenpiper D., Hsu H. P., Schaffner J., Tangonan G., Garcia R., Ontiveros S., "Low-profile, four-sector diversity antenna on high-impedance ground plane", Electronics Letters, Volume: 36, August 2000, pp: 1343 – 1345.

Chapter 7 Conclusions

This thesis reports results from diversity and beam forming measurements performed for four-element mobile arrays. Diversity combining and interference rejection using beam forming at the mobile terminals exhibit promising results as shown in Sections 5.2 and 6.2. A complete investigation was undertaken to evaluate the performance of arrays with different active element radiation pattern by using various four-element arrays listed in Table 4.1. The impedance measurement of the arrays is reported in Section 4.2.2 and their radiation patterns in azimuth are reported in Section 4.2.3. The diversity combining urban, suburban, line-of-sight and obstructed channel measurement scenarios are listed in Table 5.2 and for interference rejection measurements scenarios are listed in Table 6.1.

To study the performance at pedestrian speeds, measurements were taken using a linear positioner, run by a stepper motor. As discussed in Table 5.6 in Section 5.2.1, the linear array of four low-profile broadband omni directional monopoles (Array 1) exhibited a diversity gain of 13.7 dB in a non-line-of-sight (NLOS) obstructed urban channel (Scenario 1(b) in Table 5.2) at the 99% reliability level. Such a considerable gain allows reliable transmission at very low power levels, overcoming multipath fading and ensuring reliable communication.

Interference rejection performance of four element arrays listed in Table 4.1 was evaluated as a function of the angular separation of the desired and the interfering transmitters. As shown in Section 6.2.1, a linear array with monopole elements recorded 27.1 dB interference rejection at 1% cumulative probability with the interfering transmitter placed 90° in azimuth with respect to the desired transmitter as compared to 15.6 dB interference rejection with the

interfering transmitter placed in the same direction as the desired transmitter in suburban line-of-sight scenario (#2 (a) in Table 5.2). Performance comparison shows that the linear array performs marginally better than the square array under similar experimental setup. The results collected from interference rejection measurements indicate that the sectored square array (Array 3) performed better than other arrays described in Section 4.2 in a suburban line-of-sight environment. Moreover, the square array of four monopole elements in a suburban environment rejected interference equally well in all directions in azimuth. Interference rejection at the mobile terminals using adaptive beamforming reduces the capacity limit imposed by co-channel interference. Interference rejection using four element arrays allows effective resistance against jamming in military application.

Quality and capacity, severely limited by multipath fading and interference, can substantially be increased using adaptive antenna arrays at the mobile terminals in the urban environment [Vau88]. In mitigating fading due to the multipath arrays perform best in the urban NLOS environment providing maximum diversity gain. However, square arrays perform well to reject interference from all directions in the azimuth in both urban and suburban environments. The experiments described in this report indicate that the antenna can be used effectively for terrestrial communications.

Chapter 2 presents a brief background in mobile radio propagation and discussed some limitations in effective communications due to hostile multipath environment with interferers. Diversity combining techniques and performance parameters are briefly addressed at the end of this chapter. Adaptive beamforming and interference rejection using fixed or adaptive techniques are discussed in Chapter 3.

Carl Dietrich and Randall Nealy at Virginia Tech Antenna Group originally developed the HAAT system to investigate co-polarized and multi-polarized handheld adaptive arrays. The four-channel HAAT measurement testbed with diversity combining and adaptive beamforming software is described in Chapter 4. Antenna pattern measurements shown in Section 4.2 show a pattern gain of – 2.7 dBi in azimuth for the four-element antenna with elements mounted on a high impedance plane. This relatively low gain is comparable to built-in antennas on mobile

handsets. Element coupling measurements were performed to record the voltage standing wave ratio at 2.05 GHz. The results from these measurements are shown in Section 4.2.

The low profile four-element arrays are suitable for mounting on a vehicle rooftop. Results from diversity combining and interference rejection vehicular measurements are reported, respectively, in Sections 5.2 and 6.2. The antenna arrays performed well in the urban non line-of-sight obstructed environment and a substantial diversity gain of 9.6 dB – 13.0 dB at reliability of 99% was recorded. Switched diversity gain can be improved by reducing the threshold signal level at which switching occurs. Vehicular measurements were conducted with slow and fast moving vehicle to illustrate the effect of fast changing channel on the beamforming algorithm. The LSCMA beamforming algorithm recorded a progressive increase in interference rejection of 15 dB, 19 dB and 26 dB, respectively, for update intervals of 10 msec, 5 msec and 2.5 msec. Substantial improvement in SINR of 22 dB to 28 dB at cumulative probability of 1% was observed for a square sectorized array of four monopole elements backed by corner reflectors (Section 6.2).

The future in broadband wireless personal communications demands investigation of adaptive antenna arrays at the mobile terminals. The measurements reported in this thesis are narrowband measurements at 2.05 GHz. To ensure high data rates with sufficient reliability it is imperative to carry out wideband interference rejection measurements. The Virginia Tech Antenna Group (VTAG), working closely with the Mobile and Portable Radio Research Group (MPRG) at Virginia Tech, has put together a Wideband Antenna Array Testbed (WAAT), a four-channel wideband measurement testbed. The future work will involve testing, performing, and evaluating four–channel measurements for 3.8 MHz wide bandwidths at 2.05 GHz. In addition, the far field antenna patterns, as described in Section 4.2.3, indicate that four-wire antenna would be well suited to mobile satellite applications. The performance improvement in mobile-satellite communications using adaptive arrays has not yet been investigated. Measurements involving capturing satellite signals using adaptive arrays with diversity combining capability, mounted on vehicle rooftops, would form an interesting research topic. To harvest maximum benefits from mobile adaptive arrays there is considerable research required to make the widespread use of handheld arrays cost effective.

Vita

Gaurav Joshi was born on January 2nd, 1979 in Nagpur, Maharashtra, India. He received his Bachelor of Engineering (B.E.) in Electronics and Communications Engineering in June 2000 from Gujarat University, Ahmedabad, India. He served at Physical Research Laboratory, Ahmedabad, India as under-graduate research assistant to develop the Front End of Satellite receiving system at 150 MHz and 400 MHz. He received his Masters of Science (M.S.) in Electrical Engineering in July 2002 from Virginia Polytechnic Institute and State University, Blacksburg, Virginia. He is currently enrolled as doctoral student in Electrical Engineering at Virginia Tech.

Gaurav Joshi has served Virginia Tech Antenna Group (VTAG) as Research Assistant. At VTAG he is developing wideband four-channel receive diversity system. His research interests lie in adaptive array digital signal processing for diversity combining and interference rejection.